Potential Applications of Silk Fibroin

as a Biomaterial

by

Kevin Bailey

A thesis

presented to the University of Waterloo

in fulfillment of the

thesis requirement for the degree of

Master of Applied Science

in

Chemical Engineering

Waterloo, Ontario, Canada, 2013

Author's Declaration

I hereby declare that I am the sole author of this thesis. This is a true copy of the thesis, including any required final revisions, as accepted by my examiners.

I understand that my thesis may be made electronically available to the public.

Abstract

Fibroin is a biopolymer obtained from the cocoons of the *Bombyx mori* silkworm that offers many unique advantages. In this thesis work, fibroin was processed into a regenerated film and examined for potential biomaterial applications.

The adsorption of bovine serum albumin onto the fibroin film was investigated to examine the biocompatibility of the film, and it was found that BSA adsorption capacity increased with an increase in BSA concentration. At 10 *mg/mL* of BSA, the BSA sorption reached 0.045 mg/cm^2. This level of BSA is indicative of good blood compatibility and biocompatibility of the fibroin.

The gas permeabilities of oxygen, nitrogen, and carbon dioxide were tested for potential applications in contact lenses and wound dressings. Over a pressure range of 70 – 350 *psig*, the permeability of oxygen and nitrogen was 5 *Barrer*, while that of carbon dioxide ranged from 26 to 37 *Barrer*. The oxygen transmissibility of the fibroin films prepared in this study was on the low end required for use in daily wear contact lenses, but sufficient to aid the healing process for use in wound dressings.

The permeability and diffusivity of four model drugs in the fibroin film was investigated for potential applications in controlled drug release. The permeability at higher source concentrations leveled out to $0.8 – 4.3 \times 10^{-7}$ cm^2/s depending on the drug tested. The diffusion coefficient determined from sorption experiments was approximately 1.8×10^{-9} cm^2/s, while the diffusion coefficients from desorption experiments were determined to be $0.8 – 2.7 \times 10^{-9}$ cm^2/s. The magnitude of the drug permeability and diffusivity are consistent with many other controlled release materials, and the fibroin film showed good potential for use in controlled release.

Acknowledgements

I would like the thank my supervisor Professor Xianshe Feng for his support and guidance throughout my two years of study, as well as for his effort put into obtaining scholarships and additional funding for my research activities. I would also like to thank the members of my thesis committee, Prof. N. McManus and Prof. B. Zhao, for their time and efforts put into reading and correcting this thesis.

I would also like to thank Andrew and Margaret Stephens and the Department of Chemical Engineering at the University of Waterloo for their generous scholarship, as well as the Government of Ontario for providing me with the Queen Elizabeth II Graduate Scholarship.

I would like to thank all labmates and coworkers, in particular Dr. Gil Francisco and Usman Farooq, for their time, knowledge, and assistance with all aspects of my research.

Last but not least I would like to thank my mother, father, brother, and girlfriend, for all their support, understanding, and encouragement. I could not have done this without the help of each of you. This thesis is dedicated to you.

Table of Contents

List of Tables

List of Figures

Chapter 1: **Introduction**

Biopolymers are gaining interest in both research and industrial applications for their unique properties and advantages over synthetic materials. Evolved to serve wide ranges of uses in nature, biopolymers can display unique mechanical and chemical properties which are advantageous in many applications. Biopolymers may come from renewable and often sustainable sources, as compared to the fossil-fuel base of most synthetic polymers. As a result, interest in biopolymers over synthetic materials has grown significantly over the past decade due to increased environmental consciousness. Perhaps one of the largest advantages of biopolymers is that they are generally both biocompatible and biodegradable. This feature is of great importance in many biomedical applications, where materials are needed that do not provoke an immune response and have the ability to degrade within the body without adverse effects (Sionkowska, 2011).

Biomaterials are derived from a wide range of sources, including many different plants and animals. Some of the major natural polymers studied for use in biomaterials include chitosan, collagen, keratin, elastin, and silk (Sionkowska, 2011). Silk has been used for decades in medical sutures, and even longer in textiles, but interest in silk has grown for use as a material in contact lenses, wound dressings, controlled release of drugs, and as a scaffold in tissue engineering (Altman et al., 2003, Minoura et al., 1990, Arai et al., 2004). Silk is produced by a number of different larvae in the order *Lepidoptera*, including silkworms, spiders, scorpions, mites, and flies, with each producing a unique variety of silk (Altman et al., 2003). Most of the world's silk used for textile and other applications is produced by the domesticated *Bombyx mori* silkworm. Silk from the *Bomby mori* silkworm consists of two main proteins, fibroin and sericin.

Fibroin provides the main fibrous structure to the silkworm cocoon while sericin is a glue-like protein that holds the cocoon together. Both fibroin and sericin can be used on their own or in blends to produce membranes and films with unique chemical and physical properties (Gimenes et al., 2007).

Biodegradation refers to the ability of a material to be broken down into simpler, more easily dealt with components, through a number of different biological processes, such as bacterial metabolism or enzymatic attack. In the body, foreign materials are biodegraded through a complex interaction between biological, chemical, and physical factors. The ability of a biomaterial to biodegrade into non-harmful degradation products is important for many applications. Biodegradability is important in tissue engineering scaffolds, and the rate of biodegradation should be equal to or less than the rate of tissue growth. It is also important in controlled drug release applications in which a drug-loaded material is implanted within the body. The rate of degradation affects the rate of drug release in some instances, and full degradation is useful to avoid surgery to remove the material once the treatment is over (Altman et al., 2003).

Biocompatibility may also refer to the extent and severity of host response to a material being used in biological applications (Williams, 1999). A wide range of body responses are lumped under the concept of host response, including inflammatory or immune response, cell toxicity, thrombogenic response, and enzymatic response (Altman et al., 2003; Tang et al., 2009; Park et al., 2001). Thrombogenic response is a blood response in which circulating blood proteins and biomolecules adsorb to the foreign material and form a thrombus. A thrombus that becomes large enough and dislodges is known as an embolism, and can travel through the blood stream to the heart or brain and cause heart attack or stroke. Adsorption properties of

biomaterials should favour little to no thrombogenic response if they are to be used in the blood stream.

Bovine serum albumin (BSA), a very well characterized protein derived from bovines, is often used as a model protein in scientific investigations. In addition to being well characterized and understood, BSA is low in cost and slow to denature, which makes it ideal for research (Avremescu et al., 2003). Serum albumins, including BSA, are major components of blood, and the adsorption behaviour of BSA onto biomaterials plays a major role in limiting thrombus formation (Van Enckevort et al., 1984; Pitt et al., 1986). This investigation will look into the adsorption behaviour of BSA onto a fibroin film to determine if the film is likely to display thrombogenic response or good blood compatibility. High surface coverage of BSA adsorbed on the fibroin film would limit the adherence of thrombus forming biomolecules such as fibrinogen, limiting thrombus formation on the material surface. The extent of BSA adsorption and surface coverage on the fibroin surface will therefore be used as an indicator of thrombogenic response and blood compatibility.

Silk has long been used as a material for biomedical applications in the form of sutures. Because of the unique properties of silk (e.g. tensile strength, biocompatibility, and biodegradability), it has traditionally made for a popular material in sutures. However, silk has recently fallen out of favour for use in sutures as concerns over biological responses to silk have been raised and its biocompatibility questioned. Further research has shown that sericin in the silk is the likely cause of the unfavourable immunological response, and this has renewed interest in silk fibroin for use as a biomaterial (Altman et al., 2003). Fibroin is found to have a biological response similar to such other materials as polystyrene, and is now a popular choice for biomaterial applications (e.g. tissue-engineering scaffolds) (Sofia et al., 2001). Fibroin has

been used as a scaffold for anterior cruciate ligaments, hepatic tissue, reticular connective tissue, cartilage, and bone formation, among many others (Altman et al., 2002; Hu et al., 2006; Pra et al., 2006; Silva et al., 2008; Sofia et al., 2001). Other areas of interest for fibroin as a biomaterial include contact lenses, wound dressings, and drug delivery systems.

Contact lenses and wound dressings need to meet a number of unique requirements. Contact lenses need to be biocompatible and inert in the eye, have good chemical and mechanical stability, have good wetting ability, display appropriate optical transmission, and be very oxygen permeable (Sashina et al., 2009). Wound dressings need to be biocompatible, have good oxygen and moisture permeability, and should promote wound healing (Min et al., 2012). Both contact lenses and wound dressings require good oxygen permeability, and thus this investigation will determine the oxygen permeability of fibroin film to see if the permeability is suitable for either application.

Controlled drug release is another biomaterial application that is receiving considerable attention. The goal of controlled release is to deal with the problems of traditional drug delivery, where a large dose is often administered at one time, causing a spike in the drug concentration in the body, after which the concentration will fall as the drug is degraded and removed from the body. The spikes can potentially reach harmful concentration levels, depending on the drug and dose, and the lows can decrease the concentration below a level in which it is effective. The concentration range in which the drug is safe and effective is known as the therapeutic window. Controlled release looks to mediate drug release by encapsulating or embedding the drug within a polymer matrix and the diffusion of the drug out of the polymer or the polymer matrix degradation is used as a way to control the drug release into the body (Langer and Peppas, 1981). The biocompatibility, biodegradability, mechanical properties, and ability to be formed into a

film make fibroin attractive as a material in controlled release systems (Dyakonov et al., 2012). The present work looks to determine the permeability and diffusion coefficient of four different model drugs – tetracycline-HCl, diltiazem-HCl, ciprofloxacin-HCl, and tetrahydrozoline-HCl – in a silk fibroin film to look into its applicability as a material for controlled release applications.

1.1 Objectives

Several applications for various types of fibroin films have been reported in the literature, mainly focusing on biomaterial areas. This thesis work will focus on investigating the potential of fibroin films for such applications.

The blood compatibility and thrombogenic response of the fibroin film will be examined to determine if the film will display good biocompatibility in biomaterial applications. Therefore, the adsorption behaviour of BSA onto the fibroin film will be determined. The fibroin film will be looked into as a material for contact lenses and wound dressings as well. As an initial check of feasibility, the gas permeability, with a main focus on oxygen permeability, will be determined to see how permeable the film is to gases.

The potential of the fibroin film for use in controlled drug release will be examined by measuring the permeability and diffusivity of four different model drugs in the film. The permeability and diffusivity greatly determine the rate of release through the membranes, and knowledge of these parameters is of importance when designing controlled release systems.

1.2 Scope of Thesis

This thesis covers several aspects relevant to the potential applications of silk fibroin films, including as a biomaterial for contact lenses and wound dressings, and in controlled release systems.

Chapter 1 was an introduction to biopolymers, silk and silk fibroin, biodegradability, and biocompatibility. Biomaterial applications as contact lenses, wound dressings, and controlled release were also addressed. The objectives and aims of the thesis work were elucidated.

Chapter 2 was a literature review and in depth analysis of the topics introduced in Chapter 1 and their related concepts. These topics include fibroin, with major a focus on its biodegradability and biocompatibility, bovine serum albumin and protein adsorption, gas permeability pertinent to contact lenses and wound dressings, and drug permeability and sorption and desorption kinetics related to controlled release.

Chapter 3 outlined the materials and methods used for the fibroin film preparation, as well as experiments with BSA adsorption, gas permeability, drug permeability, and sorption/desorption kinetics.

Chapter 4 presented the results of the research, and the trends and significance of the data were discussed.

The main conclusions drawn from this work were presented in chapter 5, where the applicability of fibroin films for each of the tested applications was addressed. Recommendations for future work on the topics of this investigation were provided in chapter 6.

Chapter 2: **Background and Literature Review**

The aim of this thesis is to investigate a number of different potential applications for a novel silk fibroin film. Three different areas with respect to fibroin films are to be looked into: bovine serum albumin (BSA) adsorption, as a biomaterial in contact lenses and wound dressings, and as a material in controlled drug release. The BSA adsorption study determines the extent of BSA sorbed on the film, which has a correlation to the blood compatibility of the film. The permeability of the film to oxygen, nitrogen and carbon dioxide gases are measured to determine if the gas permeability is sufficient for use in contact lenses and wound dressings. For potential use in controlled release, the permeability and sorption kinetics of four different model drugs in the fibroin film are evaluated. The research findings from this thesis work will serve to guide future research on fibroin films for the desired applications. The following attempts to provide a general background and review prior work reported in the literature relevant to the thesis work.

2.1 Fibroin

Fibroin is a silk protein mainly derived from the cocoons of the *Bombyx mori* silkworm, along with the glue-like protein sericin. Sericin can be removed from the fibroin using a degumming process, to leave only the fibroin fibers. The main structure of fibroin is a repeating sequence of six amino acids, (Gly-Ser-Gly-Ala-Gly-Ala), which causes a homogeneous secondary structure in an antiparallel β-sheet conformation (Motta et al., 2002). Based on molecular weights, two major groups of fibroin proteins can be distinguished: the light one has a molecular weight of 25 *kDa* and the heavy one 325 *kDa* (Altman et al., 2003). While the

crystalline antiparallel β-sheet region in fibroin comprises about two-thirds of the protein, the amorphous region of the fibers represents about one-third of the protein. Together these regions provide the unique mechanical properties that silk fibroin displays (Cao and Wang, 2009). Table 2-1 displays the mechanical properties of various types of silk.

Table 2-1: Mechanical Properties of Silk (Altman et al., 2003)

Material	Ultimate Tensile Strength (MPa)	Modulus of Elasticity (GPa)	% Strain at Break
Bombyx mori silk with sericin	500	5-12	19
Bombxy mori silk without sericin	610-690	15-17	4-16
Spider Silk	875-972	11-13	17-18

In general silk has a combination of very high strength and elasticity. Fibroin also has excellent resistance to failure in compression (Altman et al., 2003). Fibroin is a natural block copolymer that contains hydrophobic and hydrophilic blocks. The hydrophobic blocks create the β-sheet conformation of the fiber through hydrogen bonding between the blocks, and these regions are responsible for the high fiber strength, insolubility, and thermal stability of fibroin (Bini et al., 2004).

Other favourable properties of silk fibroin include biodegradability and biocompatibility. Fibroin is able to be degraded *in vivo* through enzymatic degradation, resulting in harmless degradation products that can often be used by nearby cells (Cao and Wang, 2009). The foreign body response and inflammatory cell adhesion to fibroin is low, which means fibroin displays good biocompatibility (Santin et al., 1999). Fibroin can be processed into many different forms allowing for use in many applications. Besides the fiber form, fibroin can be processed into

films, sponges, gels, membranes, tissue scaffolds, and powders (Cao and Wang, 2009). The combination of unique mechanical properties, biodegradability and biocompatibility results in potential uses of fibroin for different medical applications.

The extensive hydrogen bonding between the β-sheets in silk fibroin leads to great stability and insolubility in most solvents. Solvents containing high concentration of salts such as lithium bromide, lithium thiocyanate, calcium thiocyanate, and calcium chloride have been shown to interrupt the hydrogen bonding between the β-sheets, turning the fibroin to an amorphous random coil conformation that is water soluble. Fibroin in this state can be processed into many different forms, including films, sponges, hydrogels, microparticles and many more, after which the β-sheet crystallinity can be returned through multiple methods (Wenk et al., 2011). Fibroin processed this way is referred to as regenerated silk fibroin. One of the most common processing methods involves dialyzing the fibroin-salt solution to remove the salt, then returning the β-sheet structure with methanol treatment. The novel processing method employed in this thesis is to use liquid-liquid extraction to precipitate the fibroin from the salt solution into ethanol, then dissolving the precipitated fibroin in formic acid, followed by evaporation of the formic acid, to form a uniform fibroin film.

2.1.1 Biodegradability of Fibroin

Biodegradation is the process by which a material is broken down to simpler components through such biological processes as bacterial metabolism or enzymatic attack. The biodegradability and rate of degradation play an important role in many applications. In controlled release, where a drug is encapsulated within a polymer membrane and implanted

under the skin, it would be advantageous if the membrane degrades with no harmful degradation products so surgical intervention to remove it is not needed. However, the material shouldn't degrade prematurely, or excessively high quantities of the drug could be released within the body. In tissue engineering, the scaffold biomaterial should preferably degrade, but the degradation should be matched or exceeded by the growth of the tissue (Altman et al., 2003).

In vivo biodegradation occurs via complex interactions between many different biological, chemical, and physical factors. For silk fibroin, proteolytic enzymes are the main factor for the degradation. Enzymes degrade silk fibroin through adsorption onto the fibroin surface, and then digest the material into amino acids through hydrolysis of the peptide bonds. Several enzymes are known to degrade fibroin, including chymotrypsin, actinase, and carboxylase (Cao and Wang, 2009).

Research into the degradation of silk has been ongoing for decades. In order to elucidate the structure and amino acid sequence of fibroin, Lucas et al. (1957) used chymotrypsin and carboxypeptidase to hydrolyze the peptide bonds in fibroin. It was found that the degradation products of the fibroin contained short peptide chains composed mainly of the amino acids glycine, alanine, serine, and small amounts of tyrosine.

The US Pharmacopeia's criterion for a biodegradable material is that it 'loses most of its tensile strength within 60 days' (Altman et al., 2003). Depending on the form of the fibroin, it can either meet or fail this criterion. Fibroin fibers, such as those used in sutures, will degrade in a longer time frame than when fibroin is in a film or membrane form. Arai et al. (2004) studied the effects of enzyme degradation of fibroin fibers and films using several different enzymes. They found that after incubating fibroin with enzymes for 17 days the reduction in initial weight

of the fibers was negligible, while for the films the weight reduction reached as much as 64%. On the other hand, for the tensile strength of the fibers the breaking load of the fiber was found to be reduced from 4.68 *N* for the control to 3.14 *N* for the fibers incubated with protease after 17 days, a reduction of approximately 33%. It was hypothesized that proteolytic degradation occurred in the films more readily than the fibers because the films are more amorphous and prone to swelling, allowing the enzymes greater access to cleavage sites.

Wang et al. (2008) has shown that the biodegradability of fibroin *in vivo* can be modified through the use of different processing methods and variables. Three-dimensional fibroin scaffolds were prepared using either an aqueous or organic solvent, with varying fibroin concentrations and scaffold pore sizes. The fibroin scaffolds were implanted in rats and their degradation was monitored for up to a year. The scaffolds prepared using an aqueous solvent were shown to degrade completely within 2-6 months, whereas the scaffolds prepared using an organic solvent all persisted for over one year. It was also found that the scaffolds prepared using high fibroin concentrations and small scaffold pore sizes degraded slowly. These results are important for both fibroin tissue engineering and controlled release. For tissue engineering, the fibroin scaffolds can be modified to degrade at slower or faster rates depending on the rate of the specific tissue growth, and for controlled release the fibroin can be modified to degrade at different rates depending on the length of time needed for drug delivery and release kinetics needed.

2.1.2 Biocompatibility of Fibroin

The concept of biocompatibility does not have a precise definition or even understanding as a great deal of research from a wide-range of disciplines is continuously changing what is

known about the concept. One commonly accepted definition of biocompatibility, known as the Williams definition, states that biocompatibility is "the ability of a material to perform with an appropriate host response in a specific application" (Williams, 1999). By this definition, the biocompatibility of a material is not an intrinsic material property, but dependent on the application and the host response. The host response covers a wide range of responses that the body will have to implanted foreign material. Some of these responses include inflammatory response, cell cytotoxicity of the material or the degradation products, enzymatic response, and thrombogenic response; these responses can either be localized or systemic to the whole body (Altman et al., 2003; Tang et al., 2009; Park et al., 2001). The host response may not be the same in different parts of the body, and so a material that may be biocompatible in one area for one application may not be biocompatible in another area for the same or a different application. General indicators of a biocompatible material are low and non-sustained inflammatory response, low cell toxicity, and low thrombosis formation. In order to determine the biocompatibility of a material, *in vitro* tests can be performed to see how the material interacts with various biomolecules and cells, followed by more comprehensive *in vivo* testing of animals and then humans.

Fibroin has long been used in medical applications in silk sutures. Although popular for a long time, silk sutures fell out of favour after research revealed high incidences of allergic response and sensitization to the sutures, as well as the introduction of synthetic materials with better biocompatibility. Altman et al. (2003) undertook a comprehensive review of the literature on this topic, and concluded that sericin contamination in the silk is the likely cause of the allergic response, and not the fibroin proteins. As a result, interest in fibroin as a biocompatible material in medical applications has greatly increased thereafter.

Inflammatory responses to biomaterials involve complex interactions between the biomaterial and a large number of immune system biomolecules and cells. A main trigger of inflammatory responses involves the activation of the immune system protein C3 on the surface of the biomaterial. After adhesion to the biomaterial, a disulphide bond in the C3 will be cleaved, and this will cause a cascade of adhesion of leukocytes (white blood cells) and macrophages to the material surface. Leukocytes and other inflammatory cells are also able to adhere directly to the biomaterial if certain chemical or physical interactions are present, as well as if proteins such as fibrinogen or the antibody IgG are adsorbed to the surface (Santin et al., 1999).

Santin et al. (1999) studied the *in vitro* inflammatory response of fibroin films and compared it to polystyrene and poly(2-hydroxyethyl methacrylate), and they found that the adhesion of fibrinogen to fibroin was lower, while the adhesion of C3 and IgG were comparable to the other surfaces. The activation of C3 on fibroin was also investigated, and no activation was detected. The adhesion of immune cells such as macrophages to the surface was also investigated, and fibroin was found to have significantly lower adhesion of these cells than the two other surfaces. These results indicate that fibroin has low inflammatory response, which is a good indicator of biocompatibility in a material.

Cytotoxicity is the toxicity of a material or chemical to the cells with which they make contact. Cytotoxic materials may cause a number of harmful effects on cells, including cell necrosis and eventual lysis, cell death or apoptosis, or a decrease in cell growth and viability. There are a number of ways to monitor the cytotoxicity of a material. Microscopy can be used to inspect cell morphology, and differences in the cell membrane and organelles can indicate cytotoxic effects. Cell growth and viability can be monitored using various techniques, and a reduced growth or a decrease in cell viability is an indication of cytotoxicity. Another way to

measure cytotoxicity is to look at the expression of biomolecules such as RNA or various proteins, and decreased levels of these biomolecules in the cell are indicative of cytotoxicity (Tang et al., 2009).

Tang and colleagues (2009) looked into the *in vitro* cytotoxicity of fibroin with hippocampal neurons. Extracts of fibroin and hippocampal neurons, as well as control extracts of hydroxyapatite with hippocampal neurons and organotin with hippocampal neurons were created and analyzed for cytotoxicity using several methods. The hydroxyapatite extract is the non-cytotoxic control and the organotin is the cytotoxic control. The morphology of the cells was characterized, and the fibroin extract cells displayed good morphology with no significant differences from the hydroxyapatite, and significant differences from the organotin. Cell viability was measured, and once again the fibroin cells displayed no difference from the hydroxyapatite, but significant differences from the lowered cell viability of the organotin. The expression of mRNA and other proteins associated with hippocampal neurons was determined, and once again the fibroin displayed no differences from the hydroxyapatite but significant differences from the organotin in the levels of these biomolecules. All these results indicate that fibroin is not cytotoxic to hippocampal neurons. Similar cytotoxicity work was done by Yang et al. (2007) with rat dorsal root ganglia and fibroin, and they concluded that fibroin does not display any cytotoxic effects on these cells. These results indicate that fibroin displays low cytotoxic effects on cells, and are a further indicator of the biocompatibility of fibroin.

Thrombosis is the formation of a blood clot through the aggregation of blood proteins such as platelets and fibrin. Thrombogenic response is an important reaction that prevents excessive blood loss when a blood vessel is cut or broken due to injuries. Without this response, even small cuts in the skin would result in continuous blood loss that could prove fatal if not

treated. A thrombus may also aggregate when a blood vessel is not injured, and if it grows too large it can restrict the flow of blood and oxygen downstream of the clot. A thrombosis that detaches from the vessel wall and travels through the body is known as an embolism, and can result in heart attack or stroke. The potential harmful effects of thrombosis make the thrombogenic response of a biomaterial that interacts with the blood a very important consideration. The process by which thrombosis occurs is complex and not completely understood. When a biomaterial first comes into contact with blood, plasma proteins adsorb at the polymer surface. The adsorbed proteins cause platelets to adhere to the surface, which causes a further cascade of platelet activation, aggregation, and fibrin polymerization (Pitt et al, 1986). A number of properties of the biomaterial influence thrombus formation, including surface properties such as smoothness, and various protein-polymer interactions such as charged functional groups and other electrostatic interactions, and hydrophobic or hydrophilic interactions (Park et al., 2001).

A number of studies have been conducted on the thrombogenic potential of silk fibroin. Dahlke et al. (1980) looked into the thromboginicity of black-braided silk sutures and several other materials. They found that the silk sutures induced a noticeable thrombic response within the first 7 days of post implantation, after which the thrombus gradually declined, and after 56 days only minimal thrombogenicity remained. Lee et al. (1998) studied the *in vitro* antithrombogenicity of silk fibroin and silk fibroin/s-carboxymethyl keratein (SCMK) blend films. The films were found to be relatively antithrombogenic, with lowest thrombus formation at 50/50 fibroin/SCMK blend. It was concluded that the blend films modified the polar surface free energy, which was caused by changes in the silk conformation from random coil to antiparallel β-sheet. The β-sheet conformation resulted in a heterogeneous structure and this

enhanced the films biocompatibility by increasing surface polar properties. Park et al. (2001) investigated both *in vitro* and *in vivo* thrombogenicity of silk fibroin films treated in methanol for differing periods of time. For films treated in methanol for 15 and 240 min, no thrombus formation *in vivo* was noticed in 1 and 14 days post implantation. For the film treated in formic acid, there was no thrombus formation after 1 day, but thrombus formation occured along the entire surface after 14 days. Longer methanol treatment times displayed greater transformation to a β-sheet structure and increased polar component to the film surface tension. As the treatment in increased, *in vitro* platelet adhesion increased. A discrepancy exists between the results of Lee et al. (1998) and Park et al. (2001), with the former showing decreasing thrombus formation with increasing β-sheet structure, and the later showing increasing platelet adhesion with increasing β-sheet structure. Both studies used IR crystallinity index to determine the extent of β-sheet conformation. The crystallinity index values in Lee et al. (1998) was 0.3-0.5, while the values in Park et al. (2001) was 0.575-0.675. This may suggest that there could be a value that minimizes thrombus formation between the two ranges. Other potential interpretations of the discrepancy include incompatible comparisons between the experimental procedures, or experimental error in one or both of the studies.

These studies indicate that silk fibroin generally has good antithrombogenic properties. Attention, however, should be paid to the form and conformation of silk fibroin, because any changes may result in have substantial differences on the formation of thrombus *in vivo*.

Fibroin displays good biodegradability, low inflammatory response, and good antithrombogenic properties. These features are essential for biocompatible materials, and it is expected that fibroin will be a strong candidate material for many biocompatible applications.

2.2 Bovine Serum Albumin Adsorption

As an initial assessment of the biocompatibility of the novel fibroin film, adsorption testing with bovine serum albumin was undertaken in this study. Serum albumins are one of the most common blood proteins, and they play an important role in the protein adsorption sequence that results in thrombus formation. The adsorption of the blood protein fibrinogen on a material surface will cause platelet adhesion and accumulation that result in thrombus formation. Platelets do not readily adhere to serum albumin, so the adsorption of albumin on a material surface will help to prevent thrombus formation. The adsorption of fibrinogen on a material surface has a negative correlation to the amount of albumin already adsorbed on the material. Albumin also diffuses to the surface of a material faster than fibrinogen, and so the ability of albumin to adsorb to a material surface and not be dislodged by fibrinogen molecules is of importance (Pitt et al., 1986). Kaelble and Moacanin (1977) have shown through surface energy analysis that the adsorption and retention of a plasma protein film allows for greater blood compatibility for a material. With the previous in mind, determining the adsorption capacity of BSA on the fibroin film will be an indicator of the thrombic potential and biocompatibility of the film.

2.2.1 Serum Albumin

Serum albumin is the most plentiful plasma protein in the blood of mammals, and serves a number of important functions. Albumin was identified as a major component of blood in 1839, and everything from its structure, to its functions, to its physical properties have been studied extensively since then. The main functions of albumin include the regulation of osmotic pressure in blood, transporter of fatty acids, sequestration and transportation of bilirubin, and the

maintenance of blood pH (Peters, 1975; Carter and Ho, 1994). Albumin performs many other smaller functions as well, and has the ability to reversibly bind with a very large number of different ligands.

Albumin levels in the blood are important to the overall health, with low albumin levels resulting in a number of negative effects. Typical albumin concentrations in blood are 5 g per 100 mL. Although rare, chronically lowered levels of albumin can result in hyperlipidemia and chronic fatigue (Carter and Ho, 1994). Albumin proteins are simple peptide chains that contain approximately 580 amino acids in the sequence. Albumin has a large number of the charged amino acids aspartic acid, glutamic acid, and lysine, leading to polarity in the molecule. It is also characterized by a large number of amino acids with hydrophobic side chains. While the tertiary structure of BSA has yet to be confirmed, evidence suggests it is a prolate ellipsoid with two axes of 40 Å and the third axis of 140 Å (Carter and Ho, 1994). Important physicochemical properties of albumin include small size, high solubility, a net negative charge, and many ligand binding affinities (Peters, 1975). Table 2-2 lists some properties for human and bovine albumins.

Table 2-2: Physicochemical properties of human and bovine albumins (Peters, 1975).

Property	Human Albumin	Bovine Albumin
Molecular Weight (Da)	66,248	66,210
Dimensions (Å)	38 x 150	40 x 140
Isoelectric Point	4.7	4.7
Net Charge at pH 7 per albumin molecule	-18	-18

Due to its physiological importance, abundance, ease of isolation, stability, and low cost, albumin has been used as a model protein in research. The adsorption of albumin on many different surfaces has been studied extensively. Table 2-3 summarizes some of the prior work on albumin adsorption.

Table 2-3: Adsorption capacity of BSA for various materials.

Membrane	Adsorption (μg/cm^2)	Reference
Poly(ethylene vinyl alcohol)	0.1 – 0.55	(Avramescu et al, 2003)
Silicone Rubber	0.16	(Young et al., 1998)
Poly(vinyl Chloride)	0.16	(Young et al., 1998)
Polyethylene	0.16	(Young et al., 1998)
Poly(ether urethane)	0.17	(Young et al., 1998)
Stainless Steel	0.21	(Van Enckenort et al., 1984)
Regenerated Cellulose	0.25	(Bornzin and Miller, 1982)

The adsorption of serum albumin on material surfaces and interfaces has long been shown to generally follow a Langmuir adsorption isotherm (Hitchcock, 1925). Langmuir isotherms are characterized by the adsorption of a monolayer at the surface, with the adsorption capacity increasing with increasing concentration until the monolayer covers the entire surface. Using the dimensions of the molecule adsorbed, a theoretical maximum adsorption capacity can be estimated for a monolayer. The theoretical maximum surface concentration for a monolayer of bovine serum albumin has been calculated as 0.25 $\mu g/cm^2$ (Bowen and Hughes, 1990). However, adsorption does not have to be limited to a monolayer in practice. Materials that are highly hydrophobic can have attractive forces that are strong enough to attract proteins over as far as 140 $\AA$ away from the material surface, which could potentially allow for a multilayer two

to three proteins in thickness (Kaelble and Moacanin, 1977). Multilayers may also occur through protein-protein interactions for the layers past the initial surface layer (Bornzin and Miller, 1982). It should be noted that a reported surface concentration greater than the theoretical maximum surface concentration does not necessarily indicate a protein multilayer, instead surface roughness may create a larger surface area on the microscopic level that is not accounted for in the observed surface area.

2.2.2 Protein Adsorption

Adsorption occurs when components of a fluid phase in contact with a solid phase are transferred to and held by interactions with the surface of the solid. Adsorption of molecules to surfaces is mainly governed by two types of forces, van der Waals forces and electrostatic forces. For non-polar surfaces and molecules, adsorption is governed by instantaneously induced dipoles, typically known as London dispersion forces. When the surface is polar and the molecule is non-polar, the electric field on the surface can induce a dipole in the molecules that enhances their attraction. A molecule with a permanent dipole can similarly polarize a surface and increase the adsorption. Strong adsorption can also result when the surface and the molecule are both permanently polarized (LeVan et al., 1999). Proteins contain many different charged and polar amino acids, and this leaves many areas of the molecules permanently polar and often gives the molecule a net charge. The primary amino acid structure of a protein is not the only consideration with respect to adsorption, as the secondary and the folded or tertiary structures will determine whether the polar regions are exposed to the surface or tucked away in the centre of the folded protein.

Silk has long been considered a material of interest for adsorption purposes. Linus Pauling (1945) studied the adsorption of water onto the surface of silk, and found that the number of water molecules adsorbed corresponded to the number of polar side chains in the protein. Since then the adsorption capabilities of silk fibroin have been investigated for a wide range of applications, including heavy metal removal, protein adsorption in food production, and fibroblasts for tissue engineering (Zhao et al, 2011; Baycin et al., 2007; Yamada et al., 2004). With a main repeating structure consisting of glycine, serine, and alanine, fibroin does not contain any charged amino acids to make the surface charged. Serine is considered an amino acid with a polar side chain, alanine is considered to have a hydrophobic side chain, and glycine can be either hydrophobic or hydrophilic (Voet and Voet, 2004). The adsorption behaviour of fibroin should therefore be composed mainly of hydrophobic and polar interactions.

For proteins interacting with a biomaterial surface, the affinity between the protein and the surface can be represented by an adsorption constant. There are two adsorption isotherms that protein adsorption data generally fit, the Langmuir and Freundlich isotherms (Young et al., 1988).

The Langmuir isotherm assumes adsorption occurs in a monolayer on a homogeneous flat surface (LeVan et al., 1999). The Langmuir isotherm is given by Eqn (2-1):

$$C_s = \frac{M}{AN_A}\left(\frac{KC_b}{1+KC_b}\right) \tag{2-1}$$

where, C_S is the mass of protein adsorbed per unit area, C_b is the bulk protein concentration in the solution, M is the molecular weight of the protein, K and A are adsorption constants, and N_A is the Avogadro's number.

When C_S is plotted against C_b, the Langmuir isotherm predicts that C_S will continuously increase with increasing bulk protein concentration, until a plateau is reached when C_S reaches the monolayer surface concentration. In Figure 2-1, the strongly favourable isotherm represents the behaviour of the Langmuir isotherm.

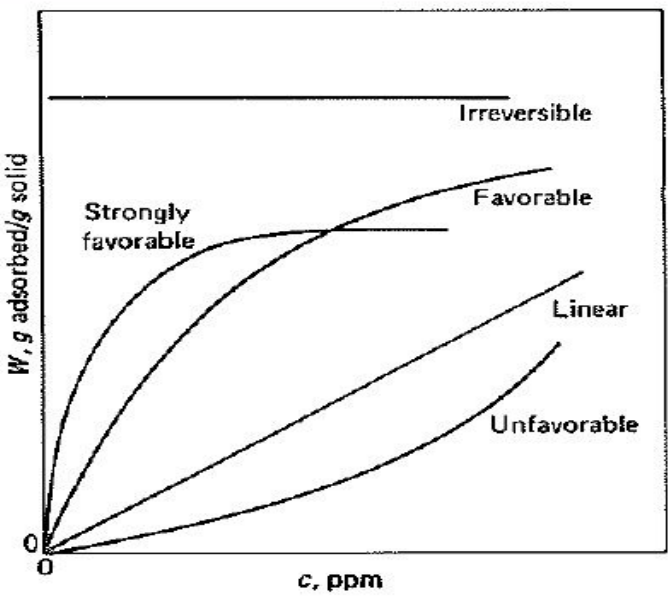

Figure 2-1: Adsorption isotherms (McCabe et al., 1993)

Although in many cases the adsorption of proteins on surfaces does not meet the assumptions behind the Langmuir isotherm, it has been found that the Langmuir isotherm still fits well. However, since the underlying assumptions are not met, the meaning behind the parameters *A* and *K* are questionable for these cases (Young et al., 1988).

The Langmuir isotherm is often used in a linearized form for data fitting.

$$\frac{1}{C_S} = \frac{AN_A}{M} + \frac{AN_A}{M}\frac{1}{KC_b} \tag{2-2}$$

If the sorption data follows the Langmuir isotherm, a plot of $1/C_S$ against $1/C_b$ should yield a straight line, from which the constants *A* and *K* can be determined from its slope and intercept.

The Freundlich isotherm is an empirical adsorption isotherm that can fit protein adsorption data. The Freundlich isotherm, also assuming adsorption occurs on a homogeneous flat surface, is given by Eqn (2-3):

$$C_s = aC_b^{1/n} \tag{2-3}$$

where *a* is a constant that's a measure of the adsorption capacity, and *1/n* is a measures the intensity of adsorption (Young et al., 1988). When C_s is plotted against C_b, the resulting isotherm will be similar to the 'favorable' isotherm in Figure 2-1. A linearized version of the Freundlich isotherm is also widely used for data fitting. The linearized form is given by Eqn (2-4):

$$\log C_S = \log a + \frac{1}{n}\log C_b \tag{2-4}$$

If the adsorption data follows the Freundlich isotherm, a plot of $log(C_S)$ against $log(C_b)$ should yield a straight line from which the constants *a* and *1/n* can be calculated.

In static sorption tests, the amount of protein adsorbed onto the membrane can be calculated based on mass balance from the difference in solution concentration that varies from the initial concentration to the equilibrium concentration.

$$m_{eq} = (C_o - C_{eq}) \cdot V_o \tag{2-5}$$

where m_{eq} is the mass of protein adsorbed on the surface, C_o is the initial protein concentration of the solution, C_{eq} is the protein concentration at equilibrium, and V_o is the volume of the solution, which remains constant over the course of the adsorption.

A useful way to compare adsorption behaviour between membranes is to normalize the quantity adsorbed by either the mass or area of the membrane used. This will provide insight on whether the adsorption occurs on the surface only. For instance, using:

$$q = \frac{m_{eq}}{A} \tag{2-6}$$

where q is the equilibrium adsorption capacity, and A is the membrane area, one will be able to compare the adsorption amount per surface area. For films of same material but with different thicknesses, the area normalized sorption uptake can also reveal whether any protein molecules will penetrate to reach the interior of the film.

2.3 Gas Permeability

2.3.1 Contact Lenses and Wound Dressings

The recent findings on the biocompatibility and biodegradability of fibroin have increased interest for fibroin as a biomedical material. Two growing areas of interest for fibroin are (1) as a material in contact lenses, and (2) for use in wound dressings. Both applications require biocompatibility but also oxygen permeability (Sashina et al., 2009; Min et al., 2012). The permeability of oxygen and other atmospheric gases through the silk fibroin membrane was to be examined in this study to determine the potential of fibroin films as a material for contact lenses and wound dressings.

The permeability of oxygen through contact lenses is of utmost importance for ocular health and comfort. Insufficient oxygen permeability in a contact lens can cause corneal edema. Corneal edema is caused when cells that normally remove fluid from the eye are damaged, resulting in corneal swelling and progressively cloudier vision (Wu, 2012). Holden and Mertz (1984) showed that if contact lenses have a high enough oxygen permeability, the residual ocular swelling after a nighttime sleeping with the lenses is no greater than sleeping without the lenses.

A wound dressing is a material placed over a wound to aid in healing and to help prevent infection. Successful wound dressings will control the moisture content of the wound to allow the transport of epithelial cells around the wound, prevent infection by acting as a barrier to bacteria, and absorb blood and other excess fluids from the healing process (Syzcher and Lee, 1992). Wounds are healed in four main phases: inflammation, migration, proliferation, and maturation. During the inflammation phase, blood clots form over the wound, bacteria and debris start to be cleared away from the wound, and blood vessels dilate to increase blood flow. During migration, macrophages move about the wound clearing damaged tissue and other materials, and this movement starts fibroblast formation and collagen synthesis. The proliferation stage sees collagen form into structural strands and epithelial cells will migrate to and form tissue on these strands, closing the wound. The last stage continues with tissue repair, as well as increasing vascularity to the healed tissue (Syzcher and Lee, 1992). Oxygen plays a very important part in the wound healing process, and as such an important property of a wound dressing is adequate oxygen permeability to the site of the wound. The major role of oxygen at the site of a wound is to control the growth of anaerobic bacteria and reduce the risk of infection, as well as decreasing tissue necrosis. Many of the cells and processes in the wound healing process require oxygen,

and there are some evidences that suggest increased exposure to oxygen at the wound site helps to oxygenate wound tissue and aids healing (Rodriguez et al., 2008).

There is considerable interest in fibroin as a material in wound dressings for not only its biocompatibility but also because the material itself has been found to enhance wound healing. Human skin fibroblasts, an essential part of the wound healing process, are able to attach to and grow on fibroin fibers to a level that is comparable to or even greater than that of collagen (Minoura et al., 1995). Yamada et al. (2004) used a proteolytic enzyme to digest fibroin and examined fibroblast adhesion and proliferation of the resulting peptide fragments. They found that two N-terminal region peptides are mainly responsible for increased fibroin growth, and the two peptides have a synergistic effect when they are together, further increasing fibroblast growth more than the individual peptides. Fibroin has also been shown to aid in the adhesion and growth of human keratinocytes, a skin cell responsible for reepitheliazation of wounds (Min et al., 2004). The adherence and growth of both fibroblasts and keratinocytes on fibroin should aid in the healing and healing time for wounds when used as a wound dressing. Roh et al. (2006) examined the healing capabilities of silk fibroin, alginate, and silk fibroin/alginate (SF/AA) blend sponges. These sponges as well as a gauze control were subjected to circular wounds surgically induced in rats, and the extent of regenerated epithelium, collagen deposition, and cell proliferation were examined. It was shown that these sponges significantly decreased wound healing time (by approximately 50%), increased collagen deposition, and increased cell proliferation compared to the gauze control. The SF/AA sponge also displayed slightly better healing capabilities than individual silk fibroin or alginate sponges. Min et al. (2012) showed that a silk fibroin sponge dressing impregnated with nano-Ag displayed impressive wound healing

capabilities and antibacterial activity, resulting in a decreased healing time of wounds as well as allowing for proliferation of a normal epidermal layer over the wound.

2.3.2 Gas Permeation

Mass transfer across a membrane will occur if there is a driving force that acts on one or more components of the systems. The driving forces may be the chemical potential gradients across the membrane caused by differences in pressure, concentration, temperature, and electrical potential. The movement of a component *i* caused by a gradient in chemical potential is described by Eqn (2-7) (Baker, 2004):

$$J_i = -L_i \frac{d\mu_i}{dx} \tag{2-7}$$

where J_i is the flux of component *i*, $d\mu_i/dx$ is the chemical potential gradient of component *i*, and L_i is a proportionality coefficient between the flux and chemical potential gradient.

The chemical potential is expressed by Eqn (2-8).

$$d\mu_i = RTd\ln(\gamma_i x_i) + \upsilon_i dp \tag{2-8}$$

where R is the gas constant, T is temperature, γ_i is the activity coefficient, x_i is the mole fraction of component *i*, υ_i is the molar volume of component *i*, and p is the pressure. Assuming ideal gas behaviour, Eqn (2-8) can be integrated to give Eqn (2-9).

$$\mu_i = u_i^{\circ} + RT\ln(\gamma_i x_i) + RT\ln p \tag{2-9}$$

where u_i° is the chemical potential of pure component *i* at the standard state.

Gas permeation through a film may be governed by two different mechanisms depending on the pore size of the film. Permeation through porous films may be described by the pore-flow model, while permeation in non-porous films is governed by the solution-diffusion model. When the pores in a film are large enough, a driving force will cause convective transfer of the gas molecules through the film. For dense films a solution-diffusion mechanism will be responsible for permeation, which is considered to take place in the following steps (Baker, 2004):

1. Gas molecules travel from bulk to the material surface.
2. Gas molecules adsorb and dissolve within the material.
3. A concentration gradient across the material will cause the diffusion of the molecules from the high concentration side to the low concentration side.
4. The gas molecules are desorbed on the low concentration side.
5. The gas molecules travel from the surface to the bulk on the downstream side of the film.

Based on this mechanism, gas transport through a material is influenced by gas solubility and diffusivity within the membrane. Based on the Fick's law of diffusion, the following equation can be derived (Wijmans and Baker, 1995):

$$J_i = \frac{D_i(c_{i_{o(m)}} - c_{i_{l(m)}})}{l} \tag{2-10}$$

where $c_{i,o(m)}$ is the concentration within the membrane at $x = 0$, $c_{i,l(m)}$ is the concentration within the membrane at $x = l$, l is the membrane thickness, and D_i is the diffusivity coefficient of component i.

The concentration of a gas within the film is related to the gas pressure, and based on Henry's law:

$$c_{i_{x(m)}} = S_i \cdot p_{ix} \tag{2-11}$$

where S_i is the sorption or solubility coefficient of the gas in the film.

Substituting Eqn (2-11) into Eqn (2-10) gives:

$$J_i = \frac{P_i^G (p_{i_o} - p_{i_l})}{l} \tag{2-12}$$

where $P_i^G = D_i S_i$ is the permeability coefficient of the gas in the film. Eqn (2-12) allows the calculation of the permeability coefficient of a film with knowledge of the flux at a certain applied pressure and film thickness. The permeability coefficient indicates the capacity of a material to permeating gas, and it is useful when comparing gas permeabilities in different materials with different film thicknesses.

2.3.3 Oxygen Permeability

Sufficient oxygen permeability is a requirement in contact lenses to prevent corneal edema, and in wound dressings to prevent the growth of anaerobic bacteria and aid in the healing process. For extended wear of contact lenses, the minimum oxygen transmissibility required to avoid corneal edema during overnight wear is 87.0 x 10^{-9} *(cm·mL O_2)/(s·mL·mmHg)* (Holden and Mertz, 1984). Oxygen transmissibility is equal to the oxygen permeability divided by the film thickness, and it is essentially the same as the so called permeance conventionally used in membrane separation. For wound dressings, the critical oxygen permeability values are not

available; however, based on the evidence for antibacterial and enhanced healing properties of oxygen at the wound site, a high oxygen permeability in wound dressings is desirable.

For regenerated fibroin films, the processing method will have an effect on the resulting polymer matrix and the resulting properties of the film. Treatment of fibroin films with methanol induces a change in the polymer matrix from an amorphous to a more crystalline structure dominated by anti-parallel β-sheets (Motta et al., 2002). Also it has been shown that the gas permeability of a material (e.g., oxygen, nitrogen, carbon dioxide permeability) changes as the material undergoes a structural change (Yasuda and Hirotsu, 1977). It is therefore important to examine the oxygen permeability of the fibroin films prepared using different methods, because differences in the structure or morphology of the polymer matrix will affect the gas permeability.

There are a few studies on the oxygen permeability of regenerated fibroin films. Minoura et al. (1990), who examined the dissolved oxygen permeability of silk fibroin films of varying crystallinities using an oxygen electrode, found that as the crystallinity of the film increased, the oxygen permeability decreased. At 20°*C*, the oxygen permeability ranged from 4-8 *Barrer* depending on the crystallinity of the film. Kweon et al. (2001) evaluated the dissolved oxygen permeability of silk fibroin/chitosan blend films, and they found that the oxygen permeability increased as the chitosan content in the film increased up to a maximum at 50/50 fibroin/chitosan, and then slightly decreased with a further increase in the chitosan content. The permeabilities of the pure fibroin and pure chitosan films were found to be 0.249 and 0.395 *Barrer* respectively, while the 50/50 fibroin/chitosan film was 0.579 *Barrer*.

Besides oxygen, the permeability of the fibroin film to the components of atmospheric air (i.e. N_2 and CO_2) is also of importance. The separation of oxygen and nitrogen from atmospheric

air and the removal of carbon dioxide from flue gases via membrane separation are receiving increased attention as alternatives to conventional separation methods. Oxygen/nitrogen gas separation is an energy intensive process typically involving cryogenic distillation. Membrane gas separation is typically an energy efficient and low operational cost process, and represents a potential alternative to cryogenic distillation for the separation of oxygen and nitrogen. Concerns over industrial greenhouse gas emissions, especially from fossil fuel based power generation, has made the separation and capture of carbon dioxide a top priority. Gas scrubbers using regenerated amine solutions are typically used for carbon dioxide separation, but membrane separation is a promising alternative (Liu, C. et al., 2005). To compete with traditional technologies, gas separation membranes must display high permeability and selectivity for the target gas.

2.4 Controlled Release

The concept of controlled drug delivery was first recognized in the 1960s by Folkman when he noticed that rabbits fell asleep when a tubing circulating their blood was exposed to anaesthetic gases on the outside. This gave him an idea that a closed off tubing containing a drug could be implanted and would deliver the drug at a constant rate (Hoffman, 2008). Since then interest in controlled drug delivery has grown considerably in an attempt to solve some of the general dose-delivery problems present in traditional methods of drug delivery. One of the major problems solved by controlled release is that of the drug concentration within the body. With pills or injections, the drug concentration within the body will quickly increase after ingestion, followed by a decline as the body metabolizes or excretes the drug. If the drugs are toxic, the

initial spike in concentration can create risks to the patient. If the drug has a minimum therapeutic concentration, once the concentration drops below this level the treatment will no longer be effective and the rest of the drug within the body is wasted. Once the drug concentration is below this level, readministration is needed, starting the cycle over again. Controlled release aims to eliminate this problem by providing a more steady rate of drug release into the body within the therapeutic window (Langer and Peppas, 1981).

One popular method to provide a sustained release of drugs within the body is slowly releasing capsules. The capsules may operate on a number of methods, including slowly dissolving coatings, or complexing the drug with other molecules to lower its solubility. While these methods have proven successful, they still suffer from a number of problems such as high patient-to-patient variability in release rates and the constant need for readministration (Langer and Peppas, 1981). Controlled drug release is expected to reduce this variability and to provide a longer time frame for drug release.

There are many advantages with controlled release systems including (Langer and Peppas, 1981):

1) Drug concentrations are maintained in a therapeutically effective range.
2) Local administration of a drug and reduce harmful effects present in systemic administration.
3) Drugs rapidly degraded *in vivo* are protected from degradation.
4) Smaller, continuous doses may reduce side effects and patient discomfort.
5) Fewer administrations should improve patient compliance
6) Less wasteful of drugs and potentially more cost effective.

7) Long operating times, from days up to years.

However, some potential disadvantages are present in these systems as well:

1) Cytotoxicity or lack of biocompatibility for the material used or its degradation products.
2) Surgical operations for implanting the system or removing a non-degradable system.
3) Pain or discomfort from the implanted system.
4) Potentially expensive material and manufacturing costs.
5) Potential for leaks or system degradation resulting in large amounts of drug release.
6) Drug release hard to stop should the need arise.

The use of polymers in controlled release applications is now of great interest. In polymer systems, the rate of drug release is controlled by the release of the drug from the polymer, which can be manipulated through different polymers, configurations, and polymer-drug preparation procedures. To combat the potential problems of toxicity, lack of biocompatibility, and lack of biodegradability, biopolymers such as silk fibroin are of significant interest in controlled release applications.

In polymeric systems, drug release may occur through different mechanisms. There are five common release mechanisms, diffusion controlled, chemically controlled, swelling controlled, osmosis controlled, and magnetically controlled. Diffusion controlled systems are the most widely used, and they rely on the drug diffusion out of either a polymer surrounded reservoir, known as membrane permeation controlled (MPC), or a polymer matrix, known as matrix diffusion controlled (MDC), to control the drug release (Jain et al., 2003). In chemically controlled systems, the drug is either distributed bound or unbound within the polymer matrix and degradation of the polymer matrix and the biodegradation of the polymer to control the drug

release. In swelling controlled systems, water penetrates a solid polymer matrix infused drug molecules, allowing a transition from a glassy to amorphous state, which lets the drug diffuse out of the matrix. Magnetically controlled systems have both drug molecules and magnetic beads dispersed in a polymer matrix, and upon exposure to an oscillating magnetic field will greatly increase the rate at which the drug is released from the matrix (Langer and Peppas, 1981).

2.4.1 Fibroin and Controlled Release

Natural biopolymers tend to show both biocompatibility and biodegradability which are advantageous in controlled release systems. However, the material properties of many biopolymers cannot be modified sufficiently for most controlled release applications. For a material to be successful in implantable controlled release applications, it must possess a number of important material properties. The material must not only be biocompatible, it should also be biodegradable with no harmful degradation products. The biodegradability should be controllable. In addition, the material should have a compatibility with the drugs or biomolecules being delivered, and display controllable release kinetics (Pritchard and Kaplan, 2011). Silk fibroin appears to display all these properties, which makes it an ideal biopolymer for controlled release applications. Silk fibroin fibers and films display excellent biocompatibility and have unique and impressive mechanical properties (Altman et al., 2003). The mechanical properties of regenerated silk fibroin films can be modified by changing the crystallinity (Motta et al., 2002). Silk fibroin is biodegradable *in vivo*, has harmless degradation products of amino acids and small peptides, and the rate of biodegradation can be controlled from days to years through modification of the β-sheet crystallinity, processing solvent, silk concentration, and porosity (Lucas et al., 1957; Horan et al., 2005; Wang et al., 2005; Pritchard and Kaplan, 2011). Fibroin films and matrices are able to encapsulate and stabilize proteins and enzymes through

intermolecular forces between the silk and biomolecules, then release the proteins undenatured and the enzymes with full activity (Lu et al., 2010). Silk fibroin can be processed and used in drug release in many different formats, including unprocessed fibers, films, nanolayers, hydrogels, sponges, and microspheres (Pritchard and Kaplan, 2011). The mass transfer and release kinetics within regenerated fibroin materials can be modified by changing the β-sheet crystalline content (Karve et al., 2011). Drug diffusion within the fibroin can also be controlled by the polymer morphology and other properties such as molecular mass (Pritchard and Kaplan, 2011). The drug release kinetics can also be modified by changing the degradation behaviour via the above mentioned, or through the co-release of proteinase inhibitors such as ethylenediamine tetraacetic acid along with the target drug to disrupt proteolytic activity (Pritchard et al., 2011).

One of the oldest uses for silk fibers was in medical sutures. Choi et al. (2004) showed that it is possible to enhance fibroin sutures using controlled release to create an infection resistant suture. Degummed silk fibroin was hydrolyzed, then two antibiotics, doxycycline and ciprofloxacin, were applied to the fibroin. The treated fibroin showed zones of inhibition of bacterial activity several centimeters in diameter for at least 24 hours in blood-flow simulated conditions. These results indicate the possibility of short-term infection resistant sutures, or even long-term infection resistant sutures that release antibiotics as the sutures degrade *in vivo*.

Regenerated fibroin films have been investigated for controlled release using both matrix diffusion controlled and membrane permeation controlled systems. In MDC systems, the drug is added to the fibroin solution before the film is cast, and this provides a uniform distribution of the drug within the film matrix. Liu et al. (2009) loaded the anticoagulant drug heparin into a polyurethane/silk fibroin blend membrane and examined the effects of film thickness, drug loading, and composition on the release kinetics. A longer sustained release of heparin occurred

when membrane thickness was greater, when drug loading was higher, and for films with higher fibroin contents. For MPC systems, there has been research using both conventional films and nano-film coatings to surround the drug reservoir. Chen et al. (1994) examined the permeability of a conventional fibroin film between two liquid reservoirs to five model drugs. The fibroin membrane was found to be an amphoteric ion exchange membrane, and would exclude one positively charged drug, while negatively charged drugs would have their permeability decrease with increasing pH, and the permeability of neutral drugs was independent of pH. The tendency for silk fibroin to form strongly interacting β-sheets allows for it to be deposited in a novel layer-by-layer nano-coating. This coating method can be utilized for controlled release applications. Wang et al. (2007a) coated several drugs and proteins with a silk nanolayer and examined the release kinetics *in vitro*. The coatings displayed excellent mechanical properties for the application, and the release kinetics could be modified by controlling the β-sheet crystallinity of the coating as well as the coating thickness.

Fibroin hydrogels have also been created for controlled release applications. Hydrogels are a network of linked polymer chains that swell considerably when water is introduced, and have the ability to retain water in the polymer matrix. Fang et al. (2006) impregnated a fibroin hydrogel with the morphine-like opioid buprenorphine and examined the release behaviour. They found that the hydrogels followed a zero-order release rate, and the release could be controlled by changing the fibroin concentration. It was also noted that polymer drug solution can be injected and form stable hydrogel matrices once inside the body.

Silk nano and microparticles have received considerable attention for drug release applications. These particles range in size from tens of *nm* to hundreds of μm in diameter. These particles can be loaded with drugs or other biomolecules and release within the body. There are a

number of methods used to prepare these particles, including emulsions, self-assembly, ionic gelation, spray drying, laminar jet, and PVA-silk casting and dissolution (Pritchard and Kaplan, 2011; Chen et al., 2012). Yan et al. (2009) synthesized silk nano-particles 40-120 *nm* in diameter and cross-linked the particles with insulin. The silk/insulin particles showed greater *in vitro* resistance to digestion and increased stability in human serum, resulting in an increase in the half-life by 2.5 times that of normal insulin. Chen et al. (2012) prepared silk nanoparticles 200-500 *nm* in diameter containing the anti-cancer drug Paclitaxel under mild conditions. Under some of the conditions tested, the nanoparticles released Paclitaxel for periods ranging from 9 days to 2 weeks, indicating the potential for use in targeted cancer therapy. Wang et al. (2007b) encapsulated the model enzyme horseradish peroxidase within silk microspheres. The enzyme retained its activity during processing and release, while the kinetics of the release could be controlled by processing conditions such as exposure to NaCl and MeOH. One of the major difficulties with silk nano-particles and microspheres is the high surface area to volume ratio of small particles. This high ratio leads to greater degradation rates compared to other drug delivery methods, but further research is being performed to improve degradation performance (Pritchard and Kaplan, 2011).

2.4.2 Membrane Permeation Controlled Diffusion

Reservoir systems in which diffusion through a membrane or film controls drug release have received much attention for their simplicity and their ability to achieve zero-order release kinetics. Zero-order systems are critical in controlled release applications because they provide a steady rate of release that does not change with time (Langer and Peppas, 1981). This steady rate

of release allows these reservoir systems to be designed to provide relatively constant drug levels in the body that are within their therapeutic windows.

Drug diffusion through a membrane follows three stages, as shown in Figure 2-2.

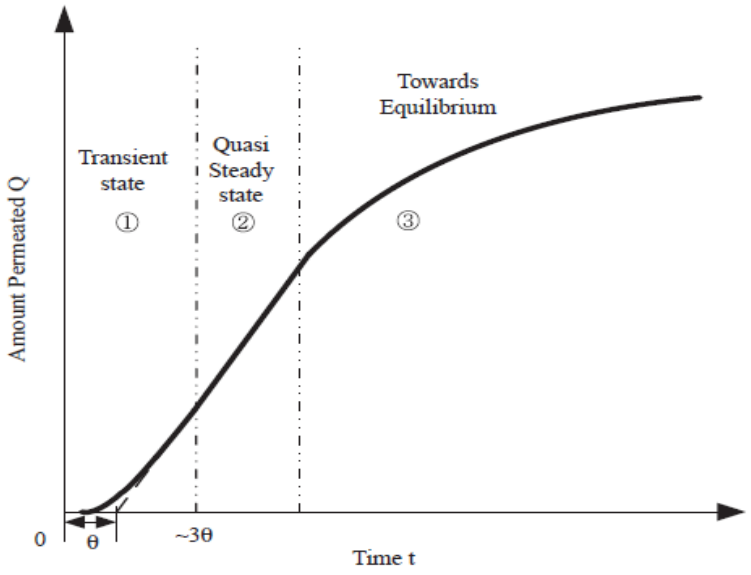

Figure 2-2: Three stages of drug permeation through a membrane (Chen et al., 2010).

The first stage is marked by an initial transient period in which the drug concentration profile within the membrane is established, which results in a "time-lag" (θ) in the permeation. The time lag is found from extrapolation of the pseudo-steady state data to the time axis. The time lag can be used to determine the start of the second phase, as the effects of the transient period can be considered to have diminished after three times the time lag (3θ). The second phase is pseudo-steady-state permeation during which period of time the concentration gradient across the membrane is relatively constant. In the third and final stage, the permeation slowly decreases with time as the concentration on the donor side depletes or on the receptor side increases to the point that the concentration gradient decreases and eventually reaches zero. The second phase of

pseudo-steady-state permeation provides the desired zero-order kinetics (Chen et al., 2010). The pseudo-steady-state phase can be extended through several techniques, including loading solid drug in the reservoir past its solubility limit to maintain a constant reservoir concentration (Langer and Peppas, 1981).

The diffusion of a drug through the membrane can be described by Fick's law,

$$J_i = -D_{im}\frac{dC_i}{dx} \tag{2-13}$$

where J_i is the drug flux through the membrane, D_{im} is the diffusion coefficient in the membrane, and dC_i/dx is the concentration gradient across the membrane. When the diffusion coefficient is independent of concentration and the membrane thickness is constant, Eqn (2-13) can be integrated to give Eqn (2-14) (Langer and Peppas, 1981).

$$J_i = -D_{im}\frac{\Delta C}{l} \tag{2-14}$$

where l is the membrane thickness. This equation shows that, as briefly discussed earlier, a constant flux will result from a constant concentration gradient across the membrane. A nearly constant concentration gradient can be obtained by keeping the donor side concentration much higher than the receptor side concentration.

Successful controlled release reservoir systems rely upon the knowledge of drug and membrane parameters such as permeability and diffusivity to tailor the controlled release system to the needs of the patient. One of the most widely used methods to determine a drug permeability coefficient within a membrane is known as the "mass balance" method. This method utilizes a mass balance on drug permeation data between the donor and receptor

reservoirs that are separated by the membrane (Chen et al., 2010). If the initial receptor drug concentration was zero, a mass balance between the two reservoirs yields Eqn (2-15).

$$V_D(C_O - C_D) = V_R C_R \tag{2-15}$$

where V_D is the volume of the donor reservoir, V_R is the volume of the receiving reservoir, C_o is the initial donor reservoir concentration, C_D is the current donor reservoir concentration, and C_R is the receiving reservoir concentration.

Eqn (2-16) gives the rate of permeation through the membrane,

$$V_R \frac{dC_R}{dt} = \frac{PA}{l}(C_D - C_R) \tag{2-16}$$

where *A* is the membrane area, and *P* is the permeability coefficient. Integrating Eqn (2-16) from *t=0* to *t=t* yields,

$$-\ln\left(\frac{m_o - V_t C_R}{m_o}\right) = \frac{PA}{l}\left(\frac{1}{V_D} + \frac{1}{V_R}\right)t \tag{2-17}$$

where m_o $(=V_D C_o)$ is the total amount of drug in the system, and V_t is the total system volume. Plotting the logarithmic term against time should yield a straight line from the slope of which the permeability coefficient can be found.

The mass balance method makes several assumptions: (1) the quantity of permeant within the membrane is negligible, and (2) the permeant is transferred through the membrane immediately from the donor side to the receiver side. These assumptions neglect the initial transient phase during which the concentration profile within the membrane is established. It is therefore important to use only the permeation data after the pseudo-steady-state phase has been established, otherwise the inclusion of the transient phase data will cause underestimation of the

permeability coefficient (Chen et al., 2010). Figure 2-3 illustrates the extent the inclusion of the transient phase will alter the slope and permeability coefficient.

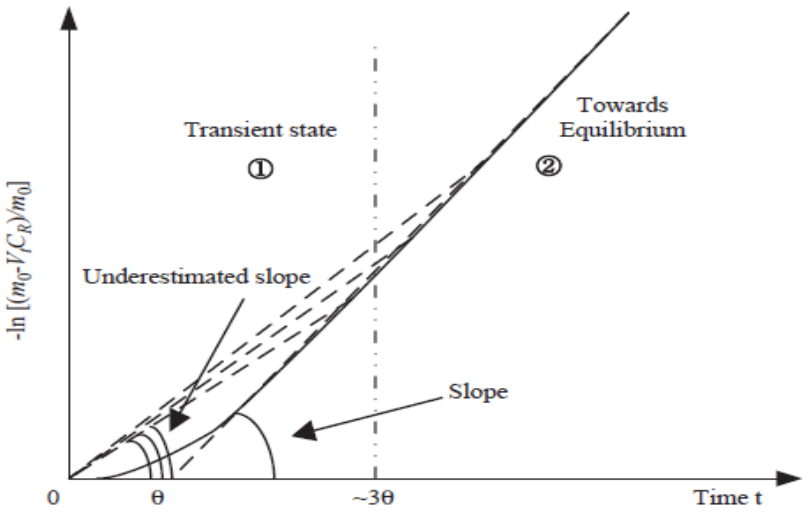

Figure 2-3: Extent of underestimation of permeability by the inclusion of the transient period (Chen et al., 2010).

While the mass balance method is able to give an accurate estimation of the permeability coefficient, another approach is needed to estimate the drug diffusivity within the membrane. One method to determine diffusivity coefficients of drugs within the membrane is to use sorption and desorption kinetics for the drugs.

For the sorption and desorption of solutes on a flat sheet in which the solution concentration changes, Crank (1975) shows an equation to estimate the diffusion coefficient:

$$\frac{M_t}{M_\infty} = 1 - \sum_{n=1}^{\infty} \frac{2\alpha(1+\alpha)}{1+\alpha+\alpha^2 q_n^2} \exp\left(-\frac{4Dq_n^2 t}{l^2}\right) \quad (2\text{-}18)$$

Where D is the diffusivity coefficient, M_t is the amount sorbed into the sheet at time t, M_∞ is the amount sorbed at equilibrium, α is ratio of the volumes of the solution and the sheet, and q_n's are the non-zero positive roots of Eqn (2-19).

$$\tan q_n = -\alpha q_n \tag{2-19}$$

To obtain the diffusivity coefficient using Eqn (2-19), non-linear regression can be used to fit the model to experimental data. D can be determined by minimizing the squared errors between the model predicted and experimental values of (M_t/M_∞).

Chapter 3: **Experimental**

3.1 Film Preparation

Bombyx mori silkworm cocoons were cut into small fragments, and washed in water to remove dirt and impurities. The cocoon fragments were degummed in deionized water at 95°*C* until all sericin was completely removed and only fibroin fibers remained. The fibroin fibers were placed in an oven at 50°*C* for three hours to remove excess water. 25 *g* of fibroin fibers were then completely dissolved in 100 *mL* of 9.5 *M* lithium bromide solution heated in a water bath to 90°*C*. The fibroin-LiBr solution was filtered to remove any residual particles. Approximately 5 *mL* of the filtered solution was then dripped slowly into 150 *mL* of well stirred ethanol, and this was repeated with fresh ethanol until the fibroin-LiBr solution was consumed. When dropped into the ethanol, the fibroin precipitates out into small particles, while the LiBr stays in solution. The fibroin particles were removed from the ethanol by filtration, and repeatedly washed in deionized water to remove any leftover lithium bromide. After all the LiBr had been removed, the fibroin particles were dried in an oven at 50°*C*. The dried fibroin particles were then dissolved in a well-stirred solution of 98% formic acid. The fibroin-formic acid solution containing 13-wt% fibroin was then cast in a petri dish, followed by evaporation of the solvent, leaving the fibroin film. The film thickness was controlled from film to film by coating the same mass of fibroin-formic acid solution for each film. After evaporation, the fibroin film was placed in deionized water to remove any residual solvent. Then the fibroin films were removed from the petri dish and stored in deionized water until use. To our knowledge, this is a novel method to prepare fibroin films without using the extremely time consuming dialysis process to remove the lithium salt from the fibroin.

The fibroin film so formed was dense and homogeneous, with no pore network capable of convective mass transfer through the film. The film thickness was measured with a micrometer. The thickness of the water wet films were in the range of 25-50 μm. The films were flexible and they displayed good strength when swollen in water, but extremely brittle when completely dried of all water.

3.2 Bovine Serum Albumin Adsorption

Batch adsorption experiments were performed with the prepared films using bovine serum albumin to examine the biocompatibility of the fibroin film. The bovine serum albumin was purchased from Sigma Aldrich Co. Ltd. Pieces of fibroin film were placed in 5 mL BSA solutions of initial concentrations ranging from 0.25 – 10 *mg/mL*, and left for 24 hours for equilibrium to be reached. The concentration of the initial solution and solution at equilibrium were measured using a Shimadzu UVmini-1240 UV-Vis Spectrophotometer at a wavelength of 285 nm. BSA calibration curves were created at 285 *nm* to relate the absorbance of the solution to BSA concentration. For each sample the film mass was recorded after drying the films for 1 hour to remove all water. The equilibrium BSA sorption uptake in the film was determined from the change in solution concentration and the film mass:

$$m_{eq} = V_o C_o - V_f C_{eq} \tag{3-1}$$

where C_o amd V_o are the initial BSA concentration and solution volume, respectively, V_f is the final volume of the solution, and m_{eq} is the equilibrium uptake at a concentration C_{eq}.

3.3 Gas Permeability

Gas permeation experiments were performed using the prepared fibroin films. The pure-gas permeability of oxygen, nitrogen, and carbon dioxide were measured at room temperatures at pressures ranging from 70 to 350 *kPa*g. The permeation experiments were performed using an apparatus shown in Figure 3-1.

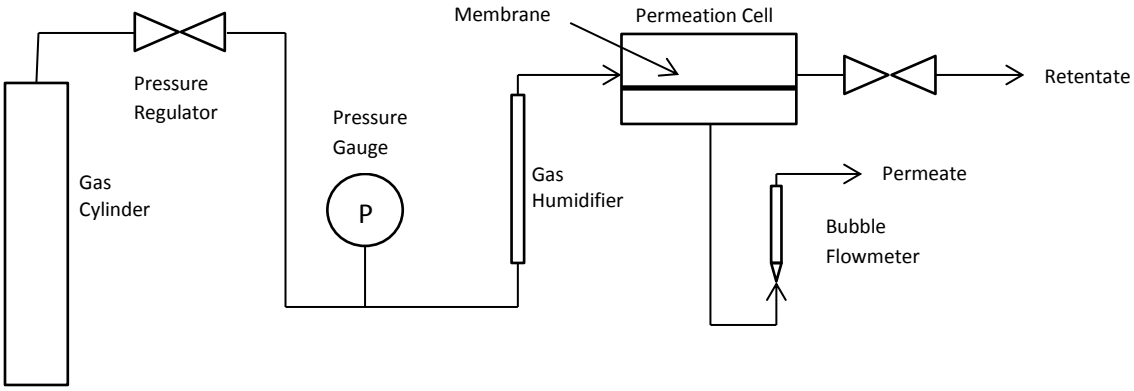

Figure 3-1: Gas permeability experimental apparatus.

Pure oxygen (O_2), nitrogen (N_2), and carbon dioxide (CO_2) were supplied by Praxair. The feed pressure was measured using a Cole-Palmer pressure gauge and controlled using a pressure regulator fitted to the gas cylinder. The pure gas was first humidified with water in a gas humidifier before reaching the permeation cell to maintain constant water saturation in the membrane. The humidified gas enters the permeation cell in which a water wet fibroin membrane had been placed on a porous metal support between two non-woven fabric supports. O-rings were used to ensure a tight seal between the permeation cell and the membrane. The retentate stream in the permeation cell was closed off after air initially present in the system was

completely purged out. The volumetric flowrate of the permeate stream through the membrane is measured using a bubble flowmeter assembled with a 1-*mL* pipette primed with Swagelok Snoop® Leak Detector fluid. The volumetric flowrates of the permeate gas stream were determined from the movement of the bubble in the bubble flowmeter at steady state permeation. The system was purged between the testing of different gases. The gas permeability was calculated from the gas flux through the membrane at each applied pressure.

3.4 Degree of Swelling

The degree of swelling of the fibroin film in deionized water (R_{sw}) was determined at room temperature from the water uptake:

$$R_{sw} = \frac{W_{sw} - W_d}{W_d} \cdot 100\% \quad (3\text{-}2)$$

where W_{sw} is the weight of the water swollen film, and W_d is the weight of the dry film.

3.5 Controlled Release

The permeability and sorption/desorption kinetics of four different model drugs with fibroin films were investigated. The model drugs used were *ciprofloxacin hydrochloride*, *(+)-cis diltiazem hydrochloride*, *tetracycline hydrochloride*, and *tetrahydrozoline hydrochloride*. All the model drugs were purchased from Sigma-Aldrich Co. Ltd. and used as received, except for *ciprofloxacin hydrochloride* which was prepared by reacting *ciprofloxacin* (supplied by Fluka BioChemica Co. Ltd.) with excess hydrogen chloride in diethyl ether to form *ciprofloxacin hydrochloride*. The details of the ciprofloxacin hydrochloride formation can be found in Chen et al. (2010). All these drugs were water soluble in their hydrochloride forms, and the drug

solutions were prepared by dissolving the pre-determined drug quantity in deionized water. Drug solutions in concentrations ranging from 50-500 *ppm* were used in the controlled release experiments. The chemical structures of the four model drugs used are shown in Scheme 1.

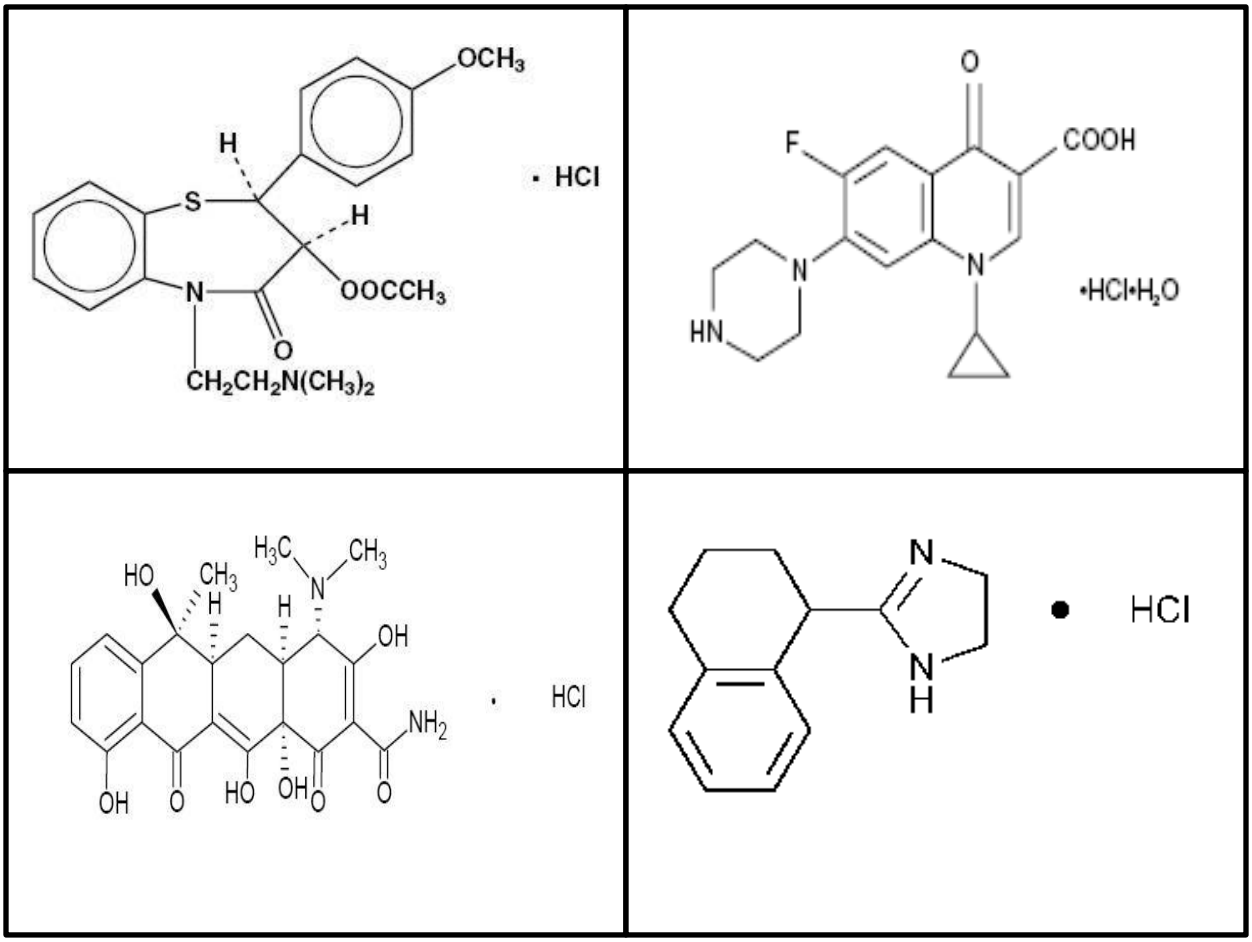

Scheme 1: Chemical structure of the four model drugs used. Top left – diltiazem-HCl; top right – ciprofloxacin-HCl; bottom left – tetracycline-HCl; bottom right – tetrahydrozoline-HCl.

Diltiazem-HCl is a calcium channel blocker and vasodilator used in the treatment of high blood pressure and angina. Ciprofloxacin-HCl is a broad-spectrum antibiotic, typically used to treat respiratory, urinary tract, gastrointestinal, and abdominal infections. Tetracycline-HCl is a broad-spectrum antibiotic commonly used to treat urinary tract and intestinal infections, as well as

acne, and was historically used in the treatment of cholera. Tetrahydrozoline-HCl is used in over-the-counter eye drops to constrict the blood vessels of the eye and relieve redness (Karch, 2012).

3.4.1 Drug Permeability

The experimental set-up for the drug permeability experiments is shown in Figure 3-2. There were 2 reservoirs; the donor reservoir was suspended partially in the receiver reservoir, with the fibroin film mounted on the bottom of the donor reservoir separating the reservoirs. The effective area of fibroin film separating the two reservoirs for drug transport was 11.3 cm^2. The receiver reservoir was filled with 2 *L* of deionized water. At time zero, 80 *mL* of drug solution at a given concentration (ranging from 50-500 *ppm*) was charged to the donor reservoir. Both reservoirs were well stirred to minimize the liquid mass transfer boundary layer resistances. The absorbance of the solution in the receiving reservoir was measured every 5 minutes using a Shimadzu UVmini-1240 UV-Vis Spectrophotometer, and the absorbance values were converted to drug concentration using calibration curves created for each drug. The wavelengths used in the spectrophotomer were 236 *nm* for *diltiazem hydrochloride*, 213 *nm* for *tetrahydrozoline hydrochloride*, 314 *nm* for *ciprofloxacin hydrochloride*, and 356 *nm* for *tetracycline hydrochloride*. The permeability coefficients were determined from the resulting data using the Mass Balance method during pseudo steady state drug release.

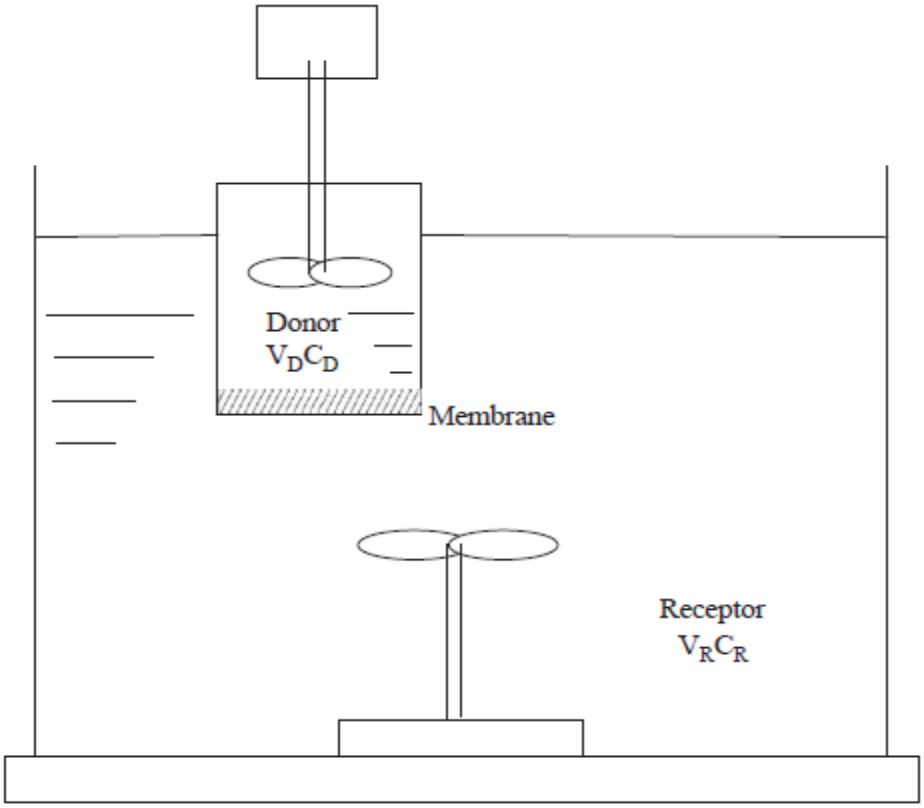

Figure 3-4: Drug permeability experimental apparatus (Chen et al., 2010).

3.5.2 Sorption/Desorption Kinetics

For the sorption experiments, water swollen fibroin films (dry mass 0.13-0.3 *g*; thickness 25-50 *μm*) were placed in 50 *mL* of aqueous drug solutions of given concentrations (ranging from 100 to 500 *ppm*). The sorption uptake was monitored by measuring the drug concentrations in solution every 5 min using the Shimadzu UVmini-1240 UV-Vis Spectrophotometer until equilibrium was reached. Further, the drug-loaded films from the sorption experiments were used for desorption experiments by immersing each drug-loaded film into 50 *mL* of deionized water. The increase in drug concentration of the solution was measured every 5 minutes using the spectrophotometer until equilibrium was reached.

Chapter 4: **Results and Discussion**

4.1 Degree of Swelling in Water

Membrane swelling affects physical properties of membranes (e.g. brittleness, strength and volume), as well as gas permeability. Water molecules between the polymer chains in a membrane will often increase mobility and free volume between the chains, thereby increasing the gas permeability. Therefore it is important to understand the degree of swelling of a material when considering applications in contact lenses and wound dressings where the material is in contact with a liquid solution. The degree of swelling of fibroin films was determined from the mass of water uptake in the films.

At equilibrium, the degree of swelling of the fibroin film in deionized water was 473% at room temperature. Comparatively, sericin/chitosan blend membranes have been observed to have a degree of swelling in the range of 265-272% (Eslami, 2011). The fibroin film swells significantly in water, which will greatly affect the gas permeability compared to a dry film.

4.2 Bovine Serum Albumin Adsorption

The adsorption of BSA onto the fibroin film was investigated to determine the biocompatibility of fibroin, specifically its blood compatibility and likelihood of thrombus formation. The results for the equilibrium adsorption, at room temperature and pH 7, can be found in Figure 4-1.

Figure 4-1 shows the uptake of BSA on the fibroin films (in mg of BSA adsorbed per g of dry film) as a function of the BSA concentration in the solution at equilibrium. The adsorption

capacity of the fibroin film increases over the concentration range tested. Referring to the adsorption isotherms found in Figure 2-1, the BSA uptake onto fibroin film fell between the 'favorable' and the 'linear' isotherms, with a slight downward concavity.

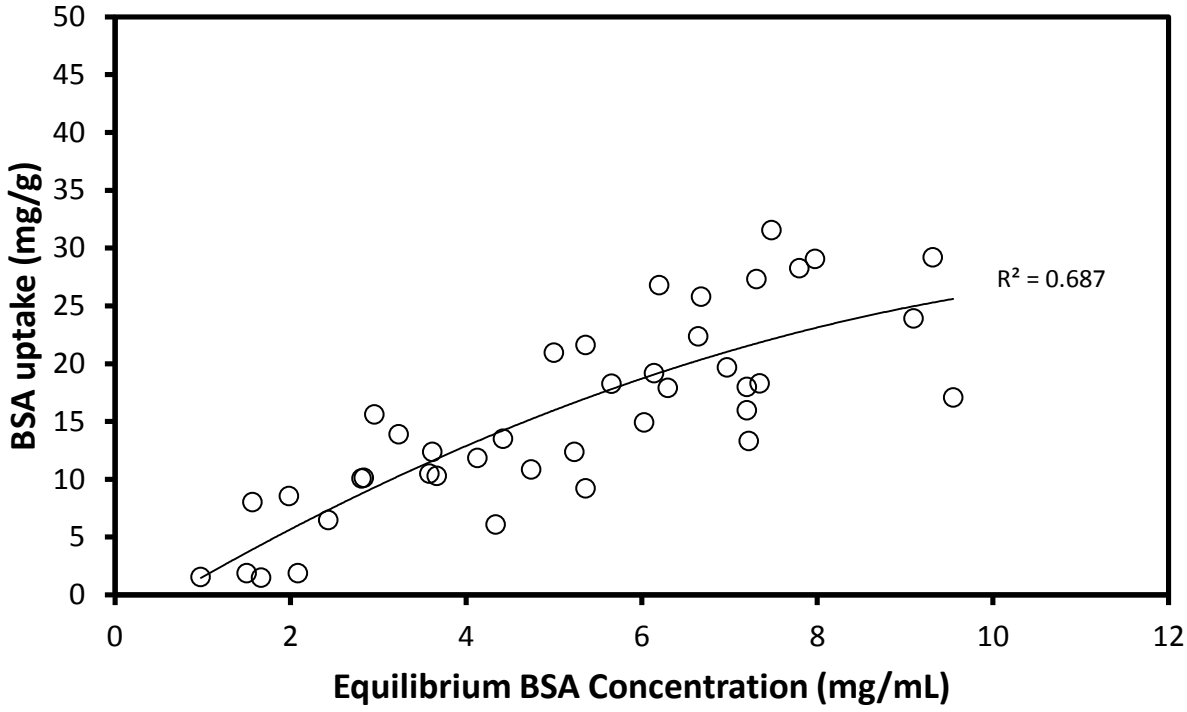

Figure 4-1: Equilibrium uptake of BSA on fibroin film per mass of dry film

Figure 4-1 shows large variability in the BSA uptake when taken on the basis of per unit mass of dry film. If the BSA is mainly sorbed to the surface of the fibroin film, then differences in the film thickness will affect the sorption uptake per mass of the film because of different surface areas per mass available for BSA uptake. Figure 4-2 shows the BSA uptake on the fibroin film per unit surface area (i.e. twice the film area), neglecting the surface area of the film edges. The area of the film edges represent <0.1% of the total surface area of the film, and can be neglected.

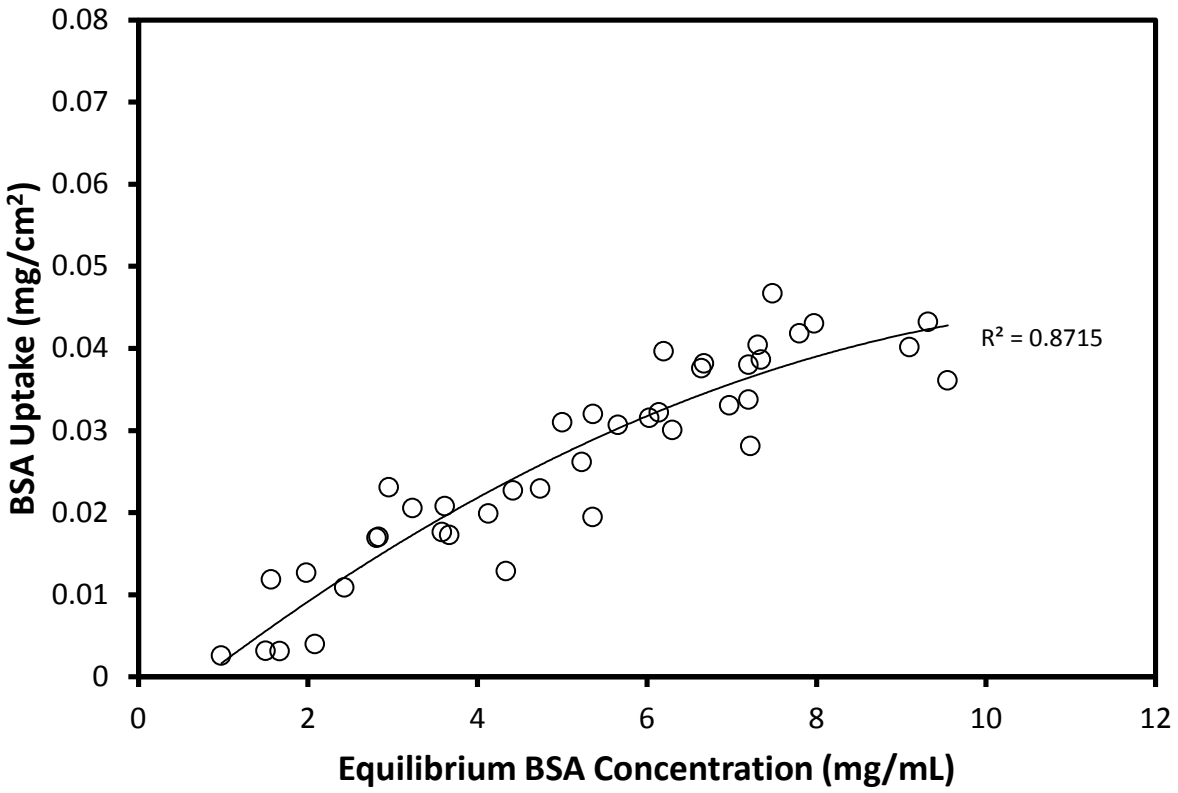

Figure 4-2: Equilibrium uptake of BSA on fibroin film per unit surface area of film

Figure 4-2 shows a reduction in the variability in the BSA uptake when based on the external surface area of the film as compared to film dry weight. This shows that the BSA uptake on the fibroin film mainly occurs on the surface of the film. While it appears that much of the BSA is sorbed to the surface of the film, a small amount of the BSA may also have entered the film.

To further investigate whether the BSA sorption follows the Langmuir or Freundlich adsorption, linearized forms of both isotherms were plotted and linear regression was used to determine the best fit of each model. For the Langmuir isotherm, the inverse of the adsorption uptake was plotted against the inverse of the bulk equilibrium concentration, as shown in Figure

4-3. For the Freundlich isotherm, the logarithm of the adsorption uptake was plotted against the logarithm of the equilibrium concentration, as shown in Figure 4-4.

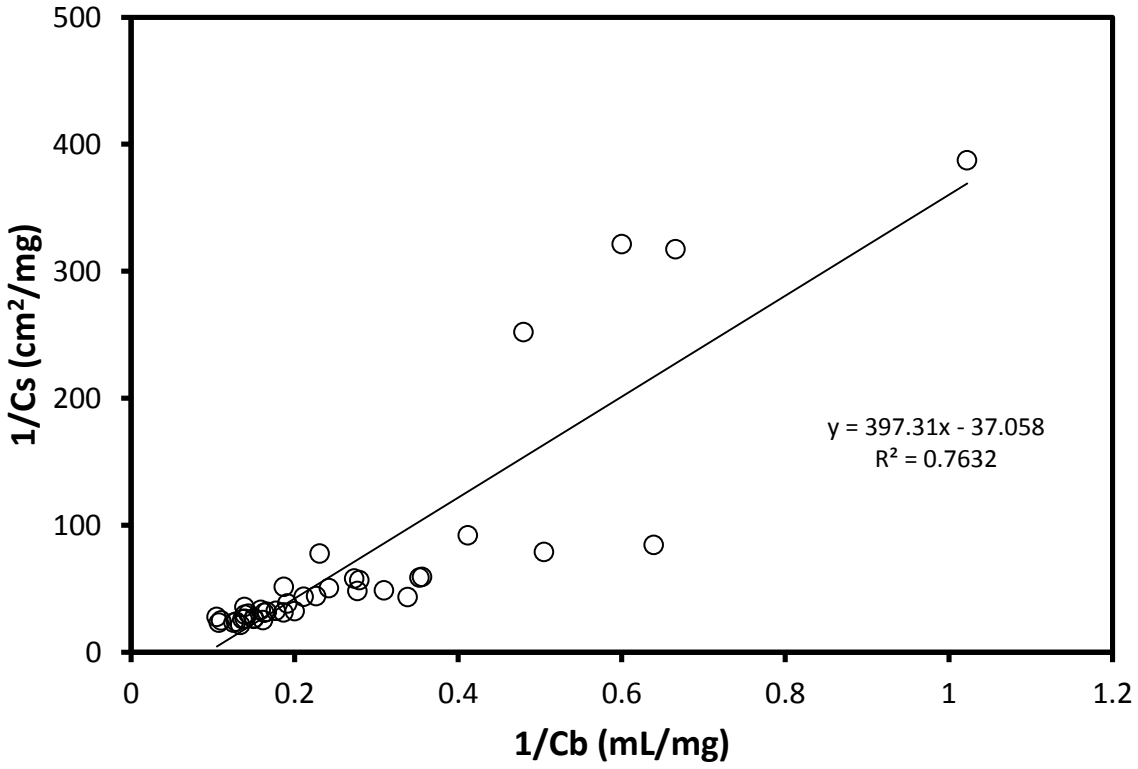

Figure 4-3: Experimental adsorption data plotted using a linearized Langmuir isotherm.

Figure 4-3 shows a moderate linear trend using the linearized Langmuir isotherm and an R^2 value of 0.763, but a close examination reveals some scatter in the data points at the far end of the range (i.e. at relatively low concentrations). This places undue importance on these data points, and can severely misrepresent the trend displayed by the majority of the data. The data at low concentrations display larger variance than the data at relatively high concentrations, and, with the influential nature of the later data points, may cause large errors in the parameter

estimation from regression analysis. The large variation is caused by a compounding of two effects. At very low concentrations, there is very little BSA uptake on the film, and this means very little change in solution concentration during the experiments. This means that any experimental errors present (i.e. from spectrophotometer calibration and measurement) greatly affect the calculated BSA uptake. In the linearized Langmuir model the reciprocal of the BSA uptake is used, and since the uptake at low concentration ranges are small and prone to large effects of error, the resulting reciprocal will display large variability. The parameter estimates for *A* and *K* were calculated from the slope and intercept of the linearized Langmuir model, and were found to both be negative. In the Langmuir isotherm, *A* represents the surface area per sorption site, and *K* is an equilibrium adsorption constant (Young et al., 1988). As such, negative values of these constants do not make physical sense, and indicate that the sorption of BSA onto fibroin film does not follow the Langmuir isotherm over the concentration range tested.

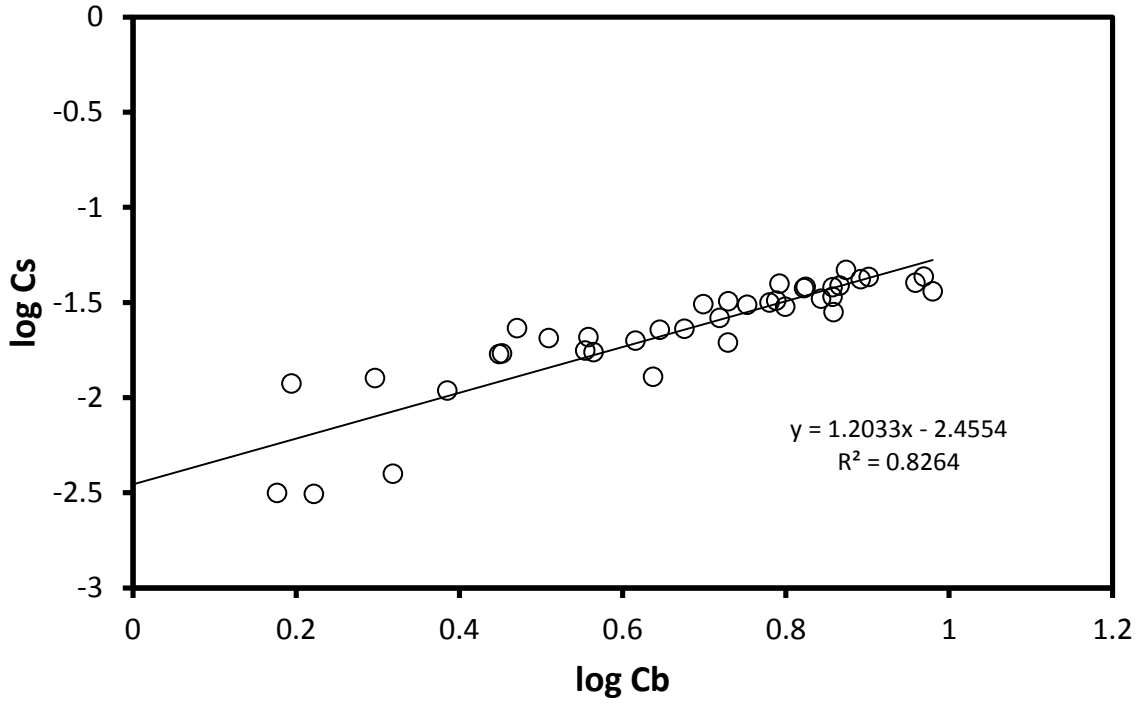

Figure 4-4: Equilibrium adsorption data plotted using a linearized Freundlich isotherm.

Figure 4-4 shows the Freundlich isotherm following a linear trend, with an R^2 value of 0.826. For the Freundlich model, the data are sparser at the beginning of the range (i.e. at relatively low concentrations), and more populated near the end of the range. While this may cause some leverage during the regression analysis for the low concentration points, the data are less spread than for the Langmuir isotherm, and as such the parameter estimates for the Freundlich model should be less error prone than the Langmuir estimates.

The model parameters for the Freundlich isotherm were estimated from the slope and intercept of the linearized Freundlich model, and are shown in Table 4-1.

Table 4-1: Freundlich parameters for adsorption of BSA on silk fibroin.

Freundlich Parameter	
A x10^3	**1/n**
3.5	1.203

Figure 4-2 shows BSA uptake increases as the equilibrium concentration increases, reaching 0.045 *mg/cm*^{2} (45 *μg/cm*^{2}) at an equilibrium concentration of 10 *mg/mL*. The equilibrium uptake of BSA on the fibroin is greater than the theoretical maximum surface concentration based on monolayer surface adsorption of 0.25 *μg/cm*^{2} (Bowen and Hughes, 1990). This high BSA uptake may be explained by discrepancies between the apparent and the effective fibroin surface area, multilayer sorption, or protein uptake within the film.

The apparent surface area of the fibroin films was measured macroscopically, which does not account for surface roughness or micropores and therefore may underestimate the effective surface area. Using a microporous poly(ethylene vinyl alcohol) membrane with an effective surface area of 4 *m*^{2}*/g* for BSA adsorption, Avramescu et al. (2003) found that BSA adsorption in

the range of 0.1 – 0.55 $\mu g/cm^2$ corresponded to 4 – 22 *mg/g* dry membrane. Akgol et al. (2004) found that *N*-methacryloyl-(L)-histidine methyl ester beads with a BET surface area of 80.1 m^2/g had a BSA adsorption capacity of 19.2 *mg BSA/g*. Lui and Bai (2005) found an adsorption capacity of 3.411 *mg BSA/g* dry membrane using a cellulose acetate/chitosan blend membrane with an internal surface area of 28.6 m^2/g. These adsorption capacities are comparable to the results found for BSA adsorption onto fibroin films, which were found to be in the range 1 – 30 *mg/g* dry membrane at equilibrium BSA concentrations from 0.25 – 10 *mg/mL*. The fibroin film is not microporous, and as a result the effective surface area for sorption will be determined primarily by external surface area. For sake of comparison, the fibroin film has an external surface area of approximately 0.06 m^2/g dry weight, with BSA adsorption capacity of 1 – 30 *mg/g* dry membrane. The fibroin film shows BSA sorption comparable to many other materials on a mass basis, but the film displays much greater sorption than the same materials on the basis of surface area. As mentioned, the high BSA uptake per film area may be caused by differences between the effective and apparent surface area, multilayer adsorption, or BSA uptake within the film.

The hydrophobic anti-parallel β-sheet regions present in silk fibroin could prove responsible for any potential multilayer adsorption. As mentioned previously, Kaelble and Moacanin (1977) showed the possibility of hydrophobic attraction over distances up to 140 *Å*. From Table 2-2, BSA has dimensions of approximately 40 x 140 *Å*, so under the right conformation up to three layers of BSA could potentially become adsorbed to the surface. Hydrophobic attraction could potentially be aided by protein-protein interactions between BSA molecules, allowing for greater retention upon the fibroin surface.

At concentrations approximately 5 – 10 times less than blood albumin concentrations, BSA displays a decent level of adsorption onto the fibroin film. Decent albumin adsorption is an indicator of good blood compatibility for the fibroin film. Albumin adsorption on the fibroin surface should lead to lower levels of fibrinogen adsorption, thus limiting thrombus and embolism formation on its surface. This indicator of blood compatibility shows promise for this fibroin film in biocompatible material applications.

While albumin adsorption is one indicator of a material's biocompatibility, more work is needed to confirm these findings. The strength of albumin adhesion on the surface is also important, so that the albumin molecules are not dislodged by fibrinogen. *In vitro* competitive adsorption experiments between albumin, fibrinogen, and other important blood biomolecules on fibroin should be performed to examine the sequential protein adsorption and blood response for the material. It should be pointed out that blood compatibility is only one indicator of biocompatibility, and to ensure complete biocompatibility of the film, appropriate experiments to determine inflammatory potential and toxicity should also be performed.

4.3 Gas Permeation

4.3.1 Permeability

The permeabilities of three gases, i.e., oxygen, nitrogen, and carbon dioxide, through water wet fibroin films were investigated, with particular attention being paid to the oxygen permeability for applications in wound dressings and contact lenses. The gas permeabilities were determined over a pressure range of 70 - 350 *kPag*. Figure 4-4 shows the gas flux through the film for the three gases, while Figure 4-5 shows the permeabilities.

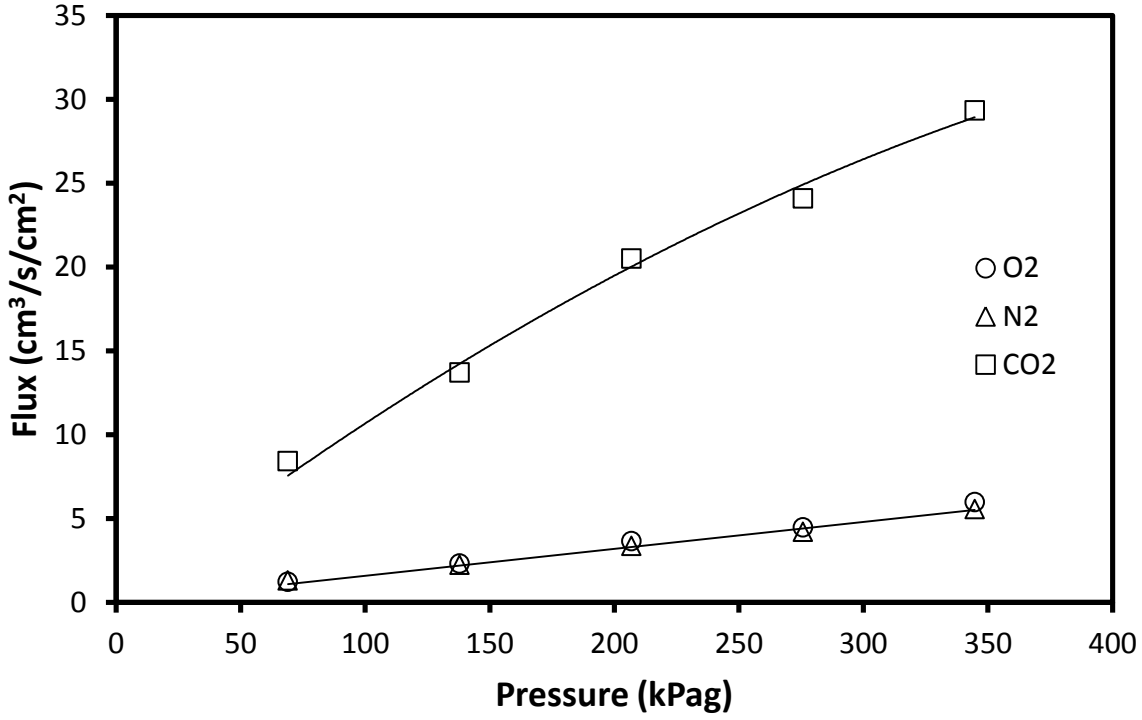

Figure 4-5: Flux of O_2, N_2 and CO_2 through fibroin film at varying pressures.

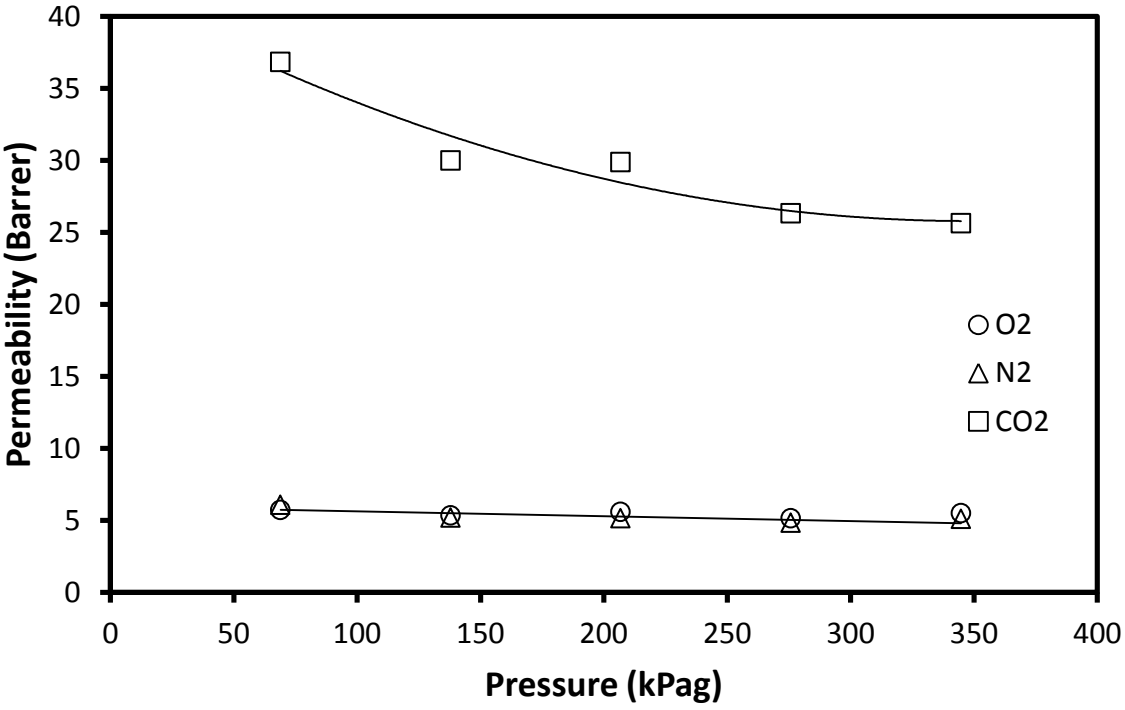

Figure 4-6: Permeability of O_2, N_2, and CO_2 through fibroin film at varying pressures.

The fluxes of all the gases increase with an increase in the applied pressure. According to Eqn 2-13, the gas flux through a film should have a linear relationship with the applied pressure for solution-diffusion situations if the diffusivity and solubility of the permeant in the membrane are pressure independent. It is shown that oxygen and nitrogen follow linear pressure dependencies of permeation flux, and the pressure dependency of carbon dioxide flux is slightly nonlinear. Both oxygen and nitrogen display similar flux through the film, while carbon dioxide displays a larger flux. The differences between the fluxes of oxygen and nitrogen and the flux of carbon dioxide are caused by differences in the solubility and diffusivity of the gases within the membrane. Table 4-2 shows the Henry's law constants and diffusion coefficients of the three gases in water.

Table 4-2: Henry's Law constants and diffusion coefficients of O_2, N_2, and CO_2 in water.

	k_H [M/atm]x10^{3} [x]	D [µm^2/s] [‡]
Oxygen	1.3	2000
Nitrogen	0.63	1880
Carbon Dioxide	34	1600

[x] Henry's law constants provided at 25°C from Sanders (1999).

[‡] Diffusion coefficients provided at 25°C from Crank et al. (1975).

The solubility of carbon dioxide in water is much greater than the solubility of oxygen or nitrogen in water, while the diffusion coefficients are relatively similar. This difference in water solubility is likely the cause of carbon dioxide's higher permeability than the permeabilities of oxygen and nitrogen. The fibroin film is water swollen during the permeability experiments, and

the presence of water in the membrane enables greater carbon dioxide solubility and thus greater flux and permeability. Oxygen is roughly twice as soluble and has a slightly greater diffusivity in water than nitrogen, but they exhibited a very similar flux through the fibroin. The solubility and diffusivity of the permeating gases in water are not the only considerations, since the solubility and diffusivity within the fibroin film matrix also play an important role. Differences between the solubility and diffusivity of oxygen and nitrogen within the fibroin matrix may offset their solubility and diffusivity in water, and this may explain the similarities in the flux and permeability.

The permeability of oxygen and nitrogen in the fibroin film are both approximately 5 *Barrer* and do not change with pressure. The permeability of carbon dioxide is shown to be 26 – 37 *Barrer* over the 70 – 350 *kPag* pressure range, with the permeability decreasing with an increase in the gas pressure. The permeability coefficient is the product of the solubility coefficient and the diffusion coefficient. A pressure-independent permeability coefficient will be observed when both the sorption and diffusion coefficients are pressure independent.

The oxygen permeability of 5 *Barrer* in the fibroin film compares closely to the oxygen permeability for fibroin film of 4-8 *Barrer* found by Minoura et al. (1990). The oxygen permeability values of Kweon et al (1990) of 0.249-0.579 *Barrer* in fibroin do not correspond as well with the results of this experiment, but are also not out of the range of plausibility. Differences in experimental technique may result in different permeability values, as the two research groups measured dissolved oxygen permeability, while this work used gas permeability. The film crystallinity and β-sheet content also play an important role in gas permeability. The crystallinity of the fibroin film created using the ethanol extraction technique used in this thesis work is not known. Differences in film crystallinity or other morphological differences between

the films may also be responsible for differences in the oxygen permeability values observed. To test this hypothesis it is suggested that the crystallinity of the fibroin film be quantified through appropriate analytical techniques such as FTIR spectroscopy, x-ray diffraction, differential scanning calorimetry, or NMR methods, and the crystallinity of the film compared to the fibroin films used by Kweon et al. (2001) and Minoura et al. (1990).

An oxygen transmissibility of 87.0 x 10^{-9} *(cm·mL O_2)/(s·mL·mmHg)* is required for water wet hydrogel contact lenses to prevent corneal edema during overnight wear. Transmissibility (also known as permeance) is the ratio of the permeability coefficient to the effective membrane thickness. The fibroin film, with an effective water wet thickness of 26 *μm* and an oxygen permeability of 5 *Barrer*, corresponds to an oxygen transmissibility of 19.2 x 10^{-9} *(cm·mL O_2)/(s·mL·mmHg)*. The oxygen transmissibility of the fibroin film is below the critical transmissibility level required to prevent corneal edema during overnight wear. The critical oxygen transmissibility to prevent corneal edema is too large for many types of hydrogel lenses to achieve, so a compromise criterion of 34.3 x 10^{-9} *(cm·mL O_2)/(s·mL·mmHg)* was suggested as this level leaves zero residual swelling of the eye shortly after eye opening (Holden and Mertz, 1984). The fibroin film still does not meet this reduced criterion of oxygen transmissibility, but the gap has been greatly reduced. According to Holden and Mertz (1984), the oxygen transmissibility required to prevent corneal edema during daily wear conditions is 24.1 x 10^{-9} *(cm·mL O_2)/(s·mL·mmHg)*. Once again the fibroin film does not meet this criterion. Based on these criteria, the fibroin film in its current state is not suitable for overnight or daily wear use as contact lenses.

Table 4-3: Oxygen transmissibility and permeability of polymers.

Membrane	Thickness (μm)	Transmissibility ($cm^3(STP))/(s \cdot cm^2 \cdot mmHg) x10^9$	Permeability (Barrer)	Reference
Poly(vinyl alcohol)	90	3.9	3.5	Henry, 2006
Hilafilcon silicone	36	22.2	8	Holden and Mertz, 1984
2-hydroxymethylmethacrylate	186	18.4	34	Holden and Mertz, 1984
(2-chlorophenyl)(2-methylphenyl)methanol	126	31.7	40	Holden and Mertz, 1984
Bucrylate	74	16.2	12	Holden and Mertz, 1984
Etafilcon A	137	133	182	Holden and Mertz, 1984
Polymacron	111	7.2	8	Holden and Mertz, 1984
Fibroin	26	19.2	5	This Work

Table 4-3 shows some polymer hydrogel materials typically used in contact lenses, along with the results for fibroin from this work. Several materials show lower oxygen transmissibility than fibroin, but while contact lens materials with oxygen permeabilities lower than the minimum criteria set by Holden and Mertz (1984) are in use, they are being replaced by higher permeability materials as evidence shows chronic ocular problems associated with their use (Fonn et al., 2005).

While the fibroin film currently does not meet the oxygen permeability requirements for daily wear or overnight contact lenses, several different modifications to the film and its preparation may increase the oxygen permeability sufficiently to meet these requirements. Minoura et al. (1990) showed that decreasing fibroin film's crystallinity increases the gas permeation, so methods that alter the β-sheet content of the fibroin film should be investigated. Treatment of fibroin films with methanol is often used to alter their crystallinity, with increasing

crystallinity resulting from longer treatment times. This suggests that exposure to ethanol may also increase crystallinity; shortening the length of exposure to ethanol in the fibroin extraction stage may result in lowered film crystallinity when preparing the films in the method used in this work. Another method to increase permeability is through blending fibroin with another biocompatible material. The blend film could potentially offer greater oxygen permeability than either of the pure materials. Potential materials could also be chosen to preferentially alter the resulting film properties to better fit other contact lens requirements, such as less brittleness or greater optical clarity. Through these or other modifications to the films, fibroin could potentially reach oxygen permeability values suitable for use in contact lenses.

There are no critical oxygen permeabilities required for wound dressings, but high oxygen permeabilities are generally considered beneficial to halt bacterial growth and aid the healing process. Sano et al. (2012) found that wound dressings with an oxygen permeance of 91.4 x 10^{-9} *(cm·mL* O_2*)/(s·mL·mmHg)* retained oxygen tension around the wound close to atmospheric levels, and showed significantly faster decreases in wound size and significantly thicker granulation tissue after seven days using a rat wound model compared to an effectively oxygen impermeable wound dressing. With an oxygen transmissibility of 19.2 x 10^{-9} *(cm·mL* O_2*)/(s·mL·mmHg),* the fibroin wound dressing should allow high oxygen permeability and display very good oxygen tension around the wound. Fibroin's good oxygen permeability and ability to aid the adherence and growth of cells responsible for wound healing suggest that fibroin films would be great assets in wound dressings.

While oxygen permeability and cell adhesion and growth are important aspects in wound dressing, other issues with the fibroin film may need to be investigated. The fibroin film has a tendency to quickly lose moisture and become extremely brittle when exposed to the atmosphere

after being swollen with water. This moisture loss may have detrimental effects on wound healing. Cells will lose mobility around the wound surface and dressing, and eventually dry out the wound surface, limiting healing. Brittleness in the wound dressing may cause the dressing to crack and break apart if the patient moves around or pressure is otherwise applied to the dressing. One approach to deal with this problem is to blend the fibroin with another polymer that helps to retain moisture and avoid brittleness. If possible the blend material could also be chosen to further aid in the wound healing process, such as the fibroin/alginate blend wound dressing created by Roh et al. (2006).

4.3.2 Selectivity for Gas Permeation

In gas separation applications, the permeability as well as the selectivity are important considerations. Selectivity represents the ability of a membrane to separate two gases. An ideal selectivity is measured by the ratio of the permeabilities of two pure gases:

$$\alpha_{ij} = \frac{P_i}{P_j} \tag{4-1}$$

where α_{ij}* is the ideal selectivity, P_i is the permeability of component *i*, and P_j is the permeability of component *j*. Table 4-4 show the selectivities of the fibroin film for the permeant oxygen, nitrogen, and carbon dioxide gases:

Table 4-4: Oxygen, nitrogen and carbon dioxide selectivities of fibroin film.

Pressure (kPag)	$\alpha_{O2/N2}$	$\alpha_{O2/CO2}$	$\alpha_{CO2/N2}$
69	0.94	0.16	6.06
138	1.03	0.18	5.78
207	1.09	0.19	5.80
276	1.07	0.20	5.45
345	1.07	0.21	5.01

The fibroin film shows an O_2/N_2 selectivity of approximately 1 throughout the pressure range. At a selectivity of 1, no separation occurs. Since the fibroin film provides no separation between O_2 and N_2, it would not be suitable as an O_2/N_2 gas separation membrane. The CO_2/N_2 selectivity decreases with increasing pressure, starting at approximately 6 at 69 kPag, and falling to 5 at 345 kPag. A CO_2/N_2 selectivity greater than 200 is estimated as a requirement for an economically competitive polymer membrane for industrial applications dealing with flue gases (Granite and O'Brien, 2005). The CO_2/N_2 selectivity of the fibroin film is considerably less than the target selectivity of 200, and the fibroin film does not show potential for CO_2 separation from flue gases, a subject that is important to greenhouse gas emission control.

4.4 Controlled Release of Drugs

4.4.1 Drug Permeability

The permeability of four model drugs, i.e., diltiazem-HCl, ciprofloxacin-HCl, tetrahydrozoline-HCl, and tetracycline-HCl, through a fibroin film was investigated for potential applications in controlled drug release. The experimental data on the drug permeation at different initial donor concentrations (50 to 600 ppm) are shown in Figure 4.7 – 4.10.

The permeation data show that as the drug concentration in the donor reservoir increases, the amount of drug permeated through the fibroin film also increases. This is consistent with Fickian diffusion through the film, in which the drug flux through the film is proportional to the concentration gradient across the film. Each permeation run shows an initial transient period in

which the rate of drug permeation gradually increases with time, followed by a pseudo steady-state period in which the rate of drug permeation is constant.

The permeability coefficients of the drug at each concentration were calculated from the pseudo steady state permeation data for each trial. The pseudo steady state data can be subjected to analysis via the mass balance method if a reference time t_o is selected at the beginning of the pseudo steady state period (Chen et al., 2010):

$$-\ln\left(\frac{m_o - V_t C_R}{m_o - V_t a}\right) = \frac{PA}{l}\left(\frac{1}{V_D} + \frac{1}{V_R}\right)(t - t_o) \qquad (4\text{-}2)$$

where $a = C_R$ at $t = t_o$. Plotting $F(t) = -\ln[(m_o - V_t C_R)/(m_o - V_t a)]$ against t will yield a straight line, and the permeability coefficient can be calculated from its slope.

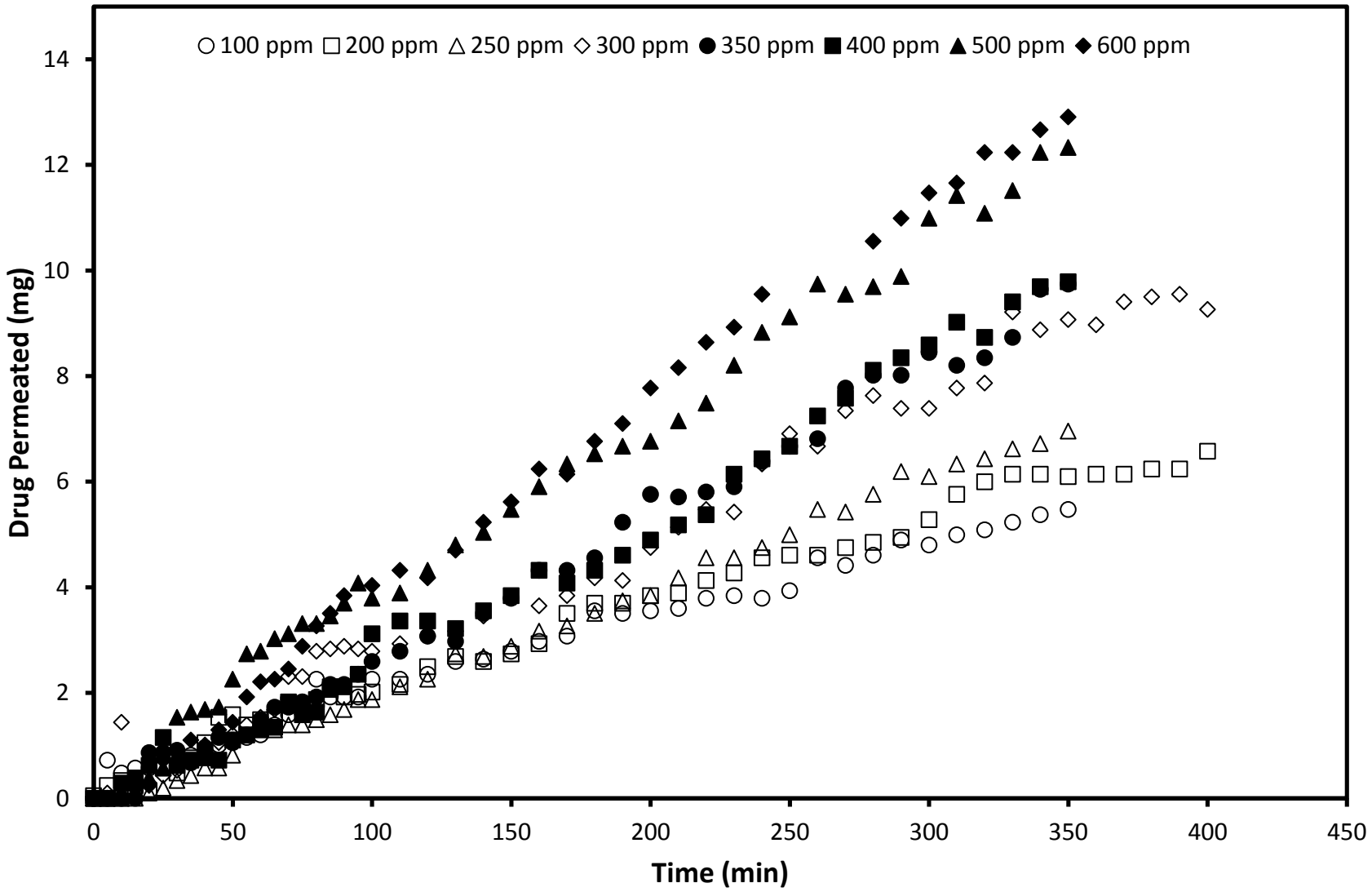

Figure 4-7: Permeation data for Diltiazem-HCl at varying initial donor reservoir concentrations.

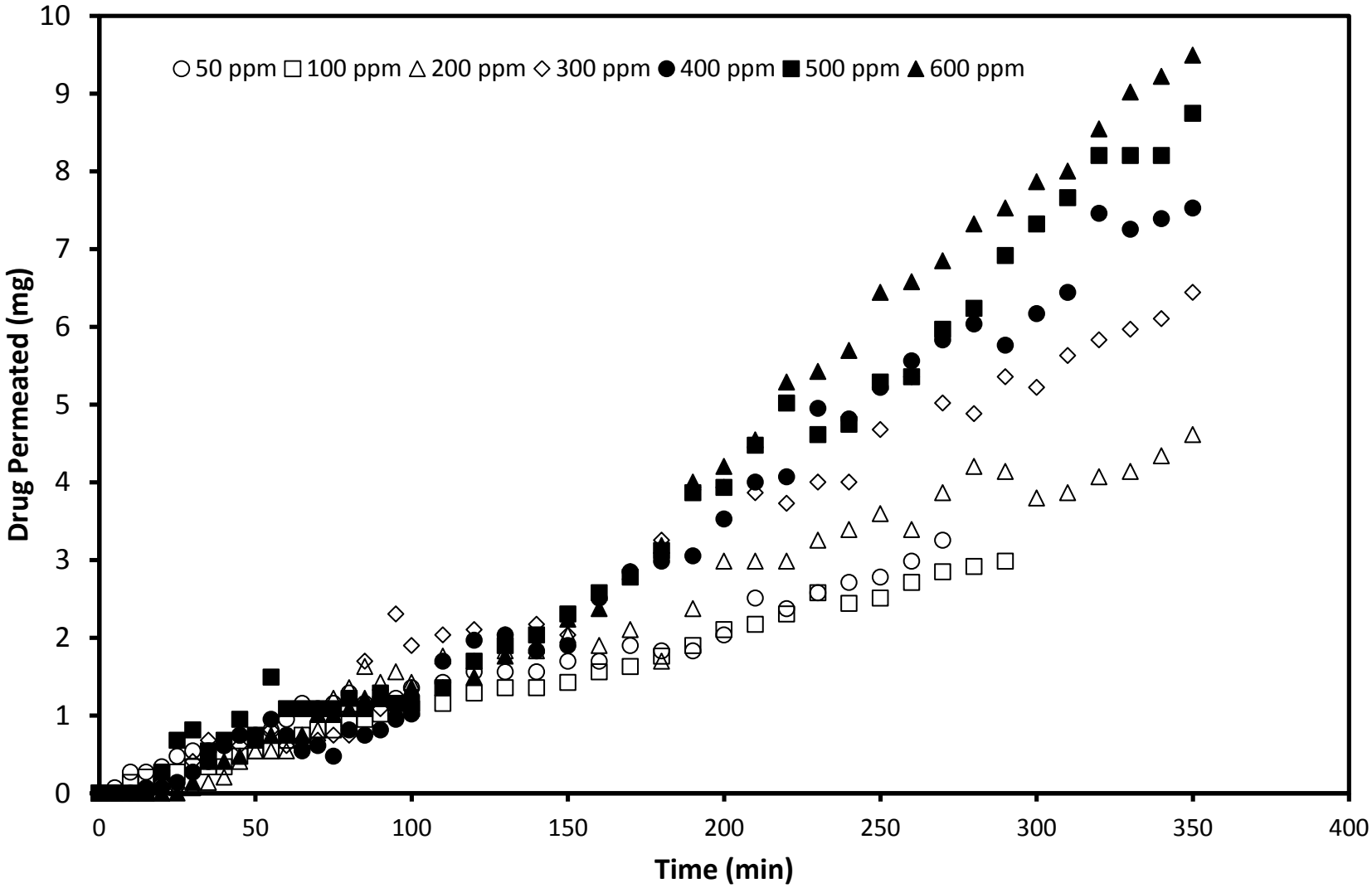

Figure 4-8: Permeation data for Ciprofloxacin-HCl at varying initial donor reservoir concentrations.

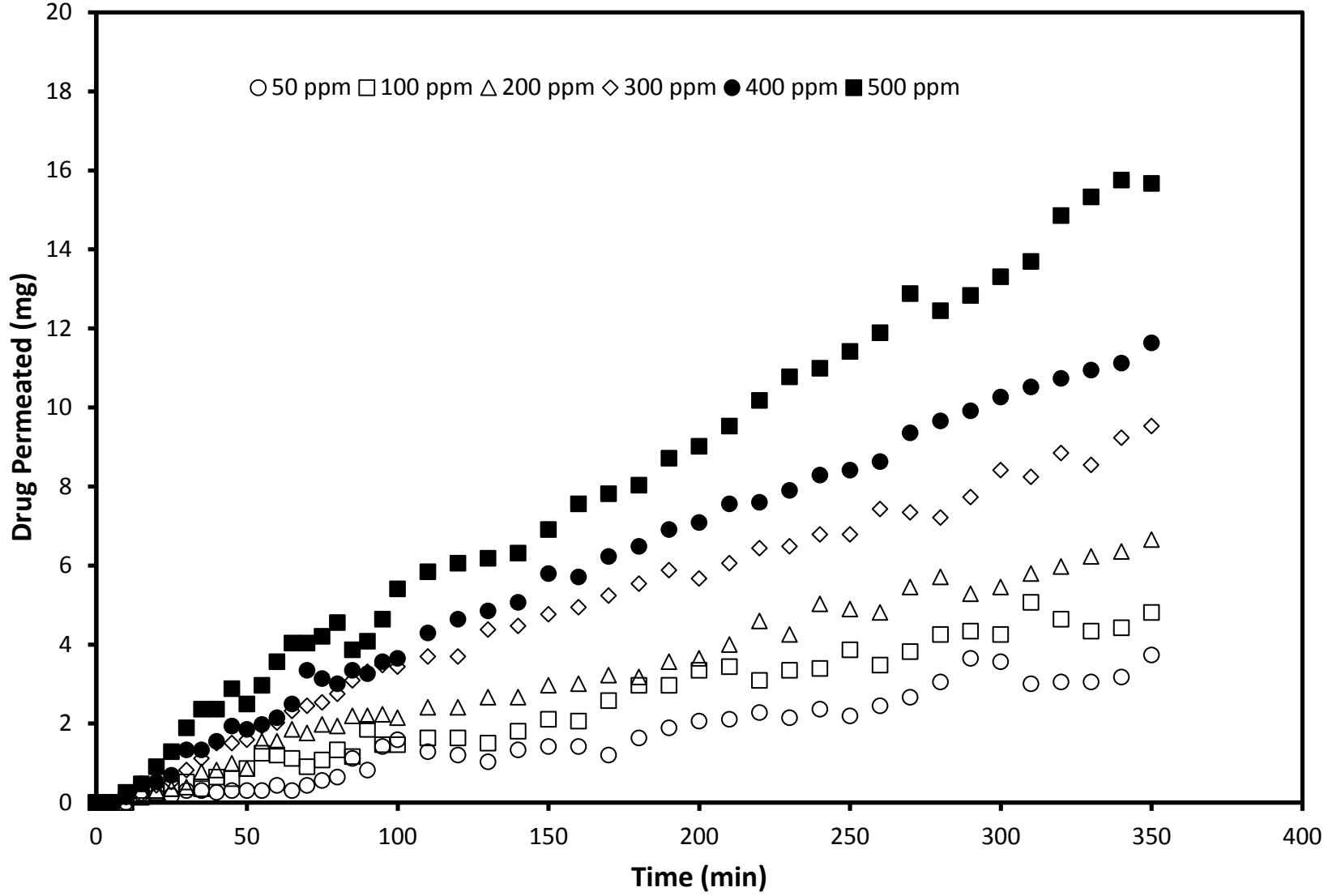

Figure 4-9: Permeation data for Tetrahydrozoline-HCl at varying initial donor reservoir concentrations.

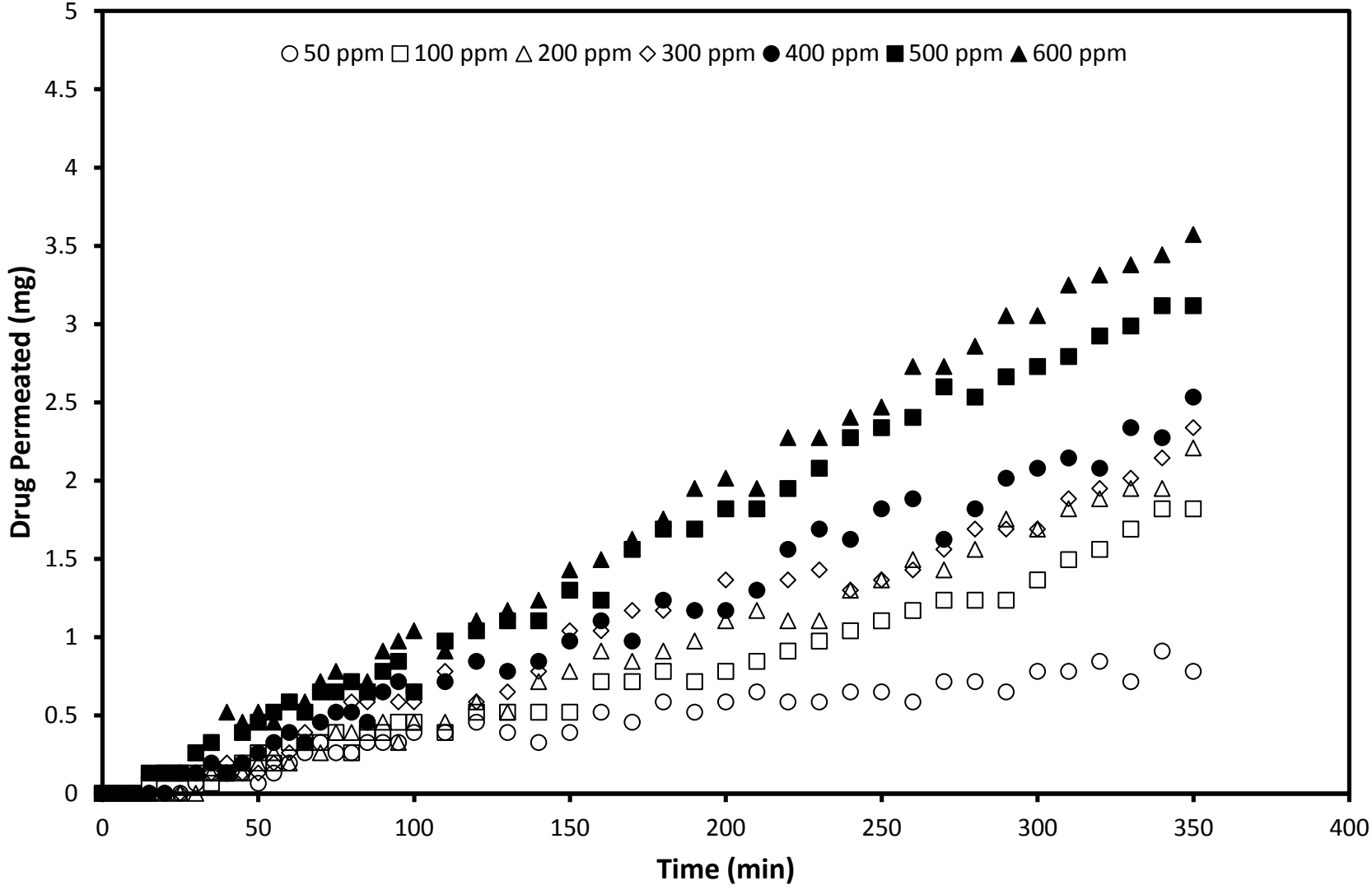

Figure 4-10: Permeation data for Tetracyline-HCl at varying initial donor reservoir concentrations.

For the purpose of illustration, Figure 4.11 shows the F(t) vs t plots for the permeation data of the four model drugs at an initial donor reservoir concentration of 500 ppm, respectively. The permeability coefficients determined from the slopes of the F(t) vs t plots are shown in Fig 4.12.

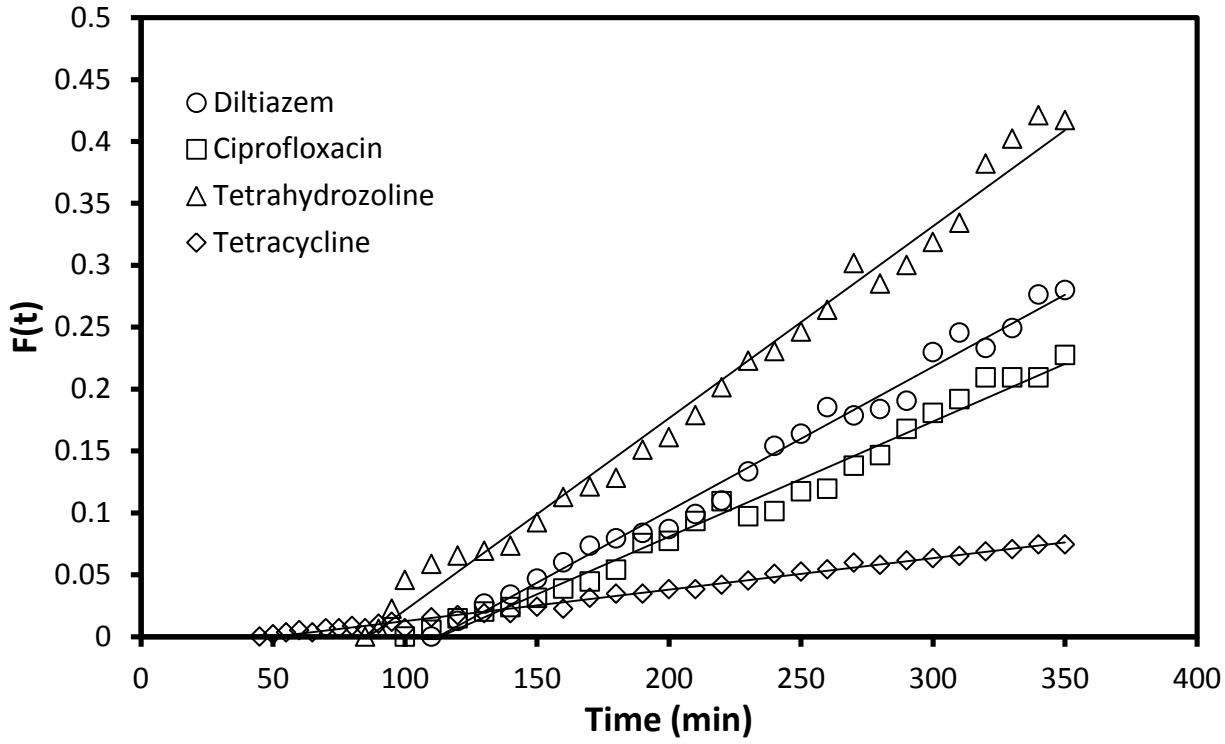

Figure 4-11: F(t) vs time plots for pseudo steady-state data. Initial drug concentration 500 ppm.

Figure 4-12 shows that at low initial donor reservoir concentrations, the permeability coefficient decreases quickly with an increase in the drug concentration. However, as the initial concentration increases above 200 *ppm*, the permeability coefficient will remain relatively constant with further increases in the drug concentration. As the initial donor concentration increases, quantity of permeated drug in the receiver increases, but the rate of the increase becomes slower, resulting in a reduction in the permeability coefficients. When increasing the initial concentration beyond a certain point (i.e., 200 *ppm*), the drug permeation rate is almost

proportional to the concentration difference between the two reservoirs, leading to nearly constant permeability coefficients.

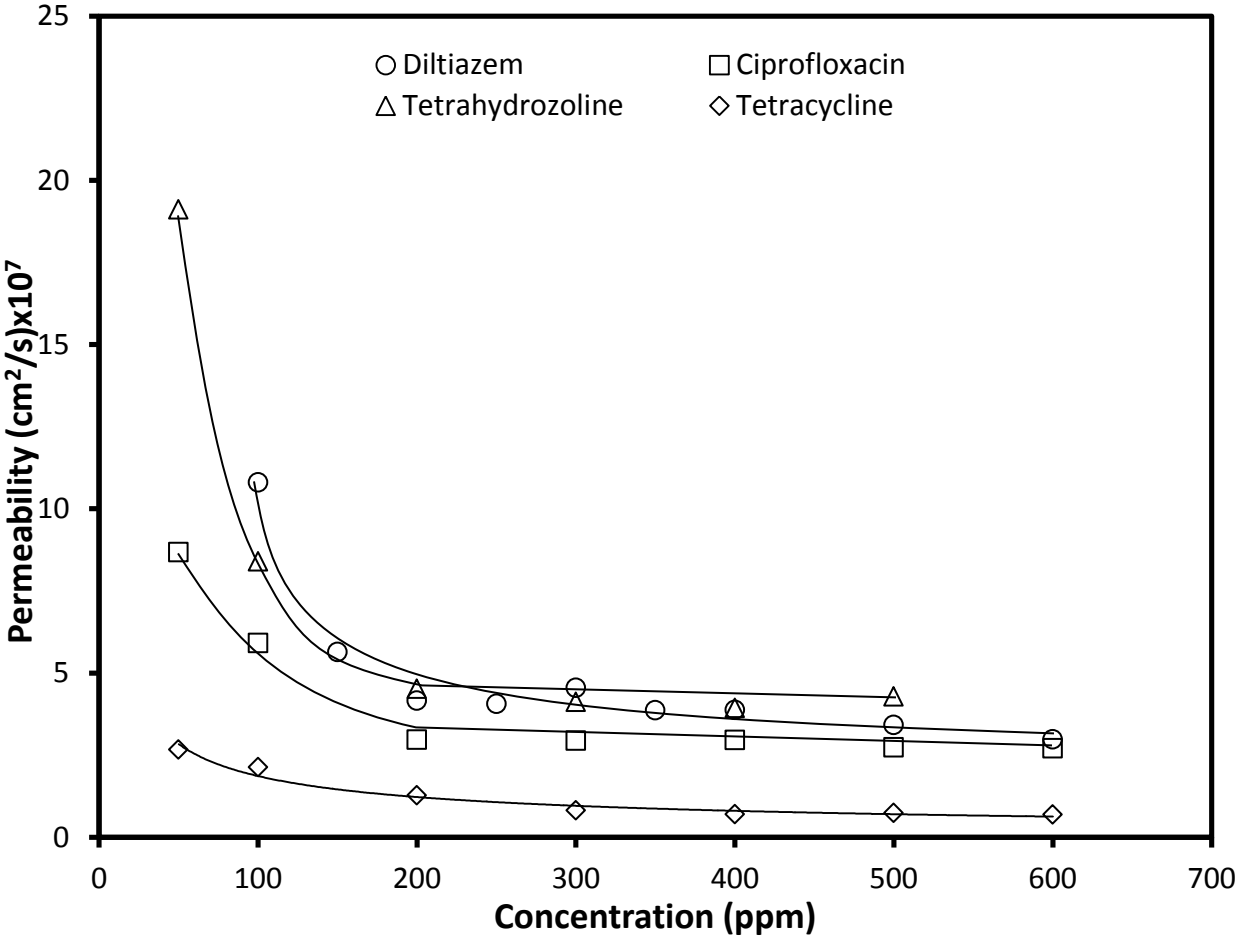

Figure 4-12: Permeability coefficients of four model drugs at varying reservoir concentrations.

Diltiazem-HCl, and tetrahydrozoline-HCl display similar permeabilities in the fibroin film, and ciprofloxacin-HCl has a slightly lower permeability, while tetracycline-HCl displays the lowest permeability among the four model drugs tested here. The permeability in the concentration independent range (200 – 600 ppm) is approximately 4.1 x 10^{-7} cm^2/s for diltiazem-HCl, 2.9 x 10^{-7} cm^2/s for ciprofloxacin-HCl, 4.3 x 10^{-7} cm^2/s for tetrahydrozoline-HCl,

and 0.8 x 10^{-7} cm^2/s for tetracycline-HCl. Permeability is affected by many factors relating to the permeant, including molecular mass, solubility, hydrophobicity, net charge, and other chemical interactions. The molecular mass for the model drugs used are shown in Table 4-5. Examining the molecular mass and permeabilities of the four model drugs, there does not appear to be a clear correlation between the two. Tetrahydrozoline-HCl has the smallest molecular mass (236 *g/mol*) and the largest permeability, and tetracycline-HCl has the largest molecular mass (480 *g/mol*) and lowest permeability. However diltiazem-HCl also has a relatively large molar mass (451 *g/mol*), but exhibited a relatively large permeability. This indicates the permeability of the drug molecules in the fibroin film is not only determined by the diffusion rate (which is primarily determined by the molecular size of the permeant), and the solubility of the drugs in the film is also important to the permeability of the drugs.

Table 4-5: Molecular mass and water solubility of model drugs.

Drug	Molecular Mass (g/mol)	Solubility in Water (mg/mL)
Diltiazem-HCl	450.98	590[*]
Ciprofloxacin-HCl	385.82	58.4[t]
Tetrahydrozoline-HCl	236.74	385[‡]
Tetracycline-HCl	480.90	26.9[t]

[*]At 37°C from McClelland et al., (1991).

[‡]At 25°C from United States Pharmacopeia, (2009).

[t]At 40°C from Varanda et al., (2006).

Table 4-5 lists the solubility in water of the four model drugs. A clear correlation can be seen between the water solubility and permeability within the fibroin film for each model drug. Diltiazem-HCl and tetrahydrozoline-HCl are highly water soluble, resulting in their relatively high permeabilities. Ciprofloxacin-HCl has a lower solubility in water, and a lower permeability

through the fibroin film. Tetracycline-HCl has the lowest water solubility and the lowest permeability.

The permeability values found in this experiment compare similarly to values from other researchers. Chen et al. (1994) looked at the permeability of five different drugs through a regenerated fibroin film using a similar reservoir setup. At pH 7, the permeabilities of 5-Fluorouracil and Resorcinol were on the order of 10^{-7} cm^2/s, benzyltrimethylammonium chloride was approximately 0.5 x 10^{-7} cm^2/s, and sodium phenolsulfonate and ascorbic acid were on the order of 10^{-9} cm^2/s. Chen et al. (2010) found that the permeability of ciprofloxacin-HCl through a chitosan membrane was approximately 5 x 10^{-7} cm^2/s using a similar reservoir setup. Eslami (2011) looked at the permeability of ciprofloxacin-HCl, diltiazem-HCl, and nitrofurazon through a chitosan/sericin blend membrane. Using the same mass balance technique, the permeability of ciprofloxacin-HCl was found to be approximately 1.5-3.0 x 10^{-7} cm^2/s, diltiazem-HCl approximately 0.5 x 10^{-7} cm^2/s, and nitrofurazon of approximately 13-17 x 10^{-7} cm^2/s. The permeability values of the four model drugs in the fibroin film are all within the range shown in the literature from both similar membranes and similar drugs.

4.4.2 Sorption Kinetics and Diffusivity

To determine the diffusivity of the four model drugs within the fibroin film, the sorption kinetics of drugs in the fibroin film were investigated at varying drug concentrations. Figure 4-13 shows the equilibrium sorption uptake of the model drugs in the fibroin film at different drug concentrations in the solution.

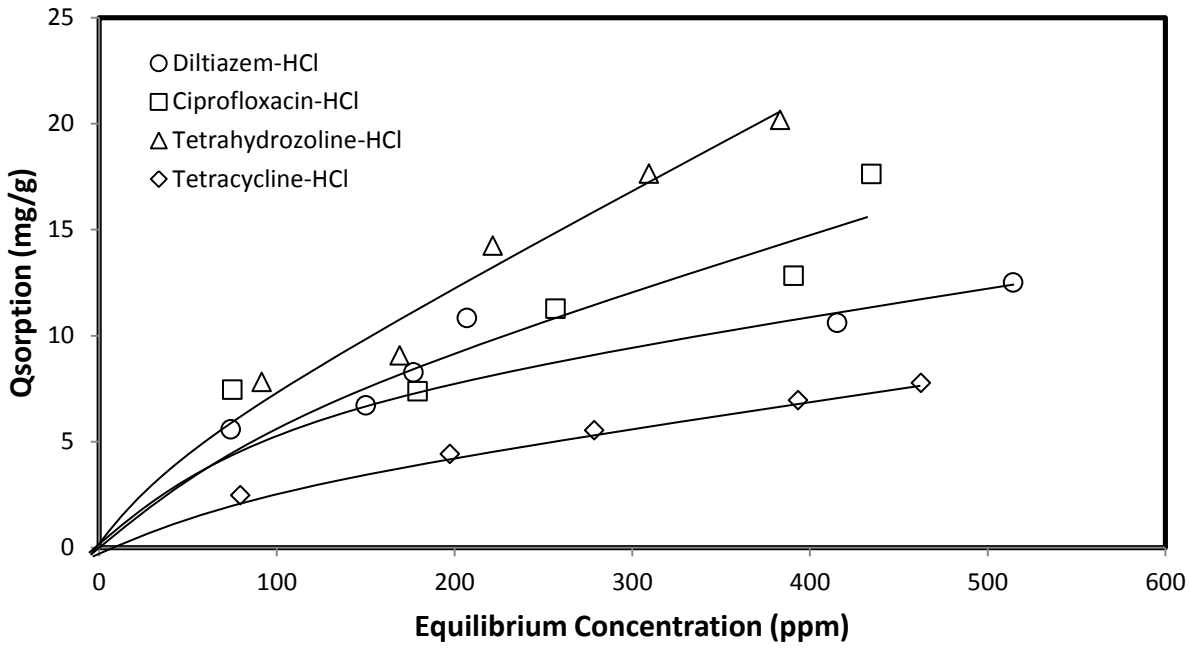

Figure 4-13: Equilibrium sorption uptake of four model drugs in fibroin film.

As expected, the equilibrium sorption uptake of each model drug into the fibroin film increases as the equilibrium drug concentration in the solution increases. Tetrahydrozoline-HCl shows the greatest sorption uptake in fibroin at approximately 20.2 *mg/g* (dry weight) of film at an equilibrium concentration of 383 *ppm*, compared to 17.6 *mg/g* (dry weight) of film at 435 *ppm* for ciprofloxacin-HCl, 12.5 *mg/g* (dry weight) of film at 514 *ppm* for diltiazem-HCl, and 7.8 *mg/g* (dry weight) of film at 462 *ppm* for tetracycline-HCl. These data show that tetrahydrozoline-HCl and ciprofloxacin-HCl interact the most strongly with the fibroin film, followed by diltiazem-HCl, and then tetracycline-HCl with the weakest interaction. The drug-fibroin interactions are important considerations in bulk-loaded films for drug delivery as it is indicative of how much drug can be loaded in the film. Strong interactions mean that more drug

can be loaded into the film, but too strong interactions will keep the drug bound to the film and lower the quantity of drug that can be released by desorption, wasting potentially expensive drug.

Figures 4-14 to 4-17 show the kinetics of sorption for the model drugs. The sorption data show the amount of drug sorbed to the film per gram (dry weight) of the film as a function of time at varying initial drug concentrations. The sorption kinetics show an initial transient period during which the drugs are quickly taken up into the fibroin film. The rate of drug uptake slows as it approaches its equilibrium point, and after approximately 100 minutes the equilibrium sorption uptake is reached and the amount of drug uptaken into the film no longer changes with time. As shown previously, the sorption uptake of drug within the fibroin film increases with increasing drug concentration, however, the drug concentration does not appear to affect the rate at which equilibrium is reached, which will be illustrated later.

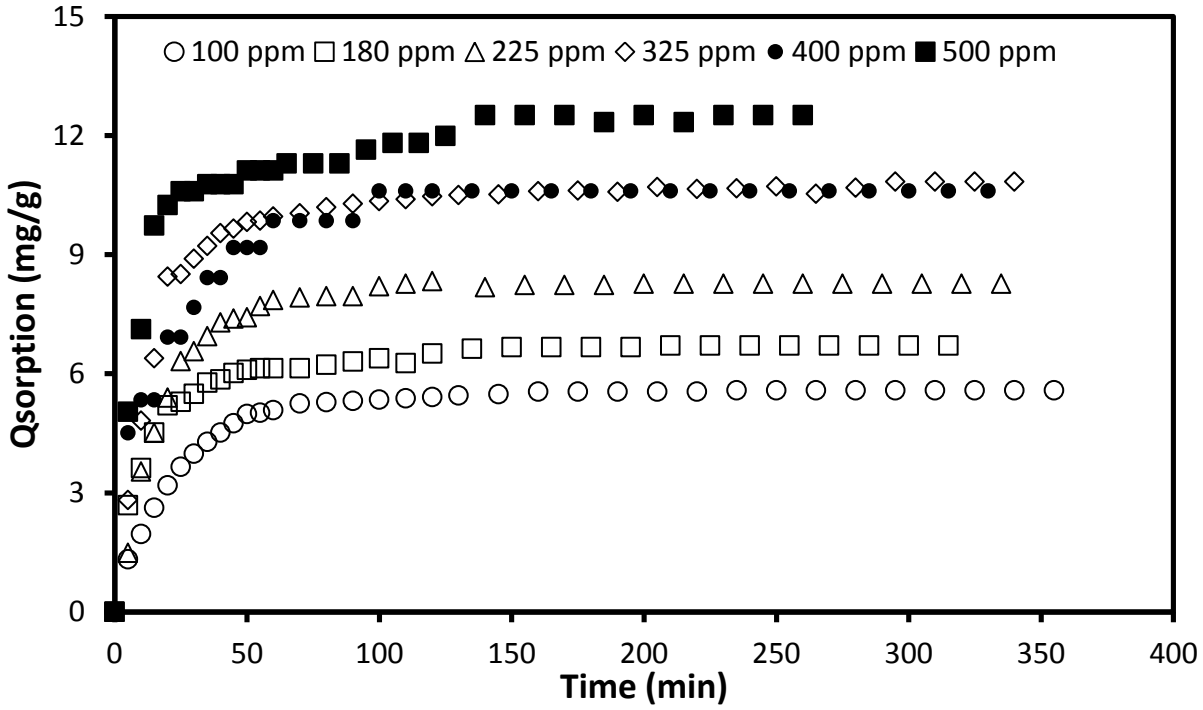

Figure 4-14: Amount of diltiazem-HCl sorbed into fibroin film at varying initial concentrations.

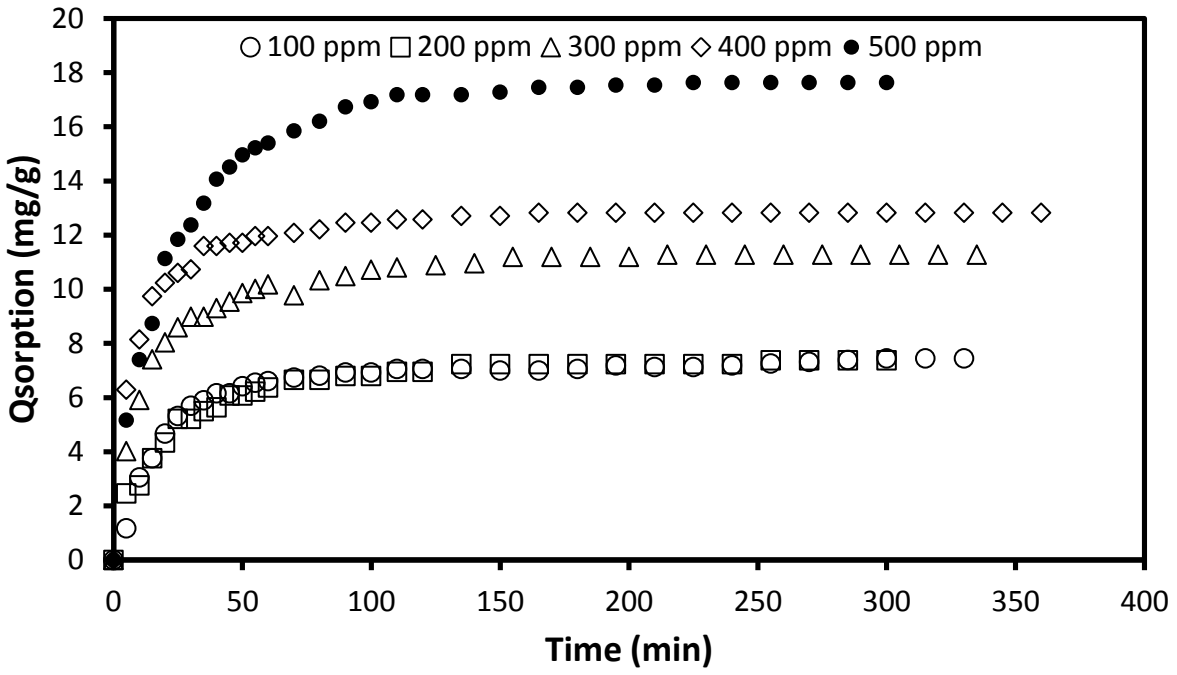

Figure 4-15: Amount of ciprofloxacin-HCl sorbed into fibroin film at varying initial concentrations.

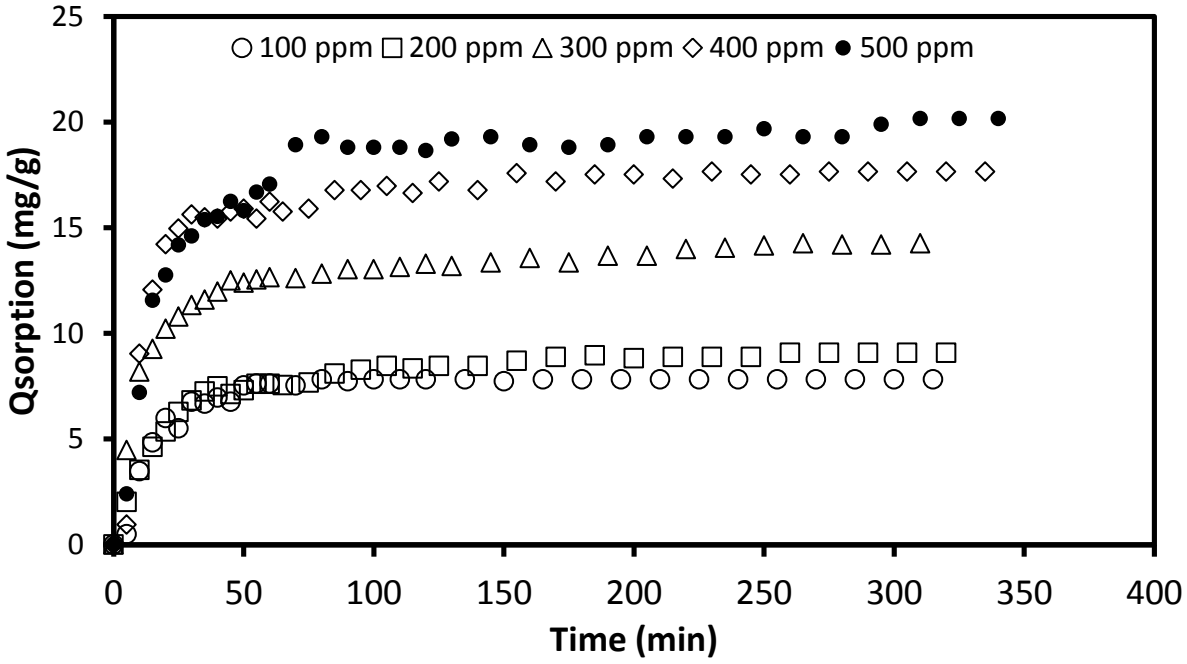

Figure 4-16: Amount of tetrahydrozoline-HCl sorbed into fibroin film at varying initial concentrations.

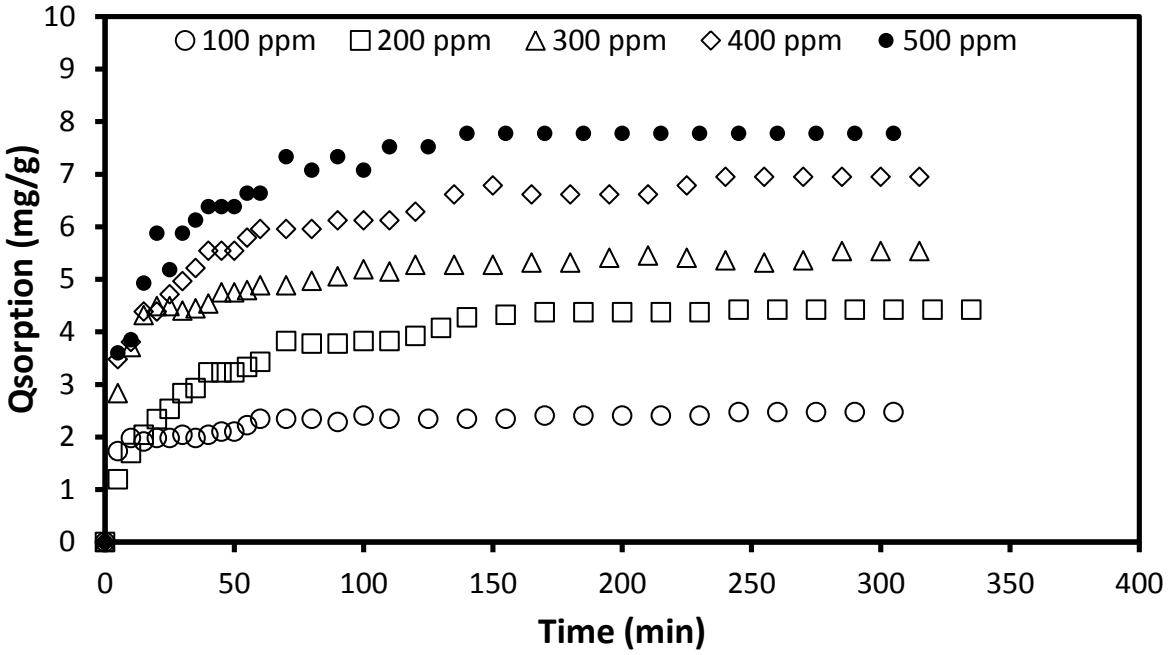

Figure 4-17: Amount of tetracycline-HCl sorbed into fibroin at varying initial concentrations.

To compare the sorption kinetics and determine drug diffusivity within the film, the experimental kinetic data were normalized by dividing the quantity of drug in the film by its equilibrium sorption uptake. The model represented in Equation 2-18 is applicable for solute diffusion into a sheet from a solution of limited volume (i.e. changing solute concentration in solution) (Crank, 1975). Most sorption kinetics trials showed minimal changes in drug concentration throughout their course (i.e. <10%), but several trials with the largest sorption uptake (i.e. with tetrahydrozoline-HCl or ciprofloxacin-HCl) showed modest changes in drug concentration of up to 25%. The diffusion coefficients for each drug concentration were estimated using non-linear regression with the normalized sorption kinetics data and the model shown in Eqn 2-18. To determine the diffusivity at each concentration, the experimental data were fit to the model shown in Eqn 2-18. An initial diffusivity coefficient was guessed, then an

iterative numerical solving method was employed to change the diffusivity coefficient until the sum of square errors between the experimental data and model was minimized. For the purposes of illustration, Figure 4-18 shows the normalized sorption kinetics data and model predictions for ciprofloxacin-HCl at 500 *ppm*.

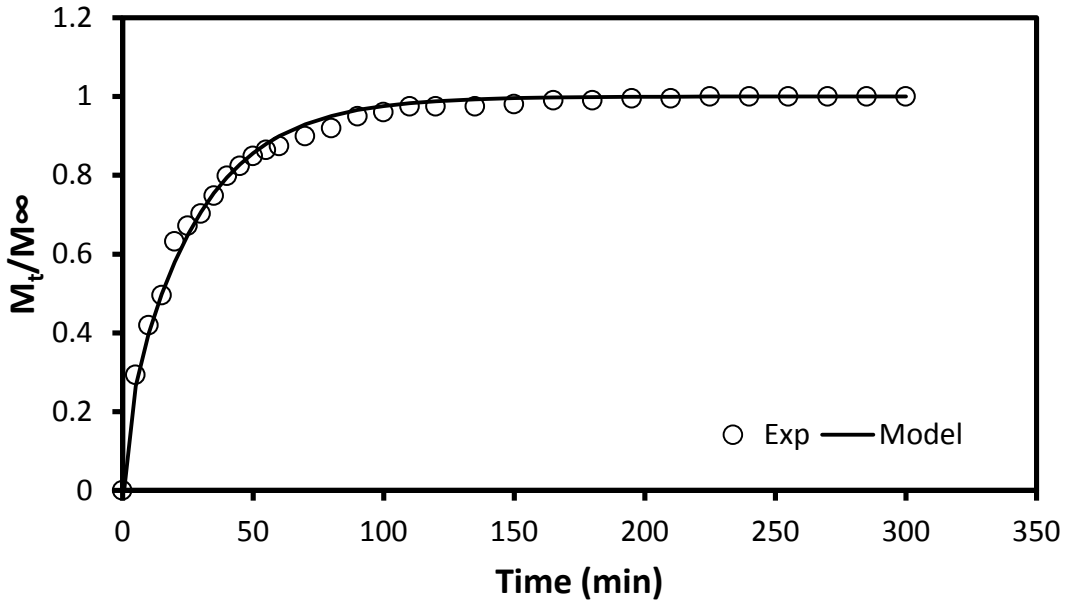

Figure 4-18: Experimental sorption kinetics and model prediction for ciprofloxacin-HCl at 500 ppm.

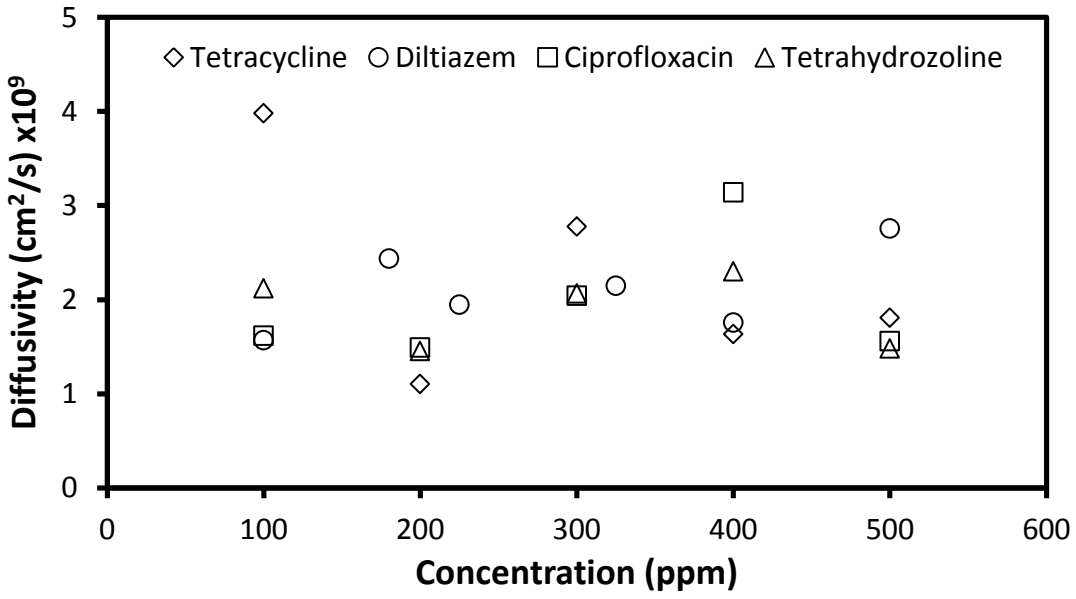

Figure 4-19: Conc. dependence of diffusion coefficients of four model drugs from sorption kinetics.

Figure 4-19 shows the model estimates of the diffusion coefficients based on the sorption kinetic data plotted against the initial drug concentration. The diffusivity based on sorption kinetics of each model drug in the fibroin film are approximately the same, and centered around 2 x 10^{-9} cm^2/s. No trend is observed between the diffusivity and the initial drug concentration for each of the four model drugs, indicating that the drug diffusivity within the fibroin film is independent of drug concentration. If the diffusivity is independent of the initial drug concentration, then the normalized sorption kinetics data at each concentration for an individual drug can be superimposed upon each other, and this is shown in Figure 4-20 to 4-23. Using non-linear regression, the diffusivity for each drug was determined from the combined data set. Table 4-6 lists the diffusivity values of the drugs so obtained, which represent the average diffusivity of the drug molecules in the fibroin film over the drug concentrations studied here. The model predictions using such diffusivity values are also presented in Figs 4-20 to 4-23, and there is a close agreement between the model calculations and the superimposed sorption kinetics data. This further supports the concentration independence of drug diffusion within the fibroin film.

Table 4-6: Model drug diffusivity estimates based on combined sorption kinetics.

Drug	$D_{Sorption}$ (cm^2/s) x 10^9
Diltiazem-HCl	1.86
Ciprofloxacin-HCl	1.81
Tetrahydrozoline-HCl	1.83
Tetracycline-HCl	1.84

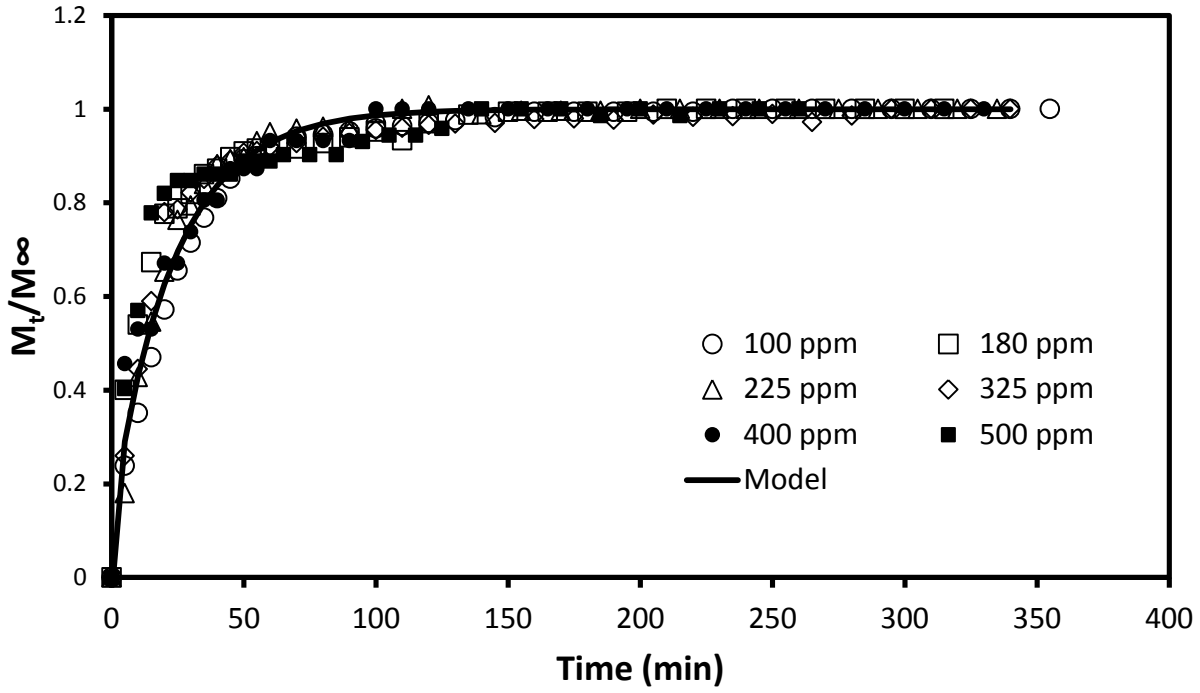

Figure 4-20: Superimposed normalized sorption kinetics in fibroin film for diltiazem-HCl.

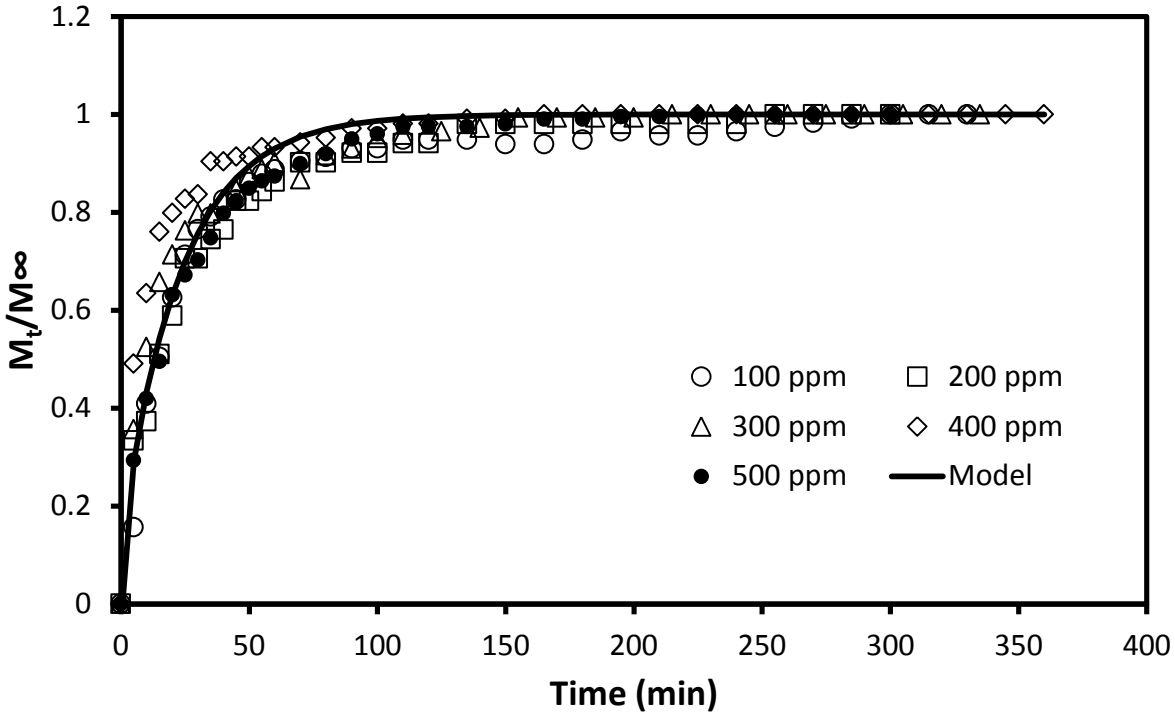

Figure 4-21: Superimposed normalized sorption kinetics in fibroin film for ciprofloxacin-HCl.

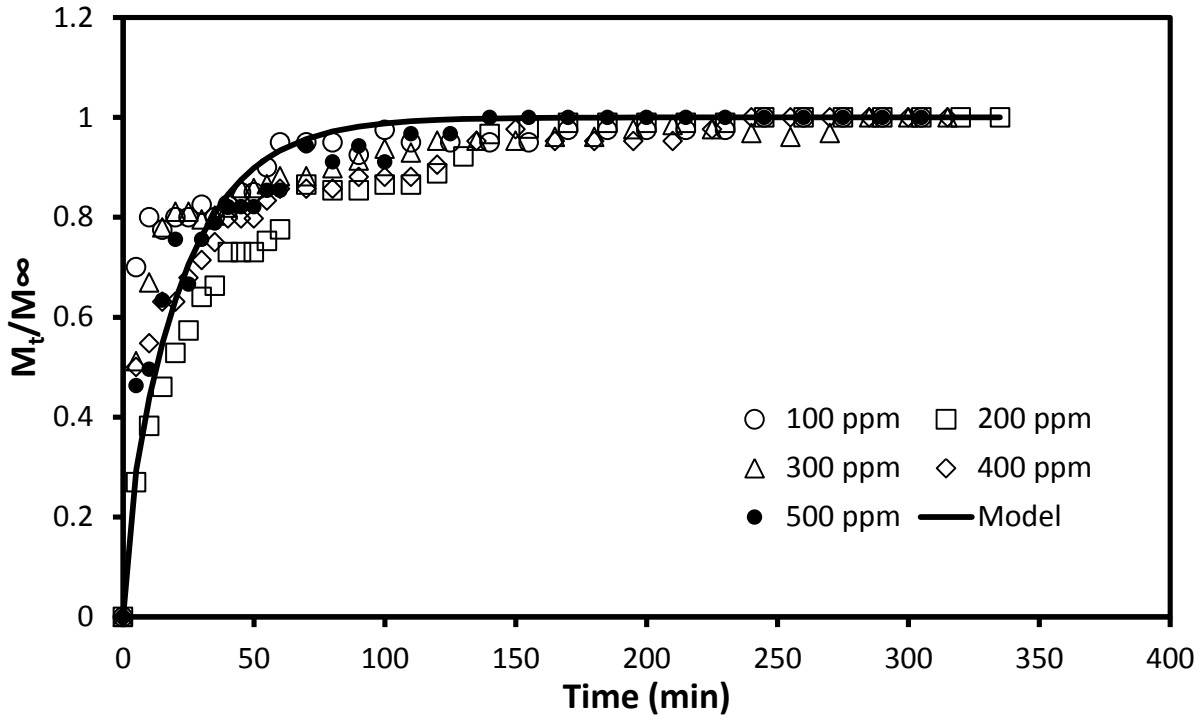

Figure 4-22: Superimposed normalized sorption kinetics in fibroin film for tetrahydrozoline-HCl at varying concentrations.

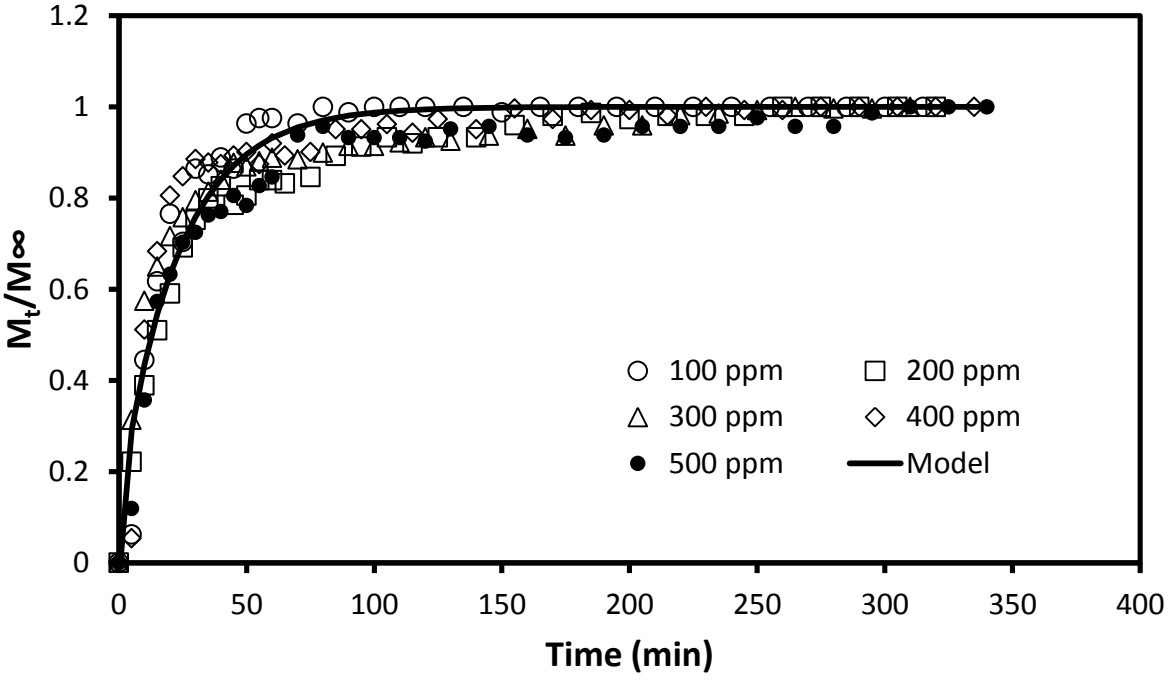

Figure 4-23: Superimposed normalized sorption kinetics in fibroin film for tetracycline-HCl at varying concentrations.

The diffusivity estimates based on sorption kinetics are very similar for each model drug, and are similar to drug diffusivities in other materials. Thacarodi and Rao (1993) examined the diffusivity of the anti-hypertensive drug nifedipine in a chitosan membrane, and found the diffusivity of the drug in the uncrosslinked membrane to be approximately 0.86 x 10^{-9} cm^2/s. Eslami (2011) found the diffusivity of ciprofloxacin-HCl and diltiazem-HCl in chitosan/sericin blend membranes from both sorption and desorption kinetic data. The diffusivity for ciprofloxacin-HCl were found to be 3.2-7.6 x 10^{-9} cm^2/s and 19.7-46.9 x 10^{-9} cm^2/s, respectively, based on the kinetics data of sorption and desorption. The diffusivity for diltiazem were 5.9-10.1 x 10^{-9} cm^2/s and 11.9-23.7 x 10^{-9} cm^2/s, respectively. Hines and Kaplan (2011) looked at the release mechanism, the effect of solute molecular mass and film crystallinity in the release of FITC-Dextran from regenerated fibroin films. They found that the release followed a diffusion model rather than an empirical exponential model, and that the diffusion coefficient decreased with increasing solute molecular mass as well as with increased crystallinity. The diffusion coefficients found to be in the range (0.30 – 4.74) x 10^{-9} cm^2/s with the lowest diffusivity resulting from high solute molecular weight and film crystallinity, while the highest diffusivity was found with low molecular weight solute and low film crystallinity. Comparing the diffusivity results from this experiment against solute molecular mass does not show a decreasing diffusivity with increasing molecular mass. This is mainly because the molecular weights of the four model drugs are not substantially different from each other, and different drugs with different interactions being compared may confound any small difference the molecular weight causes.

4.4.3 Desorption Kinetics and Diffusivity

In principle, drug diffusivity within the fibroin film can also be determined from the desorption kinetics. Figure 4-24 to 4-27 shows the kinetics of desorption of the four model drugs from the fibroin film. The desorption data show the amount of drug desorbed from the film per gram (dry weight) of the film. At a higher initial drug loading in the film, the amount of the drug desorbed from the film increases. These results are easy to understand, since an increased initial solution concentration will increase the sorption uptake, and for the drug desorption, a larger amount of drug loading in the film will result in a larger amount of drug desorbed from the fibroin film.

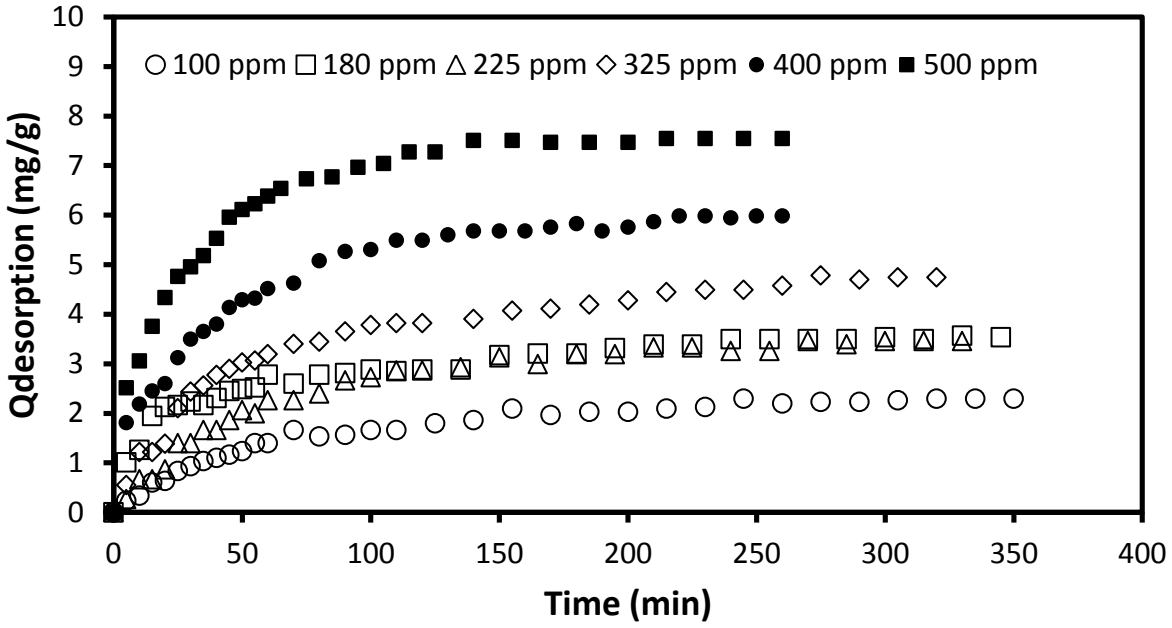

Figure 4-24: Amount of diltiazem-HCl desorbed from fibroin film at varying initial loading concentrations.

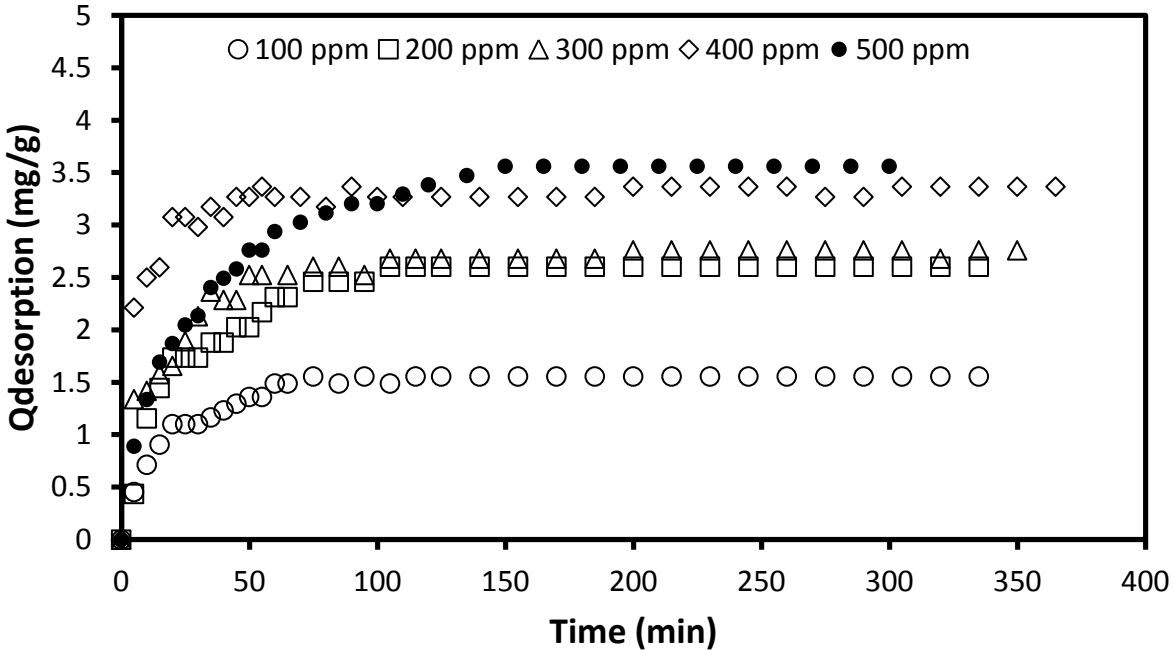

Figure 4-25: Amount of ciprofloxacin-HCl desorbed from fibroin film at varying initial loading concentrations.

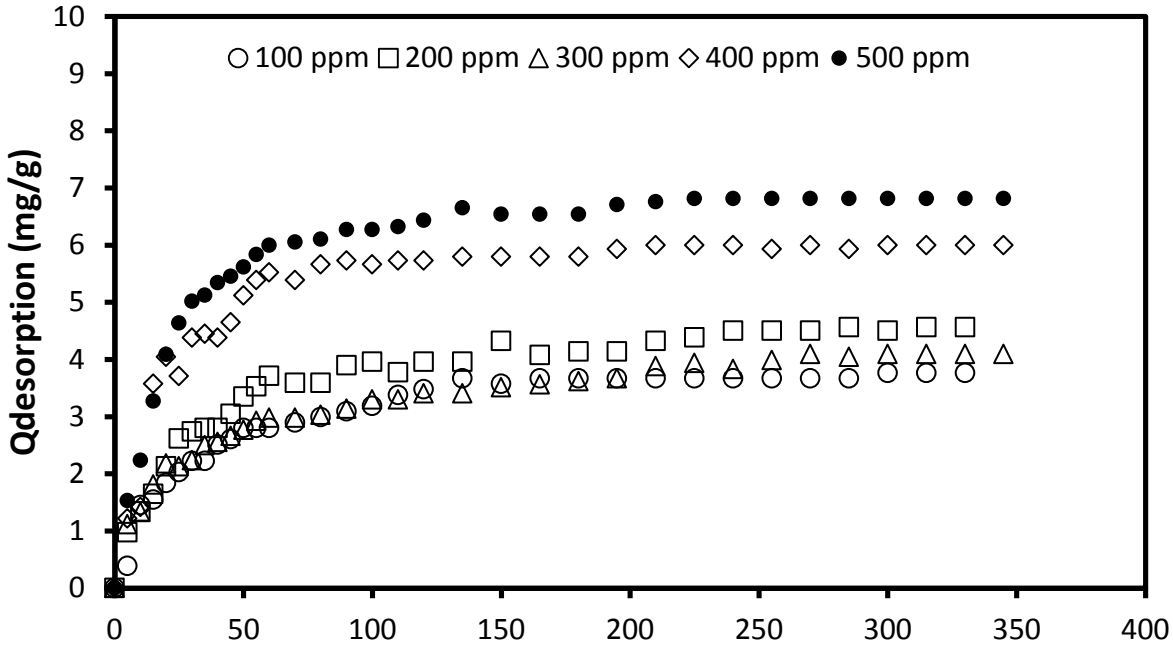

Figure 4-26: Amount of tetrahydrozoline-HCl desorbed from fibroin film at varying initial loading concentrations.

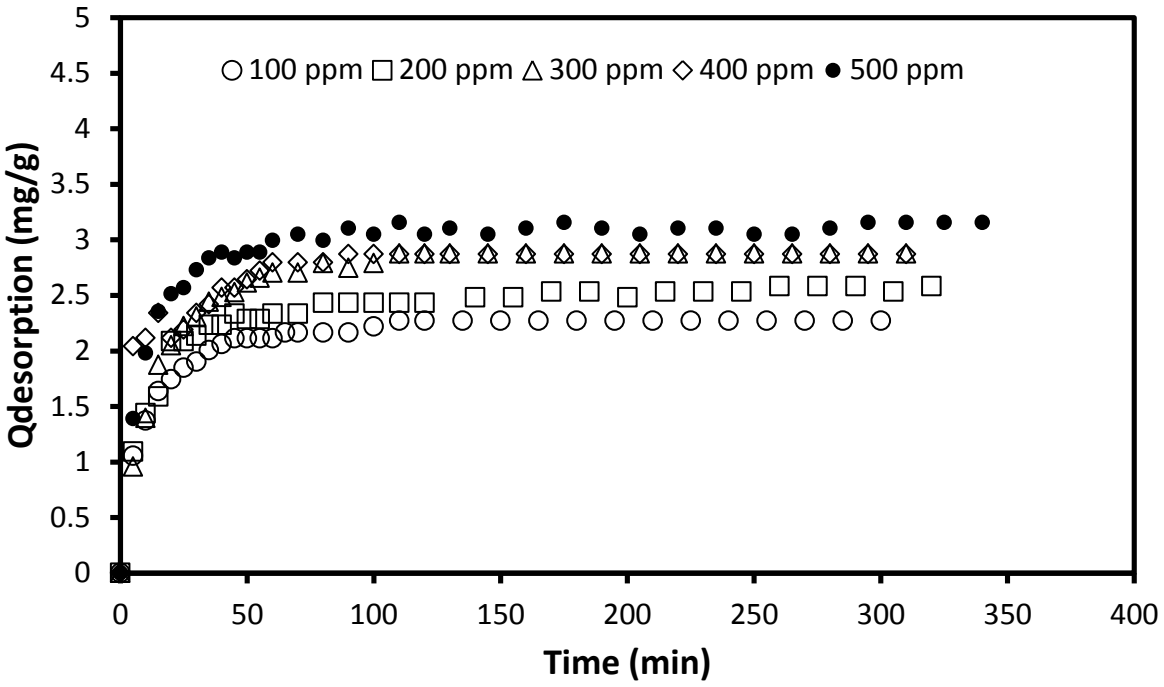

Figure 4-27: Amount of tetracycline-HCl desorbed from fibroin film at varying initial loading concentrations.

It needs to be mentioned that compared to the initial drug loading in the film, the amount of drug desorbed in a given amount of water (i.e. 50 *mL*) is less because desorption will cease to occur when the amount of drug remaining in the film is in equilibrium with the drug concentration in water. The amount of drug desorbed is 20-90% of the initial drug loading in the film, depending on the drug tested and the initial loading of the drug. This is in agreement with the equilibrium sorption isotherm shown in Fig 4-13. Table 4-7 shows the average relative amount of drug desorbed to the initial drug loading tested.

Table 4-7: Average relative drug desorption to initial drug loading.

Drug	Average Relative Desorption
Diltiazem-HCl	49%
Ciprofloxacin-HCl	25%
Tetrahydrozoline-HCl	39%
Tetracycline-HCl	57%

Tetracycline-HCl shows the largest amount of desorption, followed by diltiazem-HCl, then tetrahydrozoline-HCl, and finally ciprofloxacin-HCl which displays the least amount of desorption. This further shows that ciprofloxacin-HCl and tetrahydrozoline-HCl interact most strongly with the fibroin film which limits the amount of desorption that takes place. Conversely, tetracycline does not seem to interact with the film as strongly, and while this limits the initial loading onto the film, it leads to a higher fraction of the drug being released through desorption.

Similarly to the sorption kinetics, the desorption kinetics data was normalized by dividing the amount of drug desorbed from the film by the amount of drug desorbed at equilibrium. Non-linear regression was used with the normalized desorption data and the model (Eqn 2-18). For the purpose of illustration, the normalized desorption kinetics and model prediction are shown in Figure 4-28 for ciprofloxacin-HCl with an initial loading concentration of 500 *ppm.*

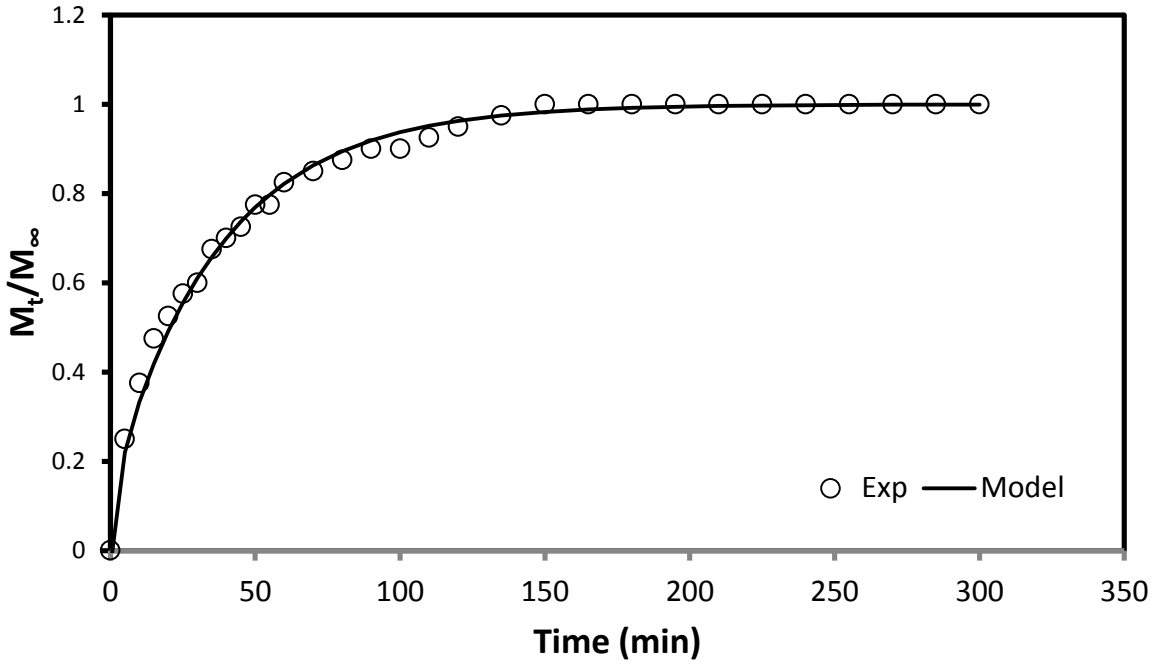

Figure 4-28: Experimental desorption kinetics and model prediction for ciprofloxacin-HCl at 500 ppm.

Figure 4-29 shows the model estimates of the diffusion coefficients based on the desorption kinetic data plotted against the initial drug loading concentration.

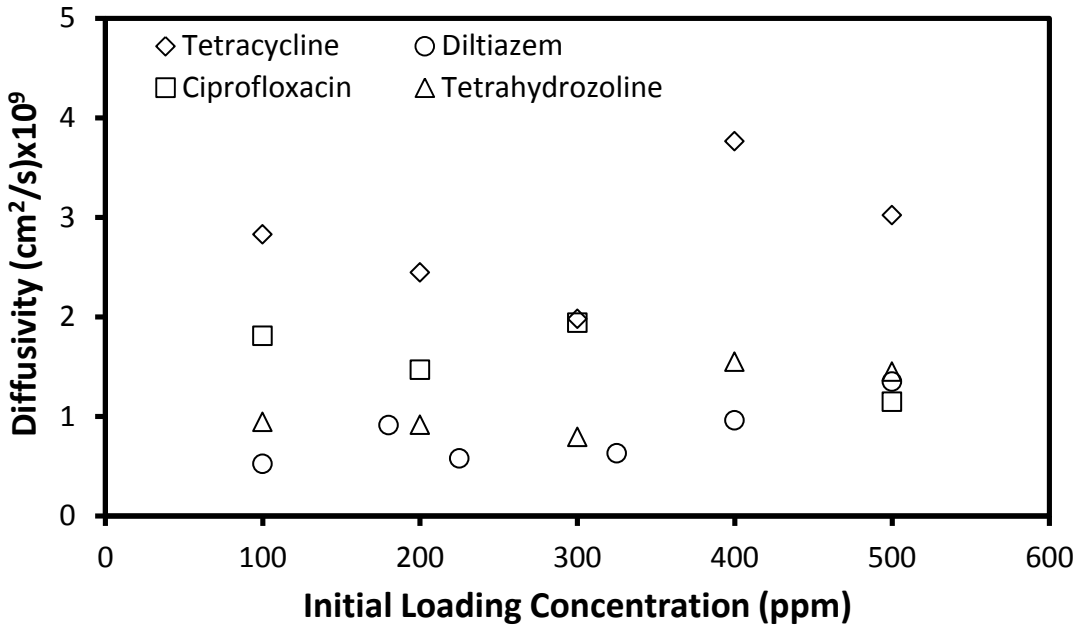

Figure 4-29: Concentration dependence of diffusivity coefficients for the four model drugs from desorption kinetic data.

The diffusivity estimates based on desorption kinetics show much greater variability drug-to-drug compared to the sorption kinetics estimates, but are still independent of concentration. Tetracycline-HCl shows the largest diffusivity of the four model drugs based on the desorption kinetics, while diltiazem-HCl and tetrahydrozoline show the lowest diffusivity.

Since the diffusion coefficients based on the desorption kinetics appear to be independent of concentration, the trials at different concentrations can be superimposed upon one another for each model drug. Figures 4-30 to 4-33 show the superimposed desorption kinetics and model predictions for the four model drugs.

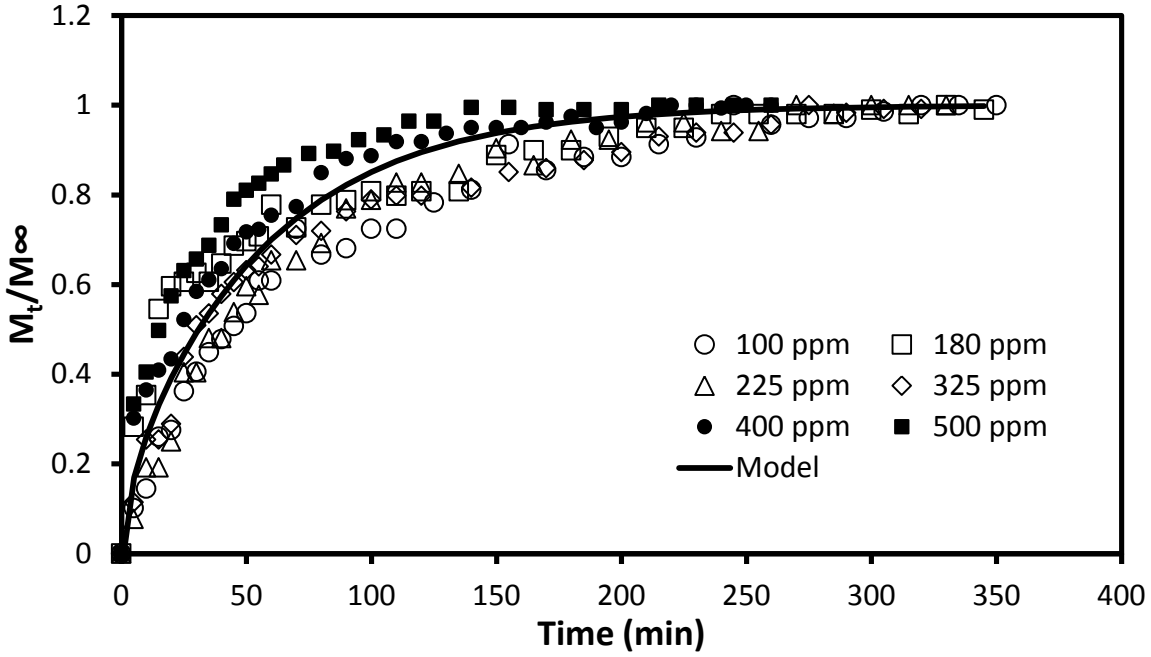

Figure 4-30: Superimposed normalized desorption kinetics for diltiazem-HCl.

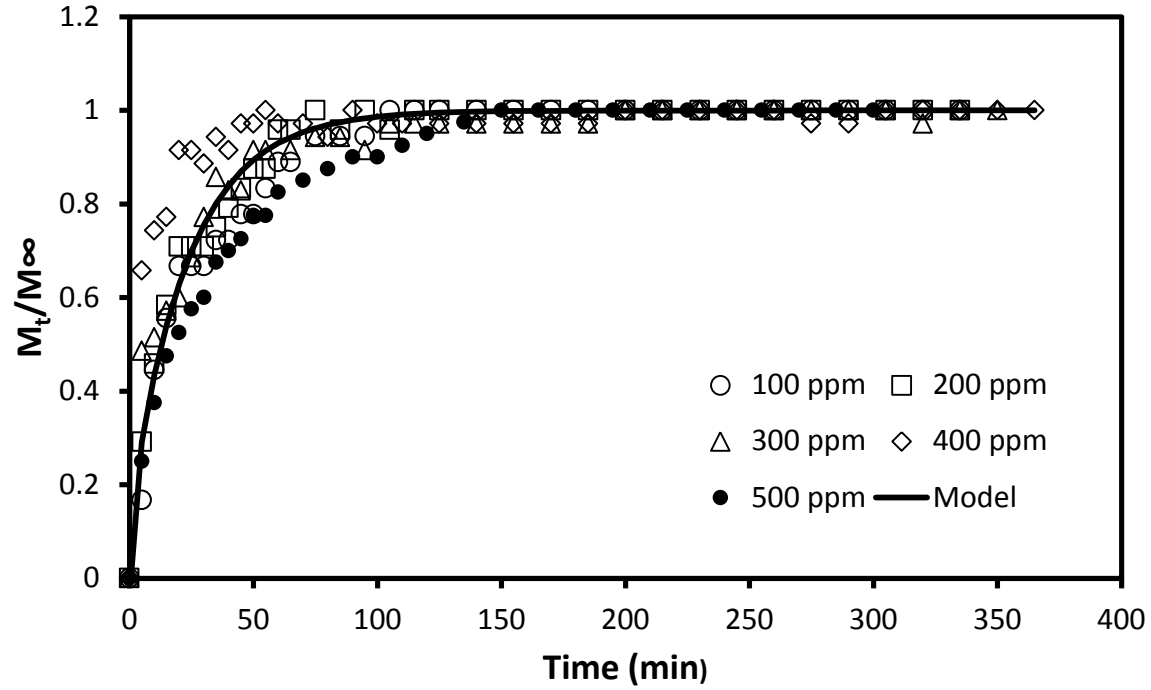

Figure 4-31: Superimposed normalized desorption kinetics for ciprofloxacin-HCl.

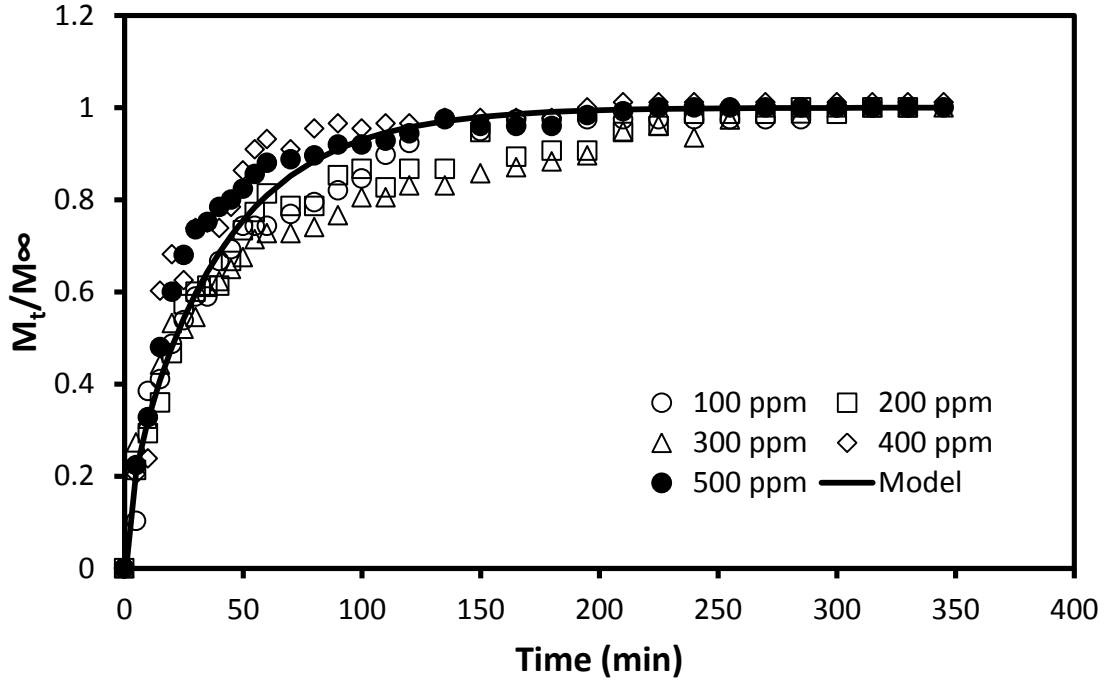

Figure 4-32: Superimposed normalized desorption kinetics for tetrahydrozoline-HCl.

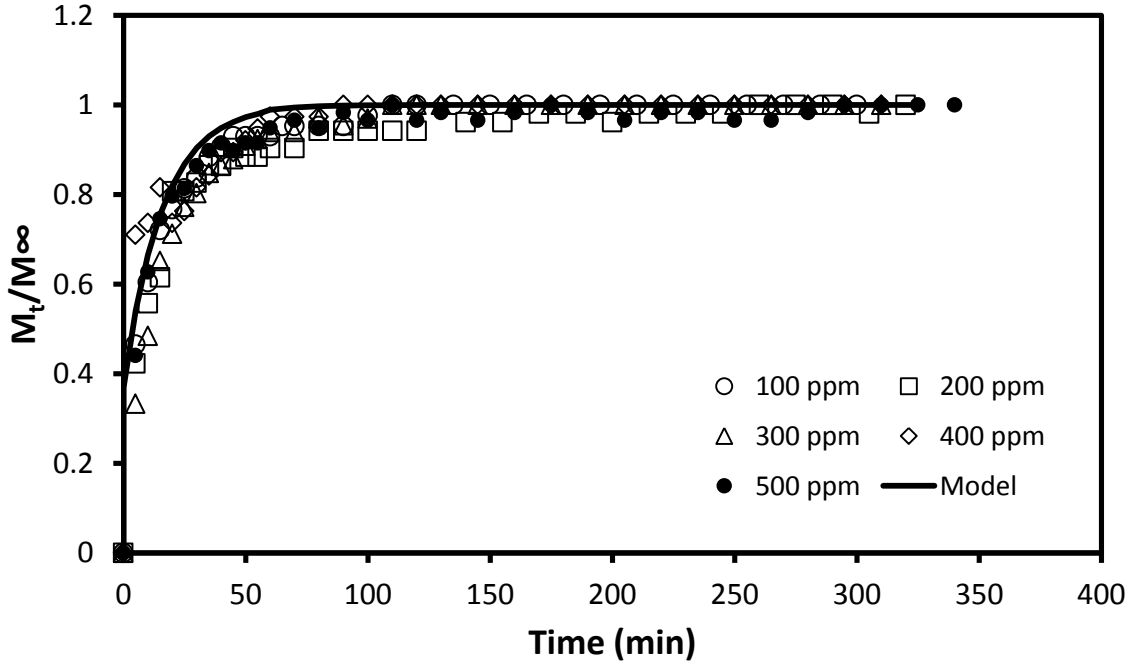

Figure 4-33: Superimposed normalized desorption kinetics for tetracycline-HCl.

The superimposed plots for the desorption kinetics shows less agreement between the different concentrations for individual drugs than the sorption kinetics. There still does not appear to be any clear trend in the desorption kinetics with concentration for any of the model drugs. The diffusivity for each model drug based on the combined desorption kinetic data set is shown in Table 4-8.

Table 4-8: Model drug diffusivity estimates based on combined desorption kinetics.

Drug	$D_{Desorption}$ (cm^2/s) x 10^9
Diltiazem-HCl	0.76
Ciprofloxacin-HCl	1.82
Tetrahydrozoline-HCl	1.09
Tetracycline-HCl	2.73

Diltiazem-HCl and tetrahydrozoline-HCl both display lower diffusivity based on the desorption kinetics than the diffusivity based on the sorption kinetics. The lower diffusivity in desorption may indicate stronger interactions between the drugs and the film that makes for quicker sorption and slower desorption. Tetracycline-HCl displays higher diffusivity from the desorption kinetics than from the sorption kinetics. This may indicate weaker or even repulsive interactions between tetracycline-HCl and the fibroin film. These results are consistent with the earlier permeability results, in which diltiazem-HCl, ciprofloxacin-HCl, and tetrahydrozoline-HCl all display greater permeability than tetracycline-HCl. Caution must be given to diffusivity estimates based on the desorption kinetics, since the model used to estimate the diffusivity is based upon sorption uptake, and the differences between sorption and desorption may make the model unreliable. In the latter case the drug concentration in the solution increases with time,

which deviates from the assumption of negligible change in drug concentration, a condition for the model to apply to the desorption process.

4.4.4 Solubility and Partition Coefficient for Drugs in Fibroin

A partition coefficient is the ratio of concentrations of a solute in two immiscible phases at equilibrium, which indicates the difference in solubility of the solvent in the two phases. The permeability of the solute is related to the partition coefficient and diffusivity. As a first approximation,

$$P = S \cdot D \tag{4-3}$$

where S is the partition coefficient. The partition coefficient can therefore be found from the ratio of the permeability and diffusivity. Figure 4-34 shows the partition coefficients for each model drug at varying drug concentrations.

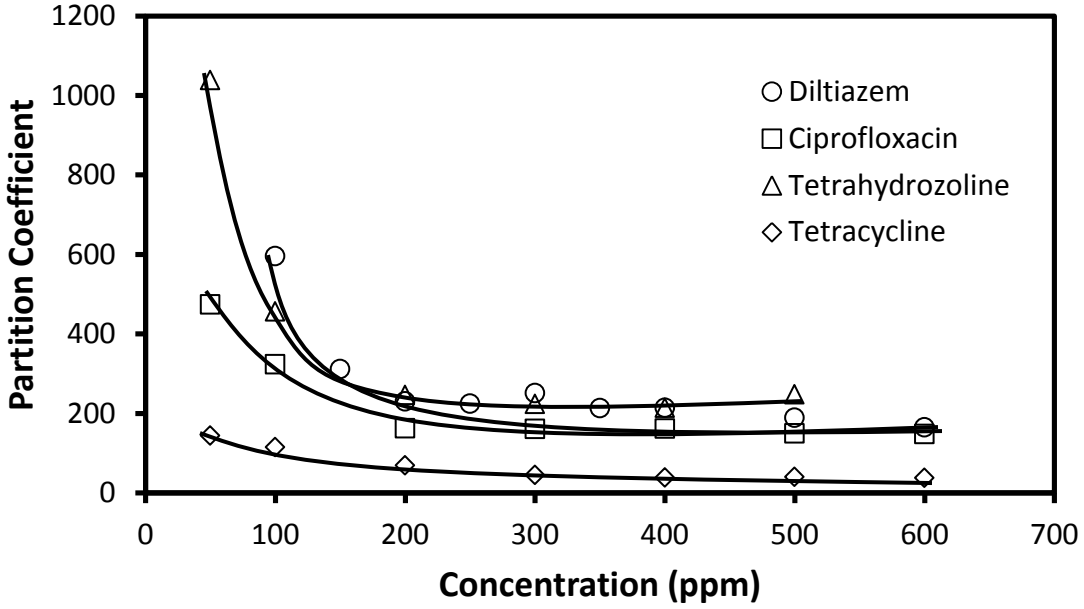

Figure 4-34: Partition coefficients of each model drug at varying drug concentration.

Since the diffusion coefficient is concentration independent, the partition coefficient follows the same trend as permeability. At low concentrations, the partition coefficient quickly decreases with increasing drug concentration, and as the concentration exceeds approximately 200 *ppm*, the partition coefficient becomes constant with further increases in drug concentration. For each model drug, the partition coefficients are well above unity (i.e. $S > 1$), indicating that the model drugs are much more "soluble" in the fibroin membrane than in water. This is consistent with the sorption data shown in Fig 4-12, which also showed that the drug molecules were substantially "enriched" in the fibroin film.

Chapter 5: **Conclusions**

Several properties of silk fibroin film were examined to determine the potential applicability of fibroin in several applications. The adsorption of bovine serum albumin to the fibroin film was conducted to explore its biocompatibility. The gas permeability of oxygen, nitrogen, and carbon dioxide was determined to gauge applicability of the fibroin film for uses in contact lenses and wound dressings where the gas transmissibility is of great interest. The permeability, diffusivity, and solubility of four model drugs in the fibroin film were determined for controlled drug release. The following conclusions can be drawn from this study:

(1) The fibroin film adsorbs bovine serum albumin at levels up to 0.045 *mg/cm*^{2} of film at an equilibrium concentration of 10 *mg BSA/mL* in solution. The BSA adsorption followed the Freundlich isotherm, with Freundlich parameters $a = 3.5x10^{-3}$ and $1/n = 1.203$. The levels of BSA adsorption suggest that the fibroin film will display good blood compatibility, which indicates strong potential for fibroin film in biocompatible material applications.

(2) Over the pressure range (70-350 kPag) tested, oxygen and nitrogen display a constant permeability of 5 *Barrer*, while carbon dioxide permeability (ranging from 26-37 *Barrer*) decreases with pressure. The oxygen transmissibility of the fibroin film is 19.2 x 10^{-9} *(cm·mL* O_2*)/(s·mL·mmHg)*, just under the critical oxygen transmissibility of 24.1 x 10^{-9} *(cm·mL* O_2*)/(s·mL·mmHg)* required to prevent corneal edema for daily wear contact lenses. While the fibroin film is not suitable for use in contact lenses in its current form as far as the oxygen transmissibility is concerned, fibroin film shows potential for use in wound dressings where the

oxygen permeability will elevate oxygen tension at the wound surface when used in wound dressings to aid in healing.

(3) For the four model drugs (i.e., diltiazem-HCl, ciprofloxacin-HCl, tetrahydrozoline-HCl, and tetracycline-HCl), an increase in the initial source drug concentration increases the permeation rate of drug through the membrane. At low drug concentrations (i.e. <200 *ppm*), the permeability coefficient of the drug decreases with an increase in the drug concentration. At relatively high drug concentrations (200 – 600 *ppm*), the drug permeability becomes independent of drug concentration, with a permeability coefficient of 4.1 x 10^{-7} cm^2/s for diltiazem-HCl, 2.9 x 10^{-7} cm^2/s for ciprofloxacin-HCl, 4.3 x 10^{-7} cm^2/s for tetrahydrozoline-HCl, and 0.8 x 10^{-7} cm^2/s for tetracycline-HCl.

(4) During sorption and desorption experiments, increasing initial drug concentration increased sorption uptake into the fibroin, which in turn increased the amount of drug desorbed. Tetrahydrozoline-HCl shows the greatest sorption onto fibroin (20.2 mg/cm^2) at an initial concentration of 500 *ppm*, compared to 17.6 mg/cm^2 for ciprofloxacin-HCl, 12.5 mg/cm^2 for diltiazem-HCl, and 7.8 mg/cm^2 for tetracycline-HCl. From the sorption kinetics data, the drug diffusivity is determined to be 1.81 x 10^{-9} cm^2/s for diltiazem-HCl, 1.83 x 10^{-9} cm^2/s for of ciprofloxacin-HCl, 1.86 x 10^{-9} cm^2/s tetrahydrozoline-HCl, and 1.84 x 10^{-9} cm^2/s for tetracycline-HCl. The fibroin film displays drug permeability and diffusivity at levels comparable to other drugs and materials, and it shows good potential for use in controlled drug release applications.

Chapter 6 – **Recommendations**

To further understand and develop fibroin film as a material for the applications investigated, further work should be undertaken and the following are recommended.

1. The film crystallinity should be quantified through FTIR analysis and compared against that of the fibroin films reported in the literature.
2. To further examine the blood compatibility of the film, competitive adsorption experiments between albumin, fibrinogen, and other blood constituent molecules on the fibroin film should be completed to determine which molecules adsorb preferentially, if any.
3. The film crystallinity should be modified through alcohol treatment and the oxygen permeability investigated to determine if changes in the crystallinity will increases the permeability enough for use in contact lenses.
4. The effects of different film blend formations on oxygen permeability for contact lenses are well as healing potential and brittleness in wound dressings should be investigated.
5. To understand the interactions between the drug and the film, the drug-loaded fibroin film may be analyzed and characterized through techniques such as FTIR and NMR spectroscopy.
6. Different model drugs with differing characteristics such as hydrophobicity or water solubility should be investigated to further understand their effects on membrane loadings and release of the drugs in fibroin films.

7. The drug release may be controlled using many different forms of the fibroin, including bulk-loading of the drugs in films during preparation, microspheres, nano-particles, and hydrogels, and these should be investigated to identify the most effective release mode.

References

Akgol, S., Turkman, D., Denizli, A. (2004). Cu(II)-incorporated, histidine-containing, magnetic-metal-complexing beads as specific sorbents for the metal chelate affinity of albumin. *Journal of Applied Polymer Science*. 93 (6), 2669-2677.

Altman, G.H., Diaz, F., Jakuba, C., Calabro, T., Horan, R.L., Chen, J., Lu, H., Richmond, J., Kaplan, D.L. (2003). Silk-based biomaterials. *Biomaterials*. 24(3), 401-416.

Altman, G.H., Horan, R.L., Lu, H.H., Moreau, J., Marin, I., Richmond, J.C., Kaplan, D.L. (2002). Silk matrix for tissue engineered anterior cruciate ligaments. *Biomaterials*. 23 (20), 4131-4141.

Arai, T., Freddi, G., Innocenti, R., Tsukada, M.. (2004). Biodegradation of bombyx mori silk fibroin fibers and films. *Journal of Applied Polymer Science*. 91 (4), 2383-2390.

Avremescu, M.E., Sager, W.F.C., Wessling, M. (2003). Functionalized ethylene vinyl alcohol copolymer (EVAL) membranes for affinity protein separation. *Journal of Membrane Science*. 216 (1-2), 177-193.

Baker, R.W (2004). *Membrane Technology and Applications*. 2nd ed. Wiley. 15-84.

Baycin, D., Altiok, E., Ulku, S., Bayraktar, O. (2007). Adsorption of olive leaf (Olea europaea L.) antioxidants on silk fibroin. *Agricultural and Food Chemistry*. 55 (4), 1227-1236.

Bini, E.,Knight, D.P., Kaplan, D.L. (2004). Mapping domain structures in silks from insects and spiders related to protein assembly. *Journal of Molecular Biology*. 335 (1), 27-40.

Bowen, W.R., Hughes, D.T. (1990). Properties of microfiltration membranes. Part 2. Adsorption of bovine serum albumin at aluminum oxide membranes. *Journal of Membrane Science*. 51 (1-2), 189-200.

Cao, Y., Wang, B. (2009). Biodegradation of silk biomaterials. *International Journal of Molecular Sciences*. 10 (4), 1514-1524.

Carter, D.C., Ho, J.X. (1994). Structure of serum albumin. *Advances in Protein Chemistry*. 45 (1), 153-203.

Chen, J., Minoura, N., Tanioka, A. (1994). Transport of pharmaceuticals through silk fibroin membrane. *Polymer*. 35 (13), 2853-2856.

Chen, M., Shao, Z., Chen, X. (2012). Paclitaxel-loaded silk fibroin nanospheres. *Journal of Biomedical Materials Research Part A*. 100 (1), 203-210.

Chen, Y., Zhang, Y., Feng, X. (2010). An improved approach for determining permeability and diffusivity relevant to controlled release. *Chemical Engineering Science*. 65 (22), 5921-5928.

Choi, H.M., Bide, M., Phaneuf, M., Quist, W., Logerfo, F. (2004). Antibiotic treatment of silk to produce novel infection-resistant biomaterials. *Textile Research Journal*. 74 (4), 333-342.

Crank, J (1975). *The Mathematics of Diffusion*. 2nd ed. Oxford University Press. 56-57.

Dahlke, H., Dociu, N., Thurau, K. (1980). Thrombogenicity of different suture materials as revealed by scanning electron microscopy. *Journal of Biomedical Materials Research*. 14 (3), 251-268.

Dyakonov, T., Yang, C.H., Bush, D., Gosangari, S., Majuru, S., Fatmi, A. (2012). Design and characterization of a silk-fibroin based drug delivery platform using naproxen as a model drug. *Journal of Drug Delivery*. 2012 (1), 1-10.

Eslami, S. (2011). *Chitosan-Sericin Blend Membranes for Controlled Release of Drugs*. MASc Thesis. University of Waterloo, Waterloo.

Fang, J.Y., Chen, J.P., Leu, Y.L., Wang, H.Y. (2006). Characterization and evaluation of silk protein hydrogels for drug delivery. *Chemical and Pharmaceutical Bulletin*. 54 (2), 156-162.

Fonn, D., Sweeny, D., Holden, B.A., Cavanagh, D. (2005). Corneal oxygen deficiency. *Eye & Contact Lens*. 31 (1), 23-27.

Gimenes, M.L., Liu, L., Feng, X.. (2007). Sericin/poly(vinyl alcohol) blend membranes for pervaperation separation of ethanol/water mixtures. *Journal of Membrane Science*. 295, 71-79.

Granite, E.J., O'Brien, T. (2005). Review of novel methods for carbon dioxide separation from flue and fuel gases. *Fuel Processing Technology*. 86 (14-15), 1423-1434.

Henry, M.A. (2006). *Oxygen/Nitrogen Separation Using Cobalt Containing Membranes*. MASc Thesis. University of Waterloo, Waterloo.

Hines, D.J., and Kaplan, D.L. (2011). Mechanisms of controlled release from silk fibroin films. *Biomacromolecules*. 12 (3), 804-812.

Hitchcock, D.LI. (1925). Protein films on collodion membranes. *The Journal of General Physiology*. 8 (2), 61-74.

Hoffman, A.S. (2008). The origins and evolution of "controlled" drug delivery systems. *Journal of Controlled Release*. 132 (3), 153-163.

Holden, B.A., Mertz, G.W. (1984). Critical oxygen levels to avoid corneal edema for daily and extended wear contact lenses. *Investigative Ophthalmology & Visual Science*. 25 (10), 1161-1167.

Horan, R.L., Antle, K., Collette, A.L., Wang, Y., Huang, J., Moreau, J.E., Volloch, V., Kaplan, D.L., Altman, G.H. (2005). In vitro degradation of silk fibroin. *Biomaterials*. 26 (17), 3385-3393.

Hu, K., Lv, Q., Cui, F.Z., Feng, Q.L., Kong, X.D., Wang, H.L., Huang, L.Y., Li, T. (2006). Biocompatible fibroin blended films with recombinant human-like collagen for hepatic tissue engineering. *Journal of Bioactive and Compatible Polymers*. 21 (1), 23-37.

Jain, S.K., Chourasia, M.K., Sabitha, M., Jain, R., Jain, A.K., Ashawat, M., Jha, A.K. (2003). Development and characterization of transdermal drug delivery systems for diltiazem hydrochloride. *Journal of Drug Delivery*. 10 (3), 169-177.

Jin, H.J., Park, J., Valluzii, R., Cebe, P., Kaplan, D. (2004). Biomaterial films of bombyx mori silk fibroin with poly(ethylene oxide). *Biomacromolecules*. 5 (1), 711-717.

Kaelble, D.H., Moacanin, J. (1977). A surface energy analysis of bioadhesion. *Polymer*. 18 (5), 475-482.

Karch, A.M (2012). *2013 Lippincott's Nursing Drug Guide*. Lippincott Williams & Wilkins. 282, 382, 1101-1103.

Karve, K.A., Gil, E.S., McCarthy, S.P., Kaplan, D.L. (2011). Effect of β-sheet crystalline content on mass transfer in silk films. *Journal of Membrane Science*. 383 (1-2), 44-49.

Kweon, H., Ha, H.C., Um, I.C., Park, Y.H. (2001). Physical properties of silk fibroin/chitosan blend films. *Journal of Applied Polymer Science*. 80 (7), 928-934.

Langer, R.S., Peppas, N.A. (1981). Present and future applications of biomaterials in controlled drug delivery systems. *Biomaterials*. 2 (1), 201-214.

Lee, K.Y., Kong, S.J., Park, W.H., Ha, W.S., Kwon, I.C. (1998). Effect of surface properties on the antithrombogenicity of silk fibroin/S-carboxymethyl kerateine blend films. *Journal of Biomaterials Science, Polymer Edition*. 9 (9), 905-914.

LeVan, M.D., Carta, G., Yon, C.M. (1999). Adsorption and Ion Exchange. In: Perry, R.H., Green, D.W., Maloney, J.O *Perry's Chemical Engineer's Handbook*. 7th ed. McGraw-Hill. 16-1 - 16-66.

Liu, L., Chakma, A., Feng, X. (2005). CO_2/N_2 separation by poly(ether block aminde) thin film hollow fiber composite membranes. *Industrial & Engineering Chemistry Research*. 44 (17), 6874-6882.

Liu, X.Y., Zhang, C.C., Xu, W.L., Ouyang, C.X. (2009). Controlled release of heparin from blended polyurethane and silk fibroin film. *Materials Letters*. 63 (2), 263-265.

Lu, Q., Wang, X., Hu, X., Cebe, F., Omenetto, F., Kaplan, D.L. (2010). Stabilization and release of enzymes from silk films. *Macromolecular Bioscience*. 10 (4), 359-368.

Lucas, F., Shaw, J.T.B., Smith, S.G. (1957). The amino acid sequence in a fraction of the fibroin of bombyx mori. *Biochemical Journal*. 66 (3), 468-479.

Lui, C., Bai, R. (2005). Preparation of chitosan/cellulose acetate blend hollow fibers for adsorptive performance. *Journal of Membrane Science*. 267 (1-2), 68-77.

McCabe, W.L., Smith, J.C., Harriot, P (1993). *Unit Operations of Chemical Engineering*. 5th ed. McGraw-Hill. 814.

McClelland, G.A., Sutton, S.C., Engle, K., Zentner, G.M. (1991). The solubility-modulated osmotic pump: in vitro/in vivo release of diltiazem hydrochloride. *Pharmaceutical Research*. 8 (1), 88-92.

Min, B.M., Lee, G., Kim, S.H., Nam, Y.S., Lee, T.S., Park, W.H. (2004). Electrospinning of silk fibroin nanofibers and its effect on the adhesion and spreading of normal human keratinocytes and fibroblasts in vitro. *Biomaterials*. 25 (7-8), 1289-1297.

Min, S., Gao, X., Han, C., Chen, Y., Yang, M., Zhu, L., Zhang, H., Lui, L., Yao, J. (2012). Preparation of silk fibroin spongy wound dressing and its therapeutic efficiency in skin defects. *Journal of Biomaterials Science*. 23 (1), 97-110.

Minoura, N., Aiba, S.I., Higuchi, M., Gotoh, Y., Tsukada, M., Imai, Y. (1995). Attachment and growth of fibroblast cells on silk fibroin. *Biochemical and Biophysical Research Communications*. 208 (2), 511-516.

Minoura, N., Tsukada, M., Nagura, M.. (1990). Physico-chemical properties of silk fibroin membrane as a biomaterial. *Biomaterials*. 11, 430-434.

Motta, A., Fambri, L., Migliaresi, C.. (2002). Regenerated silk fibroin films: thermal and dynamic mechanical analysis. *Macromolecular Chemistry and Physics*. 203 (10), 1658-1665.

Park, W.H., Ha, W.S., Ito, H., Miyamoto, T., Inagaki, H., Noishiki, Y. (2001). Relationships between antithrombogenicity and surface free energy of regenerated silk fibroin films. *Fibers and Polymers*. 2 (1), 58-63.

Pauling, L. (1945). The adsorption of water by proteins. *Journal of the American Chemical Society*, 67, 555-557.

Peters, T. (1975). Serum Albumin. In: Putnam, F.W. *The Plasma Proteins: Structure, Function, and Genetic Control*. 2nd ed. Academic Press. p133-181.

Pitt, W.G., Park, K., Cooper, S.L. (1986). Sequential protein adsorption and thrombus deposition on polymeric biomaterials. *Journal of Colloid and Interface Science*. 111 (2), 343-362.

Pra, I.D, Freddi, G., Minic, J., Chiarini, A., Armato, U. (2006). De novo engineering of reticular connective tissue in vivo by silk fibroin nonwoven materials. *Biomaterials*. 26 (1), 1987-1999.

Pritchard, E.M., Kaplan, D.L. (2011). Silk fibroin biomaterials for controlled release drug delivery. *Expert Opinion on Drug Delivery*. 8 (6), 797-811.

Pritchard, E.M., Valentin, T., Boison, D., Kaplan, D.L. (2011). Incorporation of proteinase inhibitors into silk-based delivery devices for enhanced control of degradation and drug release. *Biomaterials*. 32 (3), 909-918.

Rodriguez, P.G., Felix, F.N., Woodley, D.T., Shim, E.K. (2008). The role of oxygen in wound healing: a review of the literature. *Dermatologic Surgery*. 34 (9), 1159-1169.

Roh, D.H., Kang, S.Y., Kim, J.Y., Kwon, Y.B., Kweon, H.Y., Lee, K.G., Park, Y.H., Baek, R.M., Heo, C.Y., Choe, J., Lee, J.H. (2006). Wound healing effect of silk fibroin/alginate-blended sponge in full thickness skin defect of rat. *Journal of Materials Science: Materials in Medicine*. 17 (6), 547-552.

Sanders, R. (1999). *Compilation of Henry's Law Constants for Inorganic and Organic Species of Potential Importance in Environmental Chemistry*. Available: http://www.ceset.unicamp.br/~mariaacm/ST405/Lei%20de%20Henry.pdf. Last accessed 11th Feb 2013.

Sano H., Ichioka S., Sekiya N. (2012). Influence of oxygen on wound healing dynamics: assessment in a novel wound mouse model under a variable oxygen environment. *PLoS ONE*. 7(11): e50212. doi:10.1371/journal.pone.0050212

Santin, M., Motta, A., Freddi, G., Cannas, M. (1999). In vitro evaluation of the inflammatory potential of the silk fibroin. *Journal of Biomedical Materials Research*. 46 (3), 382-389.

Sashina, E.S., Golubikhin, A.Y., Novoselov, N.P., Tsobkallo, E.S., Zaborskii, M., Goralskii, Y. (2009). Study of possibility of applying the films of silk fibroin and its mixtures with synthetic polymers for creating the materials of contact lenses. *Russian Journal of Applied Chemistry*. 82 (5), 898-904.

Silva, S.M., Motta, A., Rodrigues, M.T., Pinheiro, A.F.M., Gomes, M.E., Mano, J.F., Reis, R.L., Migliaresi, C. (2008). Novel genipin-cross-linked chitosan/silk fibroin sponges for cartilage engineering strategies. *Biomacromolecules*. 9 (1), 2764-2774.

Sionkowski, A. (2011). Current research on the blends of natural and synthetic polymers as new biomaterials: Review. *Progress in Polymer Science*. 36, 1254-1276.

Sofia, S., McCarthy, M.B., Gronowicz, G., Kaplan, D.L.. (2001). Functionalized silk-based biomaterials for bone formation. *Journal of biomedical materials research*. 54 (1), 139-148.

Szycher, M., Lee, S.J. (1992). Modern wound dressings: a systematic approach to wound healing. *Journal of Biomaterials Applications*. 7 (2), 142-213.

Tang, X., Ding, F., Yang, Y., Hu, N., Wu, H., Gu, X. (2009). Evaluation on in vitro biocompatibility of silk fibroin-based biomaterials with primarily cultured hippocampal neurons.. *Journal of Biomedical Materials Research Part A*. 91 (1), 166-174.

United States Pharmacopeia. (2009). *Solubilities.* Available: http://www.drugfuture.com/Pharmacopoeia/USP32/pub/data/v32270/usp32nf27s0_m6h00100.html. Last accessed 22nd April 2013.

Van Enckevort, H.J., Dass, D.V., Langdon, A.G.. (1984). The adsorption of bovine serum albumin at the stainless-steel/aqueous solution interface. *Journal of Colloid and Interface Science*. 98 (1), 138-143.

Varanda, F., Pratas de Melo, M.J., Caco, A.I., Dohrn, R., Makrydaki, F.A., Voutsas, E., Tassios, D., Marrucho, I.M. (2006). Solubility of antibiotics in different solvents. 1. Hydrochloride forms of tetracycline, moxifloxacin, and ciprofloxacin. *Industrial & Engineering Chemistry Research*. 45 (18), 6368-6374.

Voet, D., Voet, J.G (2004). *Biochemistry*. 3rd ed. Wiley. 66-67.

Wang, Y., Rudym, D.D., Walsh, A., Abrahamsen, L., Kim, H.J., Kim, H.S., Kirker-Head, C., Kaplan, D.L. (2008). In vivo degradation of three-dimensional silk fibroin scaffolds. *Biomaterials*. 29 (24-25), 3415-3428.

Wang, X., Hu, X., Daley, A., Rabotyagova, O., Cebe, P., Kaplan, D.L. (2007a). Nanolayer biomaterial coatings of silk fibroin for controlled release. *Journal of Controlled Release*. 121 (3), 190-199.

Wang, X., Wenk, E., Matsumoto, A., Meinel, L., Li, C., Kaplan, D.L. (2007b). Silk microspheres for encapsulation and controlled release. *Journal of Controlled Release*. 117 (3), 360-370.

Wenk, E., Merkle, H.P., Meinel, L. (2011). Silk fibroin as a vehicle for drug delivery applications. *Journal of Controlled Release*. 150 (2), 128-141.

Wijmans, J.G., Baker, R.W. (1995). The solution-diffusion model: a review. *Journal of Membrane Science*. 107 (1), 1-21.

Williams, D.F (1999). *The Williams Dictionary of Biomaterials*. Liverpool University Press. p40.

Wu, M.C. (2012). *Corneal Edema.* Available: http://www.uwmedicine.org/patient-care/our-services/medical-services/eye-ophthalmology/pages/articleview.aspx?subid=111. Last accessed 25th Jan 2013.

Yamada, H., Igarashi, Y., Takasu, Y., Saito, H., Tsubouchi, K. (2004). Identification of fibroin-derived peptides enhancing the proliferation of cultured human skin fibroblasts. *Biomaterials*. 25 (3), 467-472.

Yan, H.B., Zhang, Y.Q., Ma, Y.L., Zhou, L.X. (2009). Biosynthesis of insulin-silk fibroin nanoparticles conjugates and in vitro evaluation of a drug delivery system. *Journal of Nanoparticle Research*. 11 (8), 1937-1946.

Yang, Y., Chen, X., Ding, F., Zhang, P., Liu, J., Gu, X. (2007). Biocompatibility evaluation of silk fibroin with peripheral nerve tissues and cells in vitro. *Biomaterials*. 28 (9), 1643-1652.

Yasuda, H., Hirotsu, T. (1977). The effect of glass transition on gas permeabilities. *Journal of Applied Polymer Science*. 21 (1), 105-112.

Young, B.R., Pitt, W.G., Cooper, S.L. (1998). Protein adsorption on polymeric biomaterials: I. Protein isotherms. *Journal of Colloid and Interface Science*. 124 (1), 28-43.

Zhou, W., He, J., Cui, S., Gao, W. (2011). Preparation of electrospun silk fibroin/cellulose acetate blend nanofibers and their applications to heavy metal ions adsorption. *Fibers and Polymers*. 12 (4), 431-437.

Appendix A: **Sample Calculations**

Adsorption Calculations

The solution concentrations were calculated from absorbance values, using a regression line fit to a calibration curve.

$$C = Slope \cdot Abs\ - Intercept\ = (1.7523)(2.568) - 0.0138 = 4.5\ mg/mL$$

The adsorption capacity was determined from the change in initial and equilibrium concentration, the solution volume, and film mass.

$$q = \frac{(C_o - C_{eq}) \cdot V_o}{m} = \frac{\left(4.486\frac{mg}{ml} - 4.339\frac{mg}{ml}\right) \cdot 5\ ml}{0.121\ g} = 6.08\frac{mg}{g}$$

Gas Permeability Calculations

The first step in the gas permeability calculations was to find the gas flowrate from the flowmeter volume and time.

$$Q = \frac{V}{t} = \frac{0.05\ cm^3}{58.2\ s} = 8.60 \times 10^{-4}\frac{cm^3}{s}$$

The gas flux can then be calculated from the flowrate and the membrane area

$$J = \frac{Q}{A} = \frac{8.60 \times 10^{-4}\frac{cm^3}{s}}{17.3\ cm^2} = 4.98 \times 10^{-5}\frac{cm^3}{s \cdot cm^2}$$

To calculate the permeability coefficient, the flowrate first needs to be converted to a standard flowrate at 0°C and 1 atm.

$$Q_{STD} = Q \cdot \frac{T_{STD}}{T} \cdot \frac{P_{STD}}{P} = 8.60 \times 10^{-4} \frac{cm^3}{s} \cdot \frac{273.15\ K}{299.15\ K} \cdot \frac{1\ atm}{1\ atm} = 7.85 \times 10^{-4} \frac{cm^3}{s}$$

The permeability coefficient can now be calculated from the standard flowrate, area, film thickness, and pressure.

$$P = \frac{Q_{STD} \cdot l}{A \cdot (p_{i_o} - p_{i_l})} = \frac{7.85 \times 10^{-4} \frac{cm^3}{s} \cdot 0.0026\ cm}{17.3\ cm^2 \cdot (258.5\ cmHg - 0)} \cdot 10^{10} \frac{barrer}{\frac{cm^3 cm}{cm^2 s\ cmHg}} = 4.6\ barrer$$

Drug Permeability Calculations

The first calculation needed is the mass of drug permeated at all the measurement times. This is found from the concentration in the receiving reservoir, and its volume.

$$m = 0.36\ ppm \cdot \frac{1 \frac{mg}{L}}{ppm} \cdot 2\ L = 0.72\ mg$$

The amount of drug in the system can be found from the volume of the donor reservoir and initial concentration.

$$m_o = V_D C_o = 80\ mL\ \cdot 100\ ppm = 8\ mg$$

The permeability coefficient is contained within the following equation

$$-\ln\left(\frac{m_o - V_t C_R}{m_o - V_t \alpha}\right) = \frac{PA}{l}\left(\frac{1}{V_D} + \frac{1}{V_R}\right) t$$

Where α is the concentration when long term permeation can said to have first occurred.

The permeability coefficient is therefore found from the slope of the logarithmic term versus time when only the long term permeation data is considered.

$$-\ln\left(\frac{m_o - V_t C_R}{m_o - V_t a}\right) = -\ln\left(\frac{8\,mg - (2.08\,L)\left(2.73\frac{mg}{L}\right)}{8\,mg - 2.08\,L \cdot 1.13\frac{mg}{L}}\right) = 0.894$$

When the slope of this plot is found, the permeability coefficient can be found from the following.

$$P = \frac{\frac{slope \cdot l}{A}}{\frac{1}{V_D} + \frac{1}{V_R}} = \frac{0.00368 \cdot 0.0026\,cm}{\frac{17.3\,cm^2}{\frac{1}{80\,mL} + \frac{1}{2000\,mL}}} \cdot \frac{1}{60\,s} = 1.08 \times 10^{-6}\frac{cm^2}{s}$$

Sorption/Desorption Kinetics Calculations

First the experimental amount of drug adsorbed at time t divided by the amount of drug adsorbed at equilibrium as calculated from the concentrations. For adsorption:

$$\frac{M_t}{M_\infty} = \frac{C_o - C_t}{C_o - C_\infty} = \frac{219.6 - 213.6}{219.6 - 197.4} = 0.27$$

For desorption:

$$\frac{M_t}{M_\infty} = \frac{C_t}{C_\infty} = \frac{5.48}{13.0} = 0.423$$

M_t/M_∞ was then found using the following model.

$$\frac{M_t}{M_\infty} = 1 - \sum_{n=1}^{\infty} \frac{2\alpha(1+\alpha)}{1 + \alpha + \alpha^2 q_n^2} \exp\left(-\frac{D q_n^2 t}{l^2}\right)$$

Where

$$\tan q_n = -\alpha q_n$$

And α is the ratio of the volumes of the solution and the film.

For α = 25, the positive roots of $\tan(q_n) = -\alpha q_n$ and pre-exponential term for the model are shown in Table A-1.

Table A-1: Non-zero positive roots of $\tan(q_n) = \alpha q_n$, and pre-exponential term for α = 25

q_n	Pre-Exp
0	50
1.544910	0.856549
4.703886	0.093828
7.848885	0.033741
10.99194	0.017209
14.13434	0.010409
17.27644	0.006968
20.41839	0.004989
23.56025	0.003747
26.70204	0.002917
29.84379	0.002335
32.98551	0.001912

The summation was truncated at n = 12, as the addition of more terms did not change the results.

The resulting model was:

M =

1-0.856549*exp(-(1.544910)^2*A*t)-0.0093828*exp(-(4.703886)^2*A*t)-…-0.001912*exp(-(32.98551)^2*A*t)

where $A = 4D/l^2$

An initial value of $A = 0.01$ was guessed, which provided a model estimate of M_t/M_∞. Estimates at each time interval were calculated, and the total sum of square errors between the model and the experimental value of M_t/M_∞ was obtained. Using the Solver function in Microsoft Excel, A was varied until a minimum was found in the sum of square errors. The diffusivity that minimized the errors was taken as the drug diffusivity within the membrane

For Ciprofloxacin-HCl at 500 ppm, *A = 0.01496* minimized the square errors, and the resultant output was:

Time (min)	M act	M pred	Mbar	SE
0	0	0.034604045	-0.03460404	0.001197
5	0.2929293	0.265244682	-0.02768461	0.000766
10	0.4191919	0.397237295	-0.02195462	0.000482
15	0.4949495	0.498010789	0.003061294	9.37E-06
20	0.6313131	0.5805155	-0.05079763	0.00258
25	0.6717172	0.649187866	-0.02252931	0.000508
30	0.7020202	0.706566056	0.004545854	2.07E-05
35	0.7474747	0.754549626	0.007074878	5.01E-05
40	0.7979798	0.794684817	-0.00329498	1.09E-05
45	0.8232323	0.828256879	0.005024555	2.52E-05
50	0.8484848	0.856339343	0.007854495	6.17E-05
55	0.8636364	0.879829909	0.016193545	0.000262
60	0.8737374	0.899479429	0.025742056	0.000663
70	0.8989899	0.929664908	0.030675009	0.000941
80	0.9191919	0.950785942	0.031594023	0.000998
90	0.9494949	0.965564508	0.016069559	0.000258
100	0.959596	0.975905196	0.016309236	0.000266
110	0.9747475	0.983140662	0.008393187	7.04E-05
120	0.9747475	0.988203379	0.013455904	0.000181
135	0.9747475	0.993095483	0.018348008	0.000337
150	0.979798	0.995958813	0.016160833	0.000261
165	0.989899	0.997634709	0.007735719	5.98E-05
180	0.989899	0.998615604	0.008716614	7.6E-05
195	0.9949495	0.999189718	0.004240223	1.8E-05
210	0.9949495	0.999525745	0.00457625	2.09E-05
225	1	0.999722421	-0.00027758	7.71E-08
240	1	0.999837534	-0.00016247	2.64E-08
255	1	0.999904909	-9.5091E-05	9.04E-09
270	1	0.999944344	-5.5656E-05	3.1E-09
285	1	0.999967425	-3.2575E-05	1.06E-09
300	1	0.999980934	-1.9066E-05	3.64E-10

$$D = \frac{A \cdot l^2}{4} = \frac{(0.01496)(0.005)^2}{4} \cdot \frac{1\ min}{60\ s} = 1.56 \times 10^{-9}\ cm^2/s$$

Appendix B – **Supporting Data**

B.1 Bovine Serum Albumin Adsorption Data

Table B-1: Bovine serum albumin adsorption data

Membrane Area (cm^2)	Solution Volume (mL)	Initial Concentration (mg/mL)	Final Concentration (mg/mL)	Mass Adsorbed (mg)	Capacity (mg/cm^2)
57.2	5	4.49	4.34	0.74	0.013
75.6	5	3.85	3.58	1.33	0.018
79.8	5	3.08	2.81	1.35	0.017
59.1	5	1.70	1.67	0.18	0.003
108.4	5	1.57	1.50	0.34	0.003
14.9	5	4.19	4.13	0.30	0.020
36.5	5	3.38	3.23	0.75	0.021
28.0	5	2.49	2.43	0.30	0.011
34.0	5	1.00	0.98	0.09	0.003
19.9	5	2.10	2.08	0.08	0.004
28.6	5	2.93	2.83	0.49	0.017
30.4	5	3.74	3.62	0.63	0.021
9.5	5	9.62	9.55	0.34	0.036
16.9	5	7.64	7.48	0.79	0.047
12.2	5	6.77	6.68	0.46	0.038
14.2	5	2.02	1.98	0.18	0.013
16.9	5	3.03	2.96	0.39	0.023
13.7	5	3.72	3.67	0.24	0.017
14.3	5	4.49	4.42	0.32	0.023
9.0	5	4.78	4.74	0.21	0.023
79.7	5	5.87	5.36	2.55	0.032
42.6	5	6.54	6.20	1.69	0.040
26.2	5	7.15	6.97	0.87	0.033
71.0	5	8.39	7.80	2.97	0.042
31.0	5	9.35	9.10	1.24	0.040
62.5	5	6.54	6.14	2.01	0.032
67.9	5	6.71	6.30	2.04	0.030
38.3	5	7.46	7.20	1.29	0.034
49.7	5	7.50	7.22	1.40	0.028

83.1	5	1.76	1.57	0.98	0.012
95.9	5	7.37	6.65	3.60	0.038
98.0	5	5.61	5.00	3.03	0.031
141.9	5	10.54	9.32	6.13	0.043
63.1	5	6.04	5.66	1.94	0.031
44.0	5	6.31	6.03	1.39	0.032
77.0	5	8.64	7.97	3.31	0.043
95.1	5	7.92	7.20	3.61	0.038
29.8	5	5.48	5.36	0.58	0.019
56.8	5	5.53	5.23	1.48	0.026
95.1	5	8.08	7.35	3.67	0.039
96.0	5	8.08	7.31	3.88	0.040

B.2 Gas Permeability Data

Oxygen Permeability

Table B-4: Oxygen gas permeability data

Pressure (psig)	Temp (°C)	Avg. Time (s)	Volume (mL)	Flux 10^5 (cm^3/cm^2s)	Permeability (barrer)
10	26	232.0	0.05	1.25	0.57
20	26	124.0	0.05	2.33	0.54
30	26	79.0	0.05	3.66	0.56
40	26	64.5	0.05	4.49	0.51
50	26	48.4	0.05	5.98	0.55

Nitrogen Permeability

Table B-5: Nitrogen gas permeability data

Pressure (psig)	Temp (°C)	Avg. Time (s)	Volume (mL)	Flux 10^5 (cm^3/cm^2s)	Permeability (barrer)
10	26	252.5	0.05	1.32	0.61
20	26	134.3	0.05	2.26	0.52
30	26	90.0	0.05	3.37	0.52
40	26	69.5	0.05	4.21	0.48
50	26	53.3	0.05	5.57	0.51

Carbon Dioxide Permeability

Table B-6: Carbon dioxide gas permeability data

Pressure (psig)	Temp (°C)	Avg. Time (s)	Volume (mL)	Flux 10^5 (cm^3/cm^2s)	Permeability (barrer)
10	26	35	0.5	8.42	3.68
20	26	21.3	0.5	13.7	3.00
30	26	14.2	0.5	20.5	2.99
40	26	12.2	0.5	24.1	2.63
50	26	9.9	0.5	29.3	2.56

B.3 Drug Permeability Data

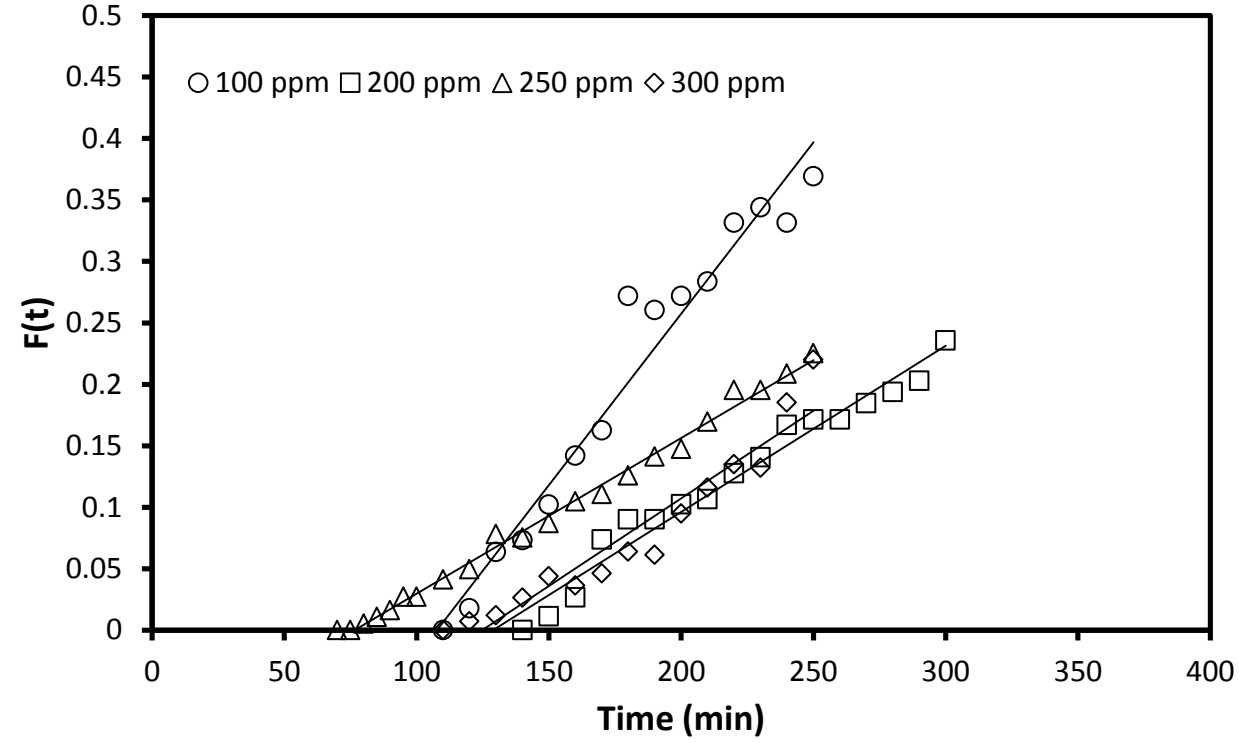

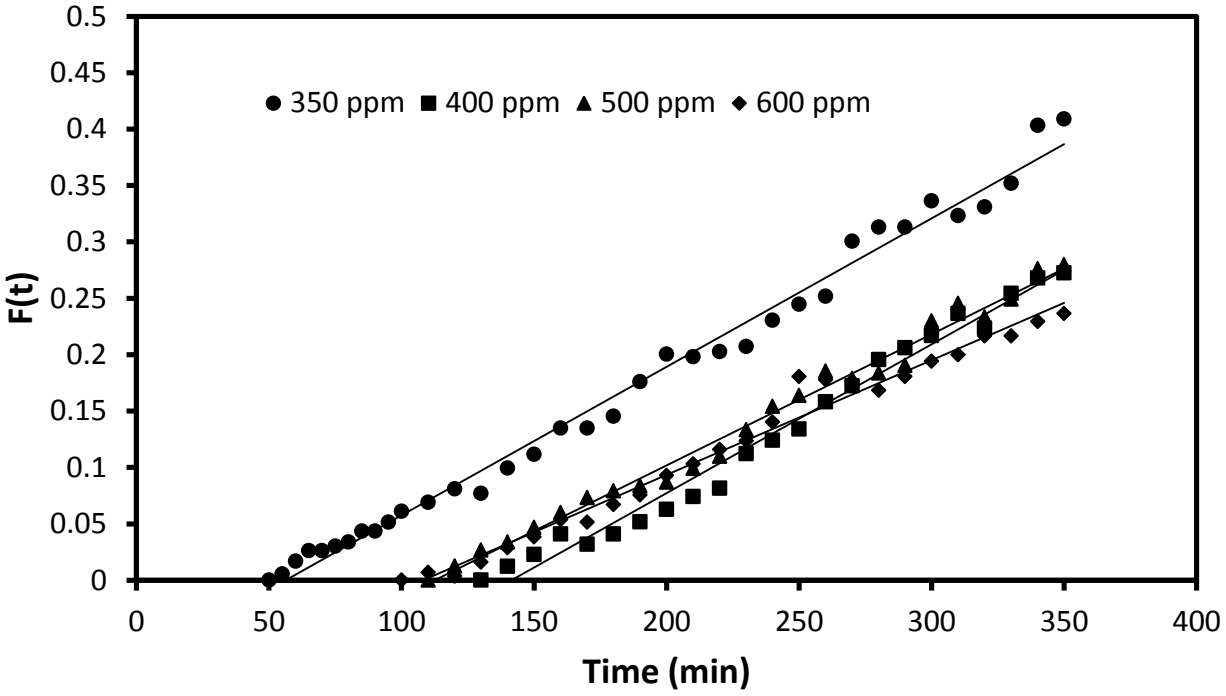

Figure B-1: Pseudo steady-state data for diltiazem-HCl.

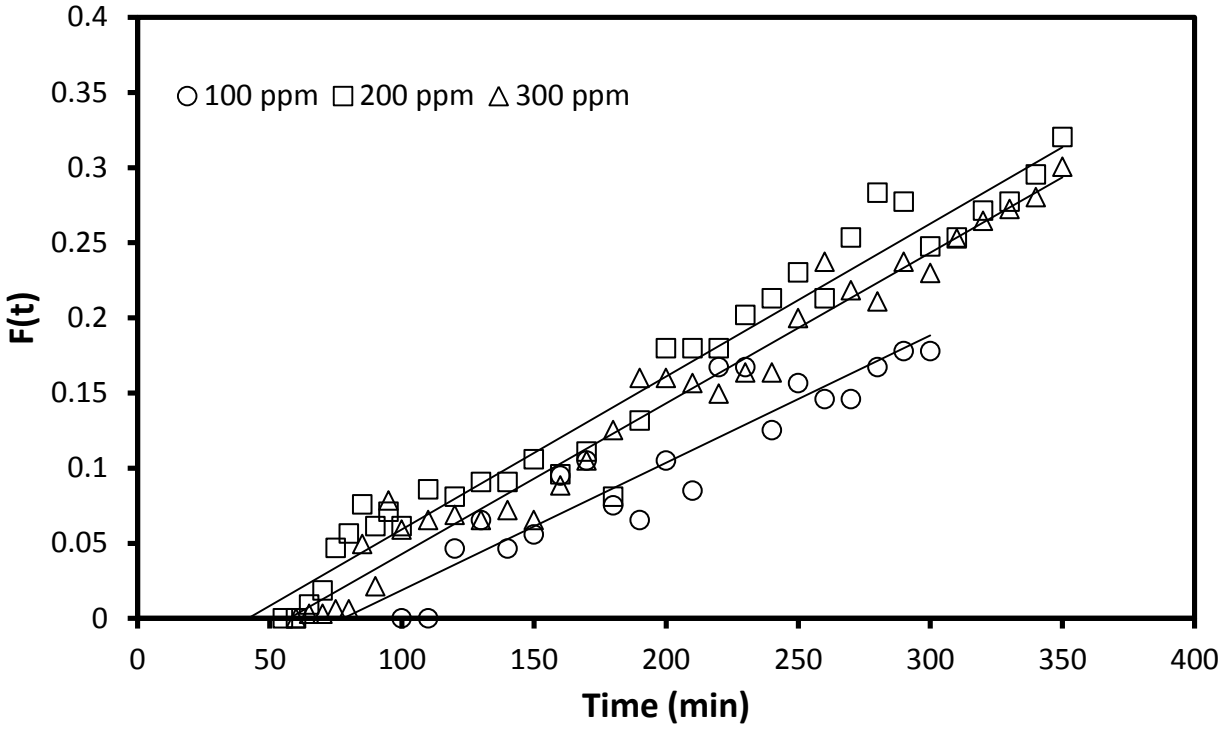

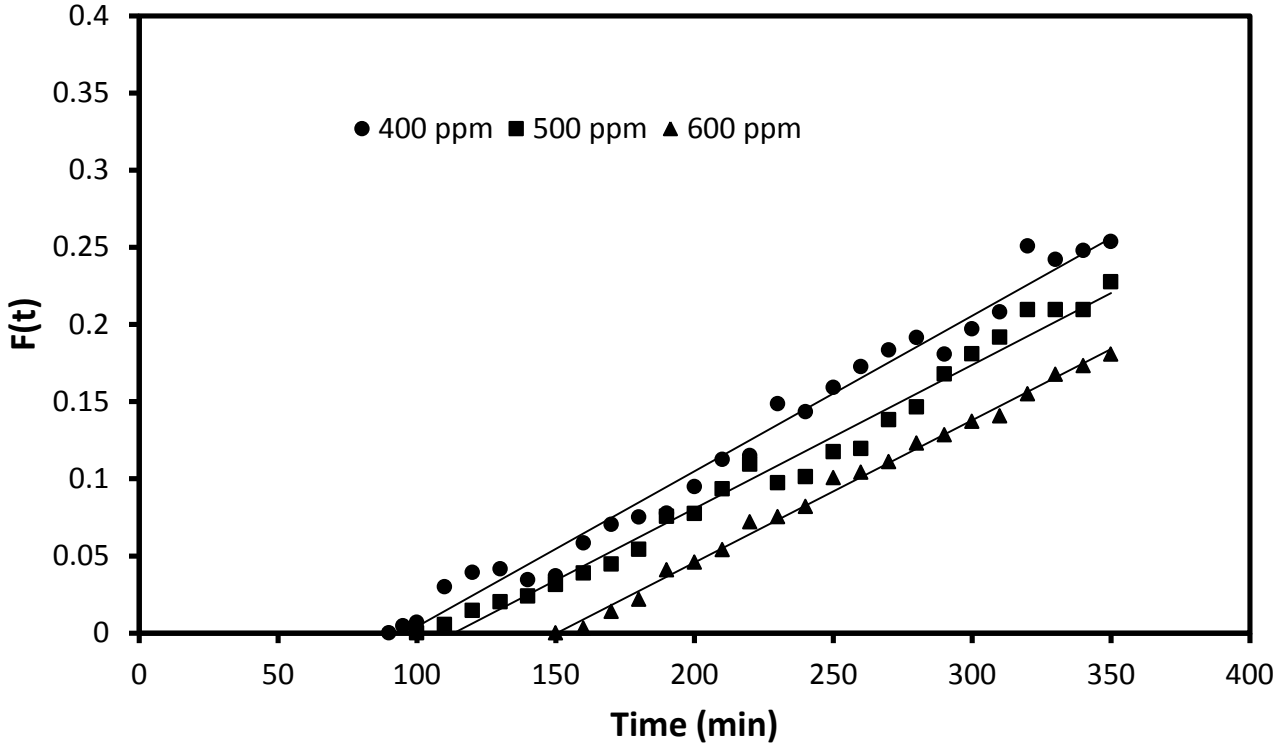

Figure B-2: Pseudo steady-state data for ciprofloxacin-HCl

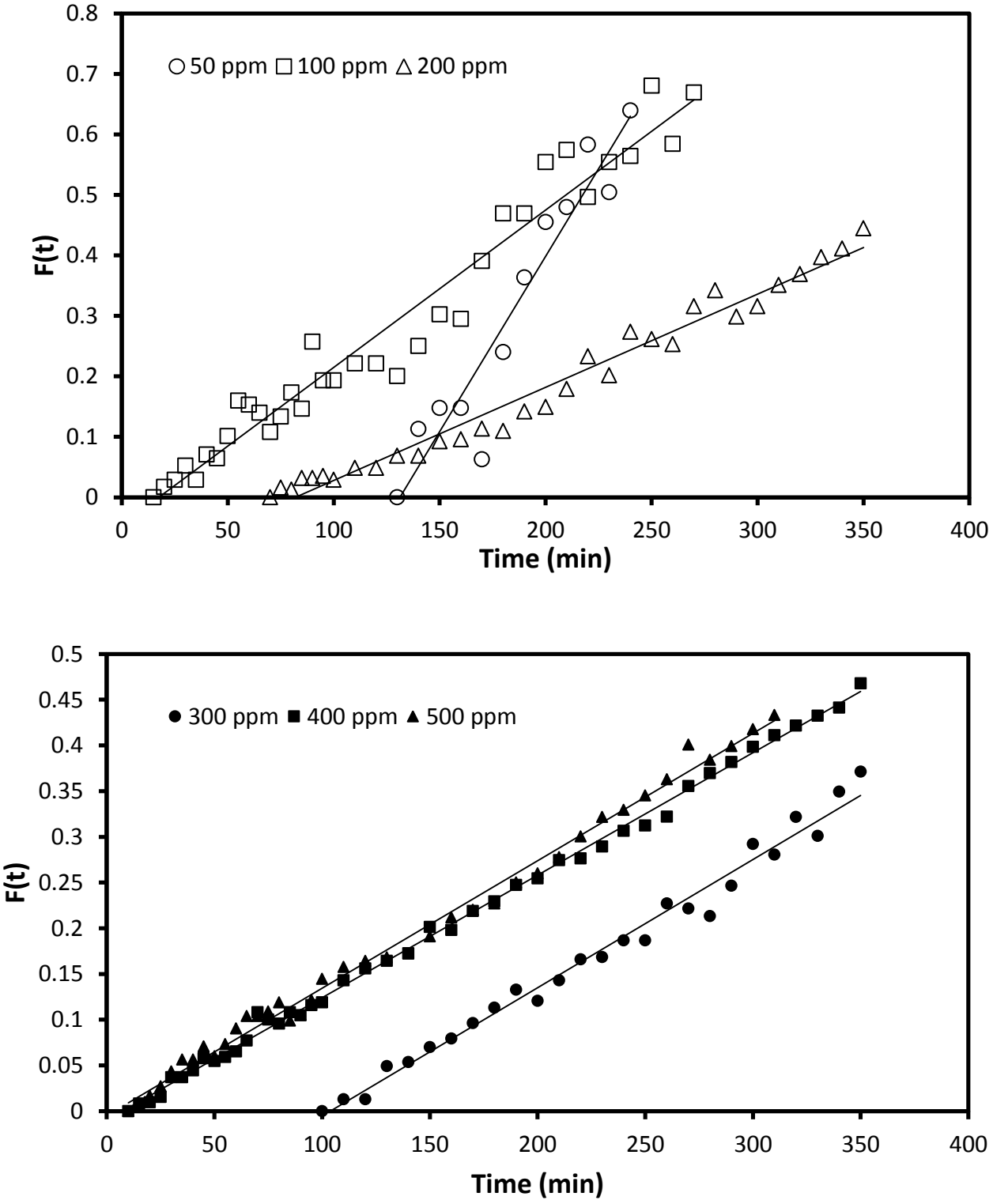

Figure B-3: Pseudo steady-state data for tetrahydrozoline-HCl

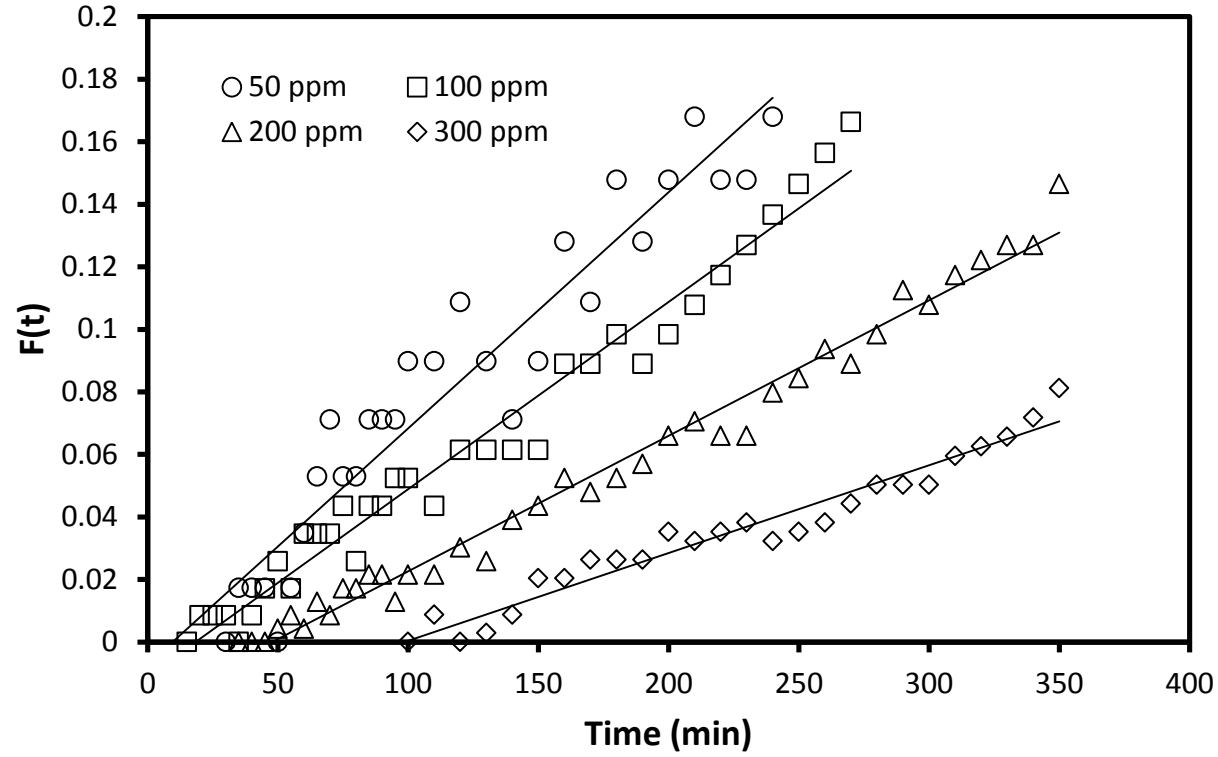

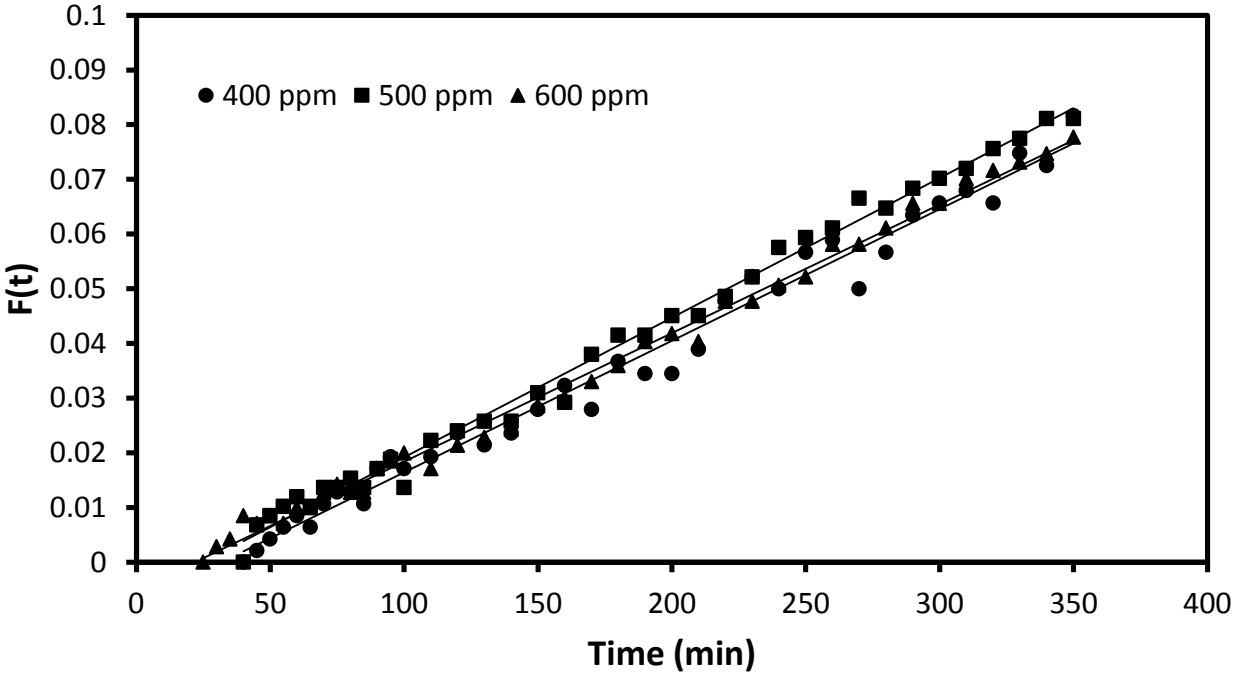

Figure B-4: Pseudo steady-state data for tetracycline-HCl

B.4 Drug Sorption/Desorption

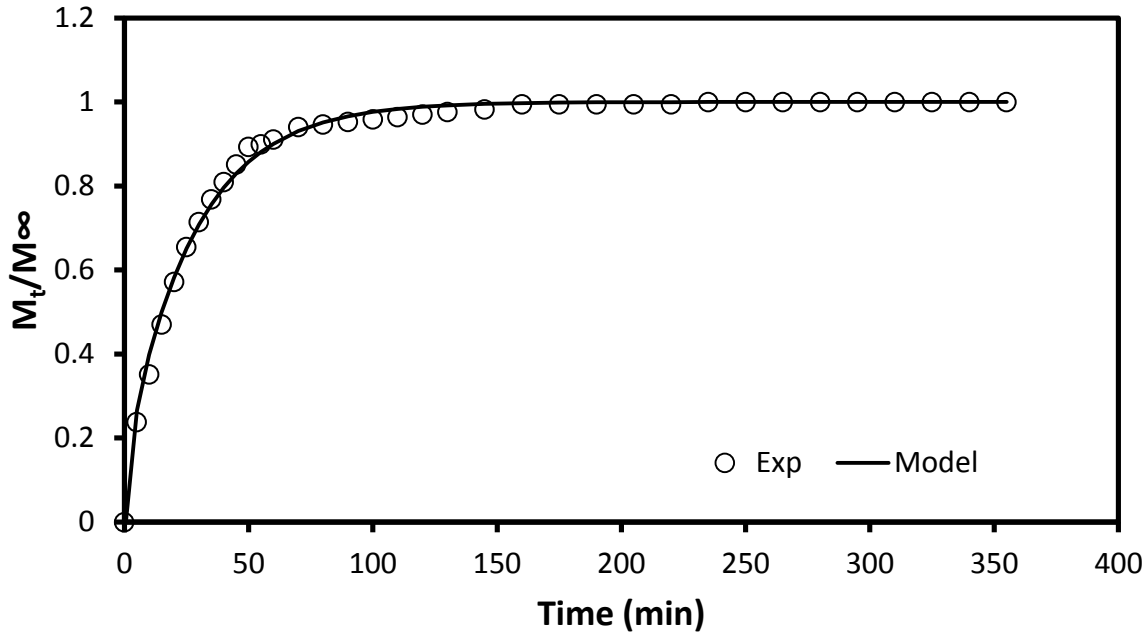

Figure B-5: Diltiazem-HCl sorption kinetics, 100 ppm.

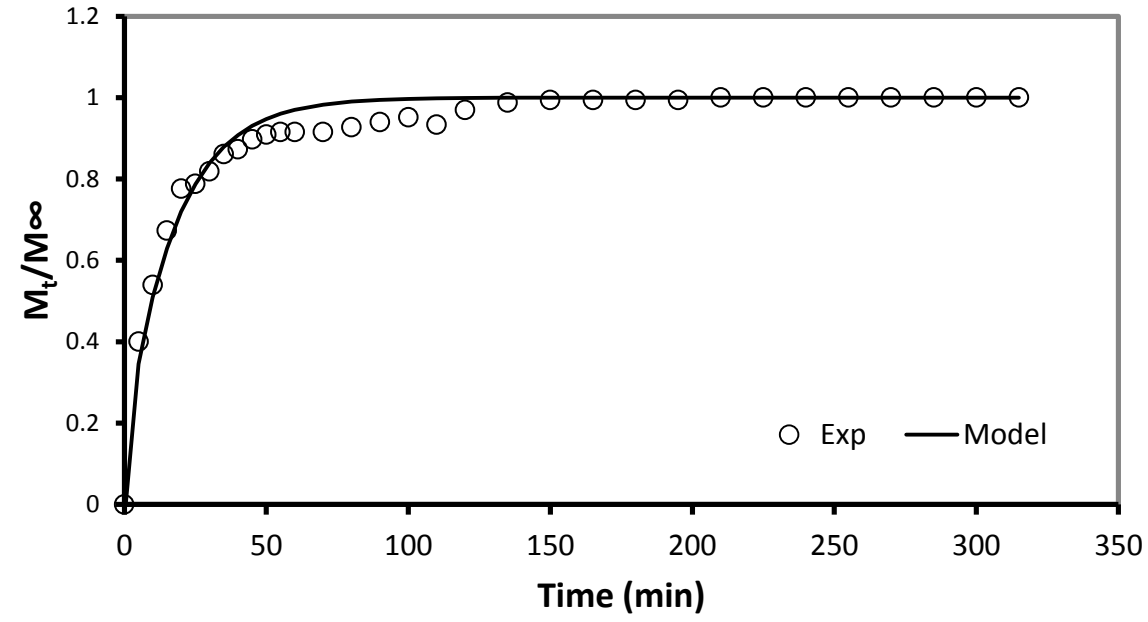

Figure B-6: Diltiazem-HCl sorption kinetics, 180 ppm.

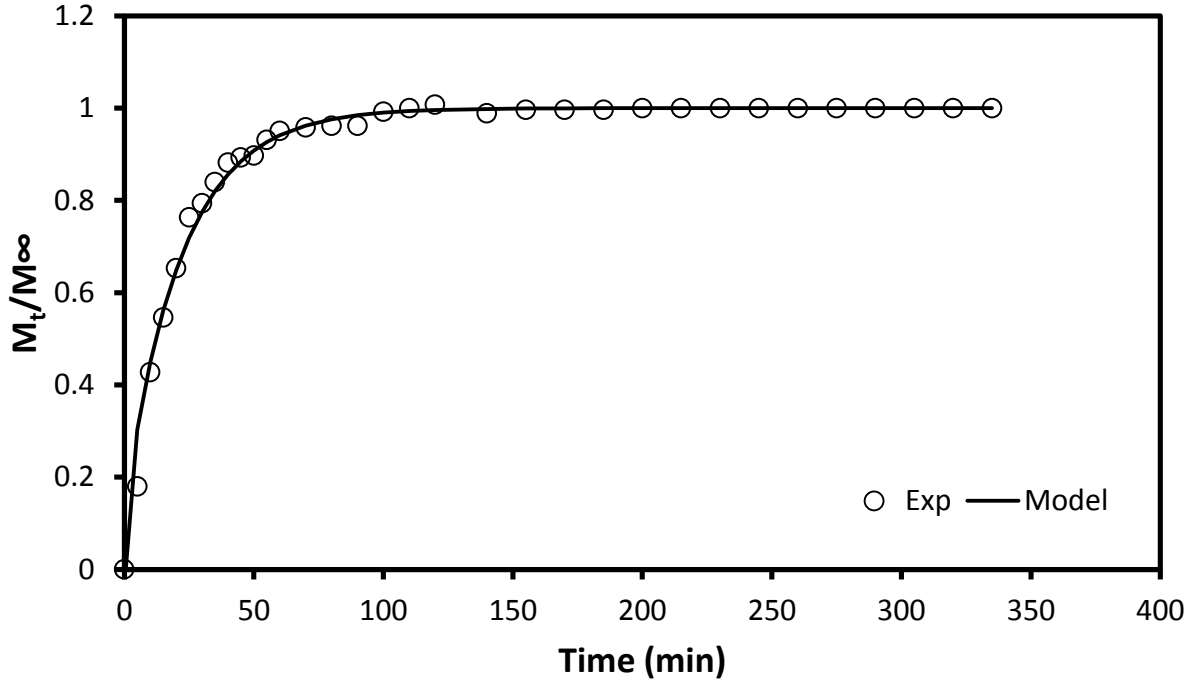

Figure B-7: Diltiazem-HCl sorption kinetics, 225 ppm.

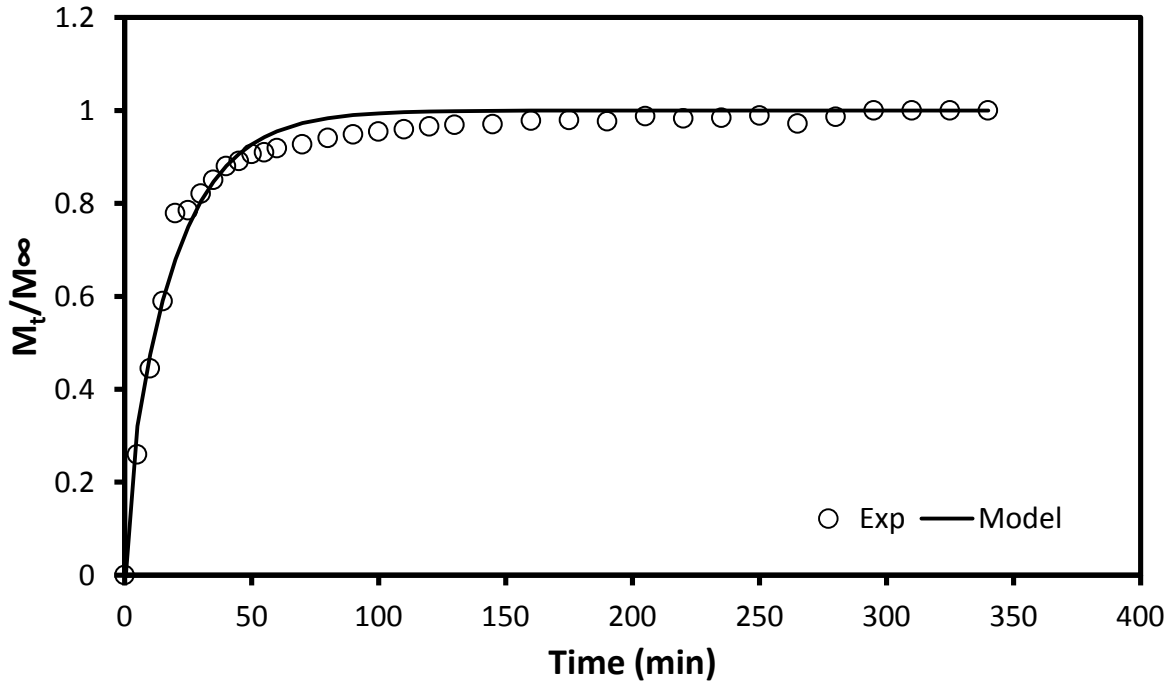

Figure B-8: Diltiazem-HCl sorption kinetics, 325 ppm.

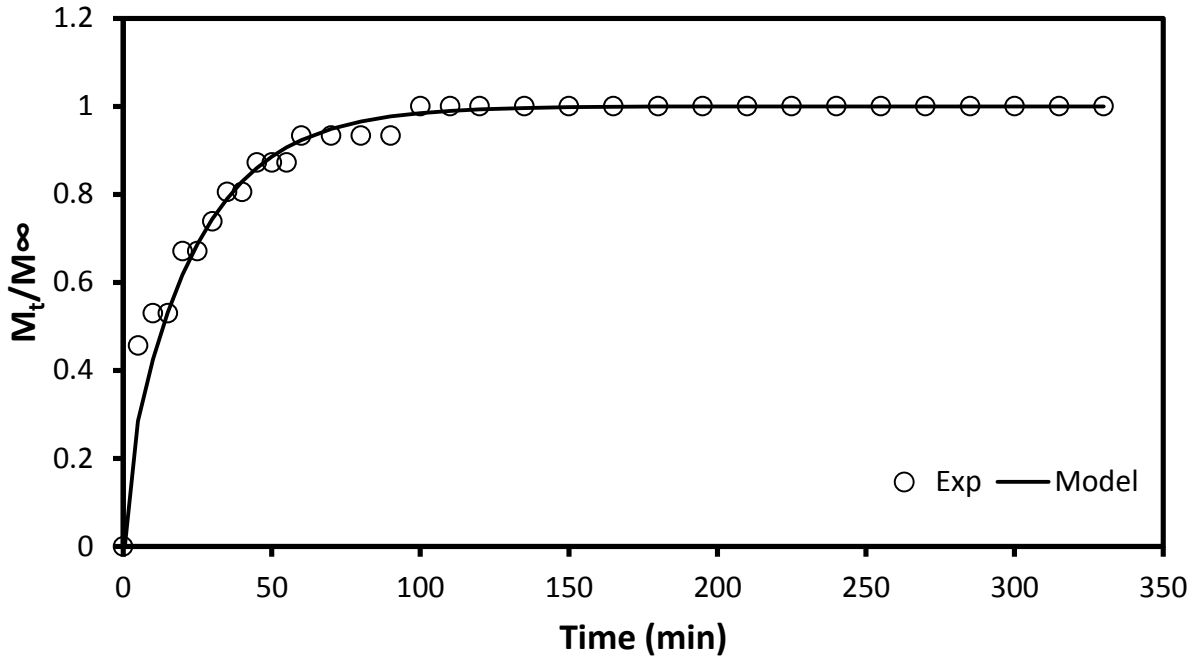

Figure B-9: Diltiazem-HCl sorption kinetics, 400 ppm.

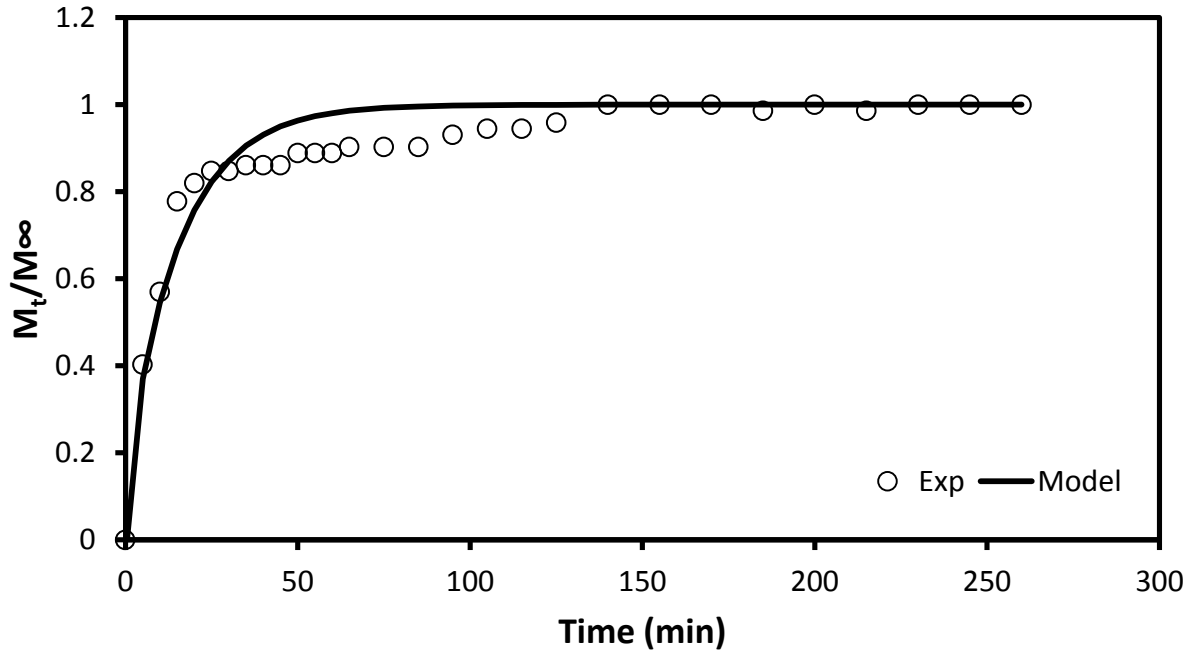

Figure B-10: Diltiazem-HCl sorption kinetics, 500 ppm.

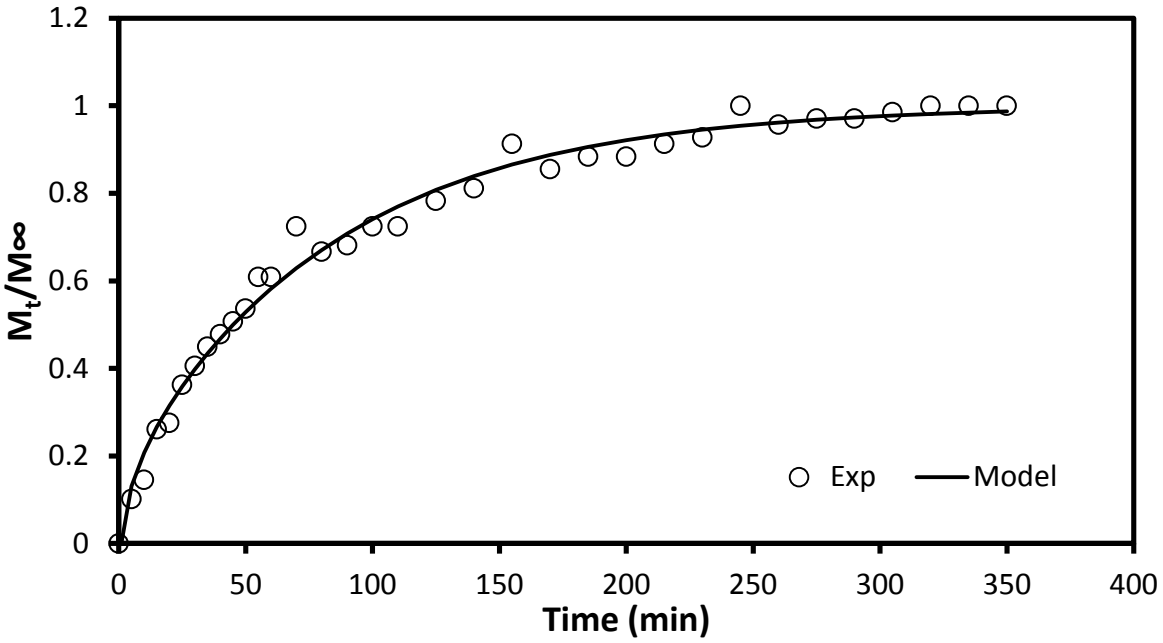

Figure B-11: Diltiazem-HCl desorption kinetics, 100 ppm.

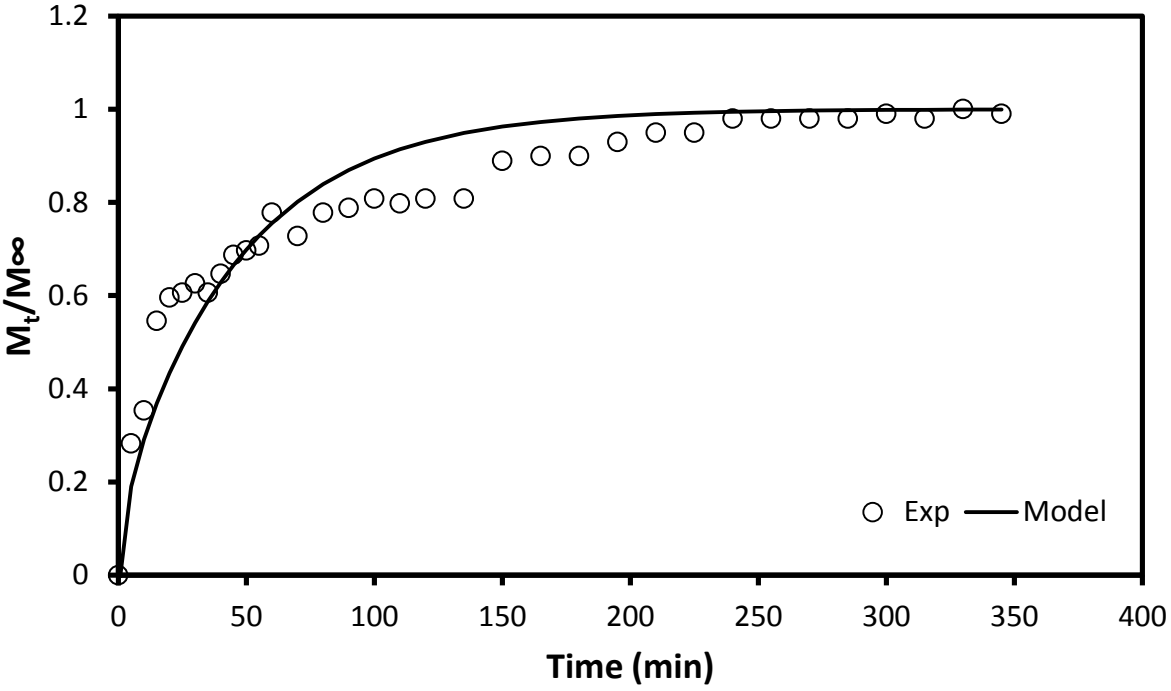

Figure B-12: Diltiazem-HCl desorption kinetics, 180 ppm.

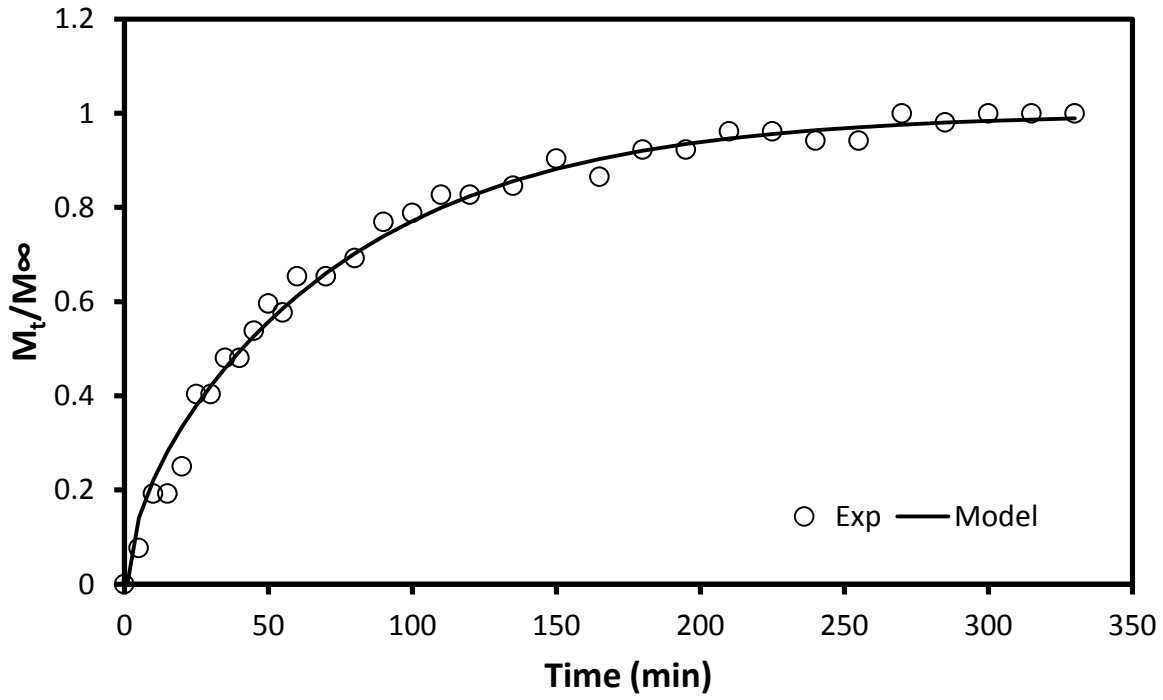

Figure B-13: Diltiazem-HCl desorption kinetics, 225 ppm.

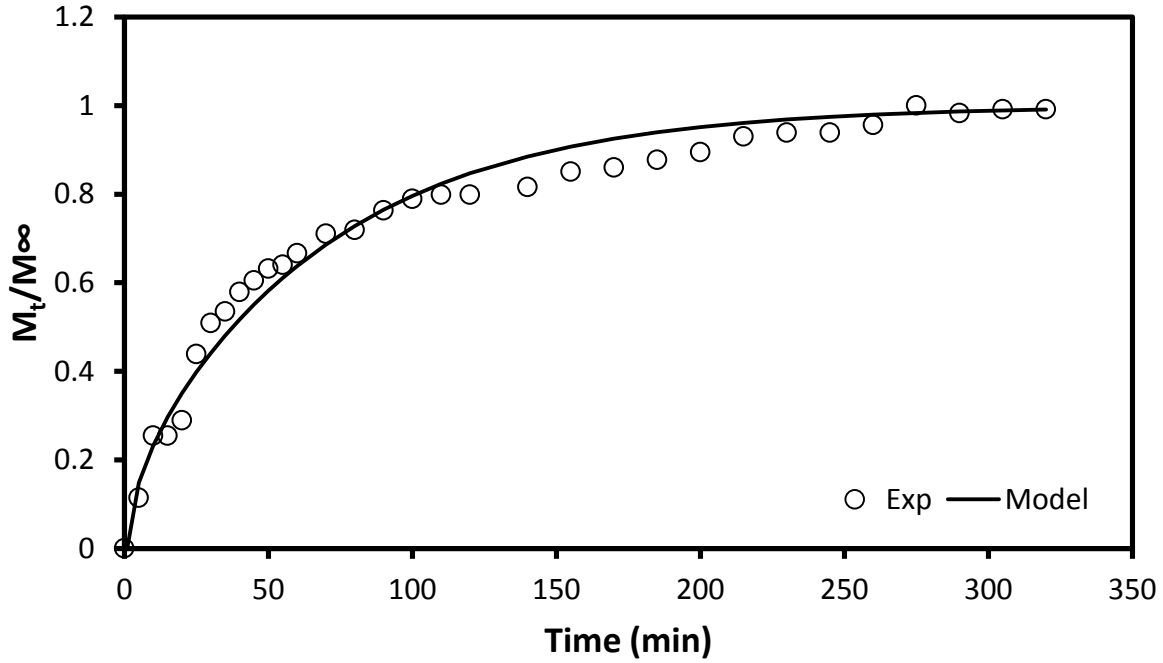

Figure B-54: Diltiazem-HCl desorption kinetics, 325 ppm.

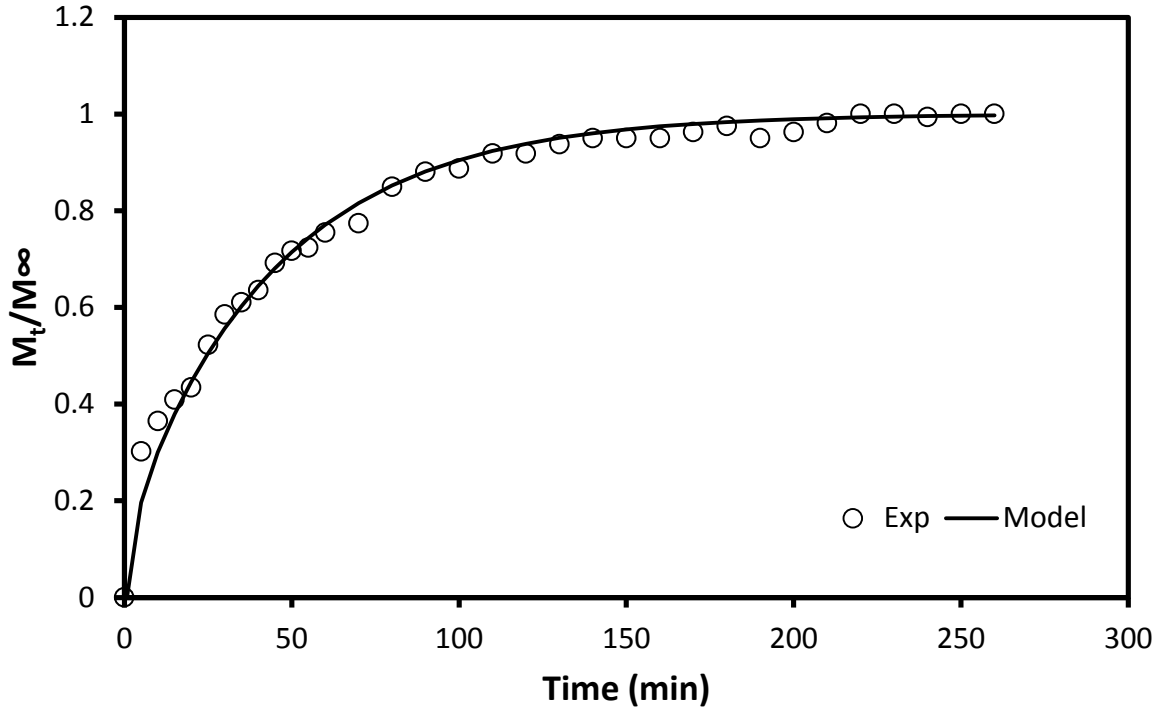

Figure B-65 Diltiazem-HCl desorption kinetics, 400 ppm.

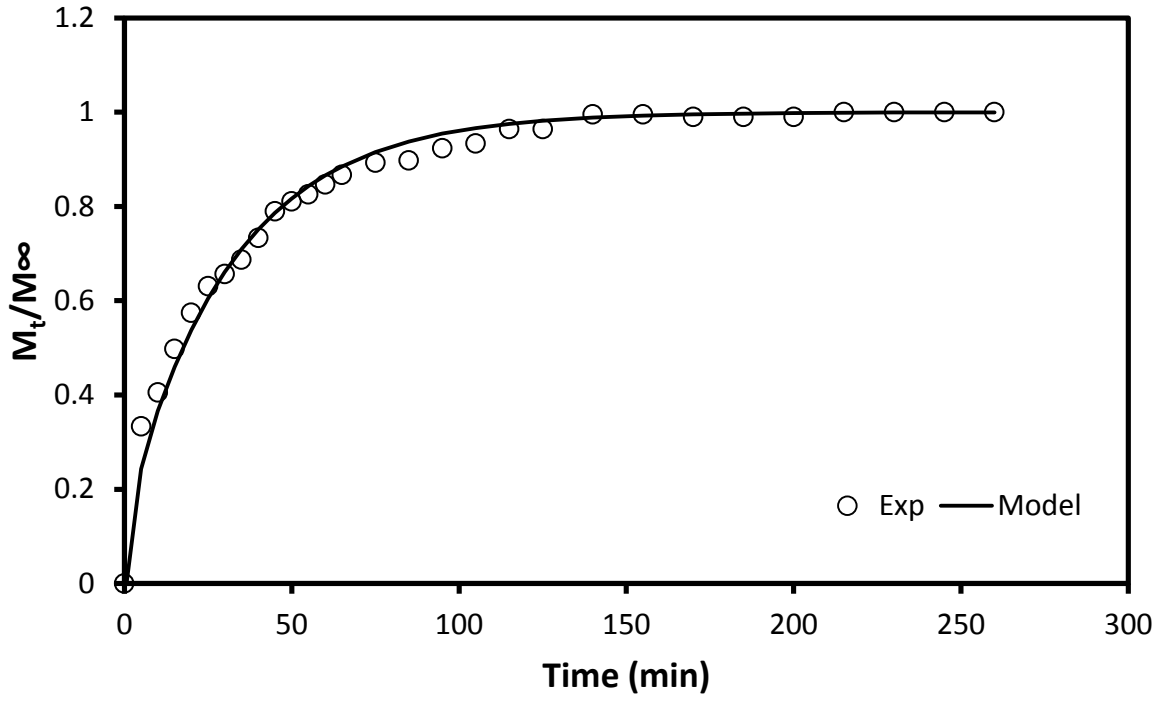

Figure B-16: Diltiazem-HCl desorption kinetics, 500 ppm.

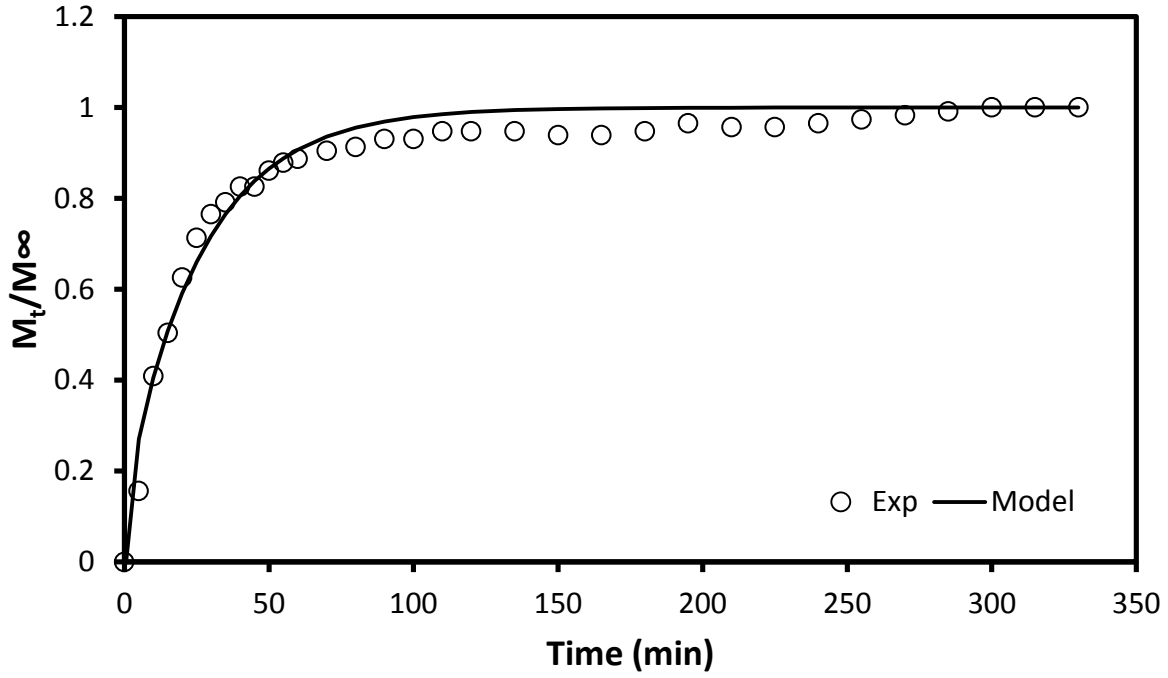

Figure B-17: Ciprofloxacin-HCl sorption kinetics, 100 ppm.

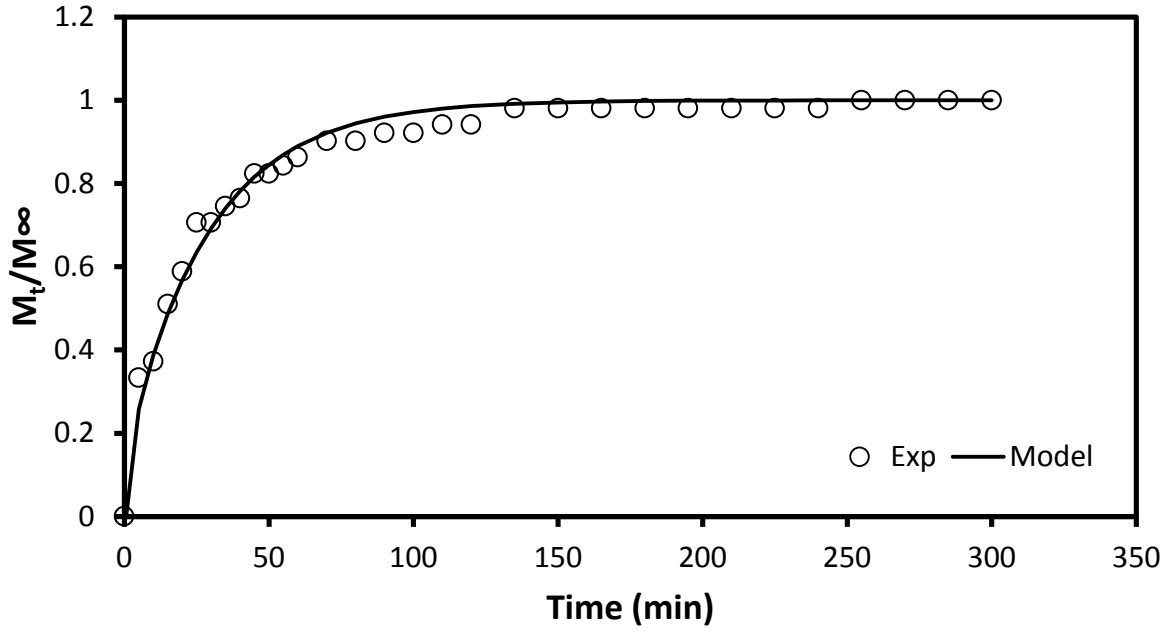

Figure B-18: Ciprofloxacin-HCl sorption kinetics, 200 ppm.

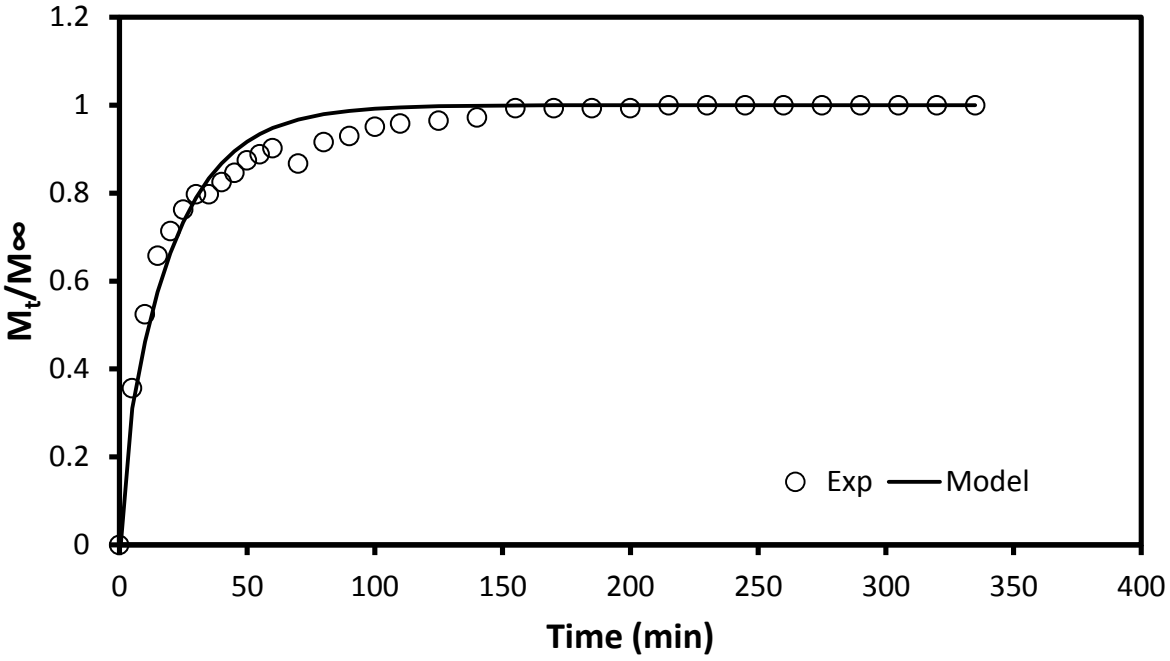

Figure B-19: Ciprofloxacin-HCl sorption kinetics, 300 ppm.

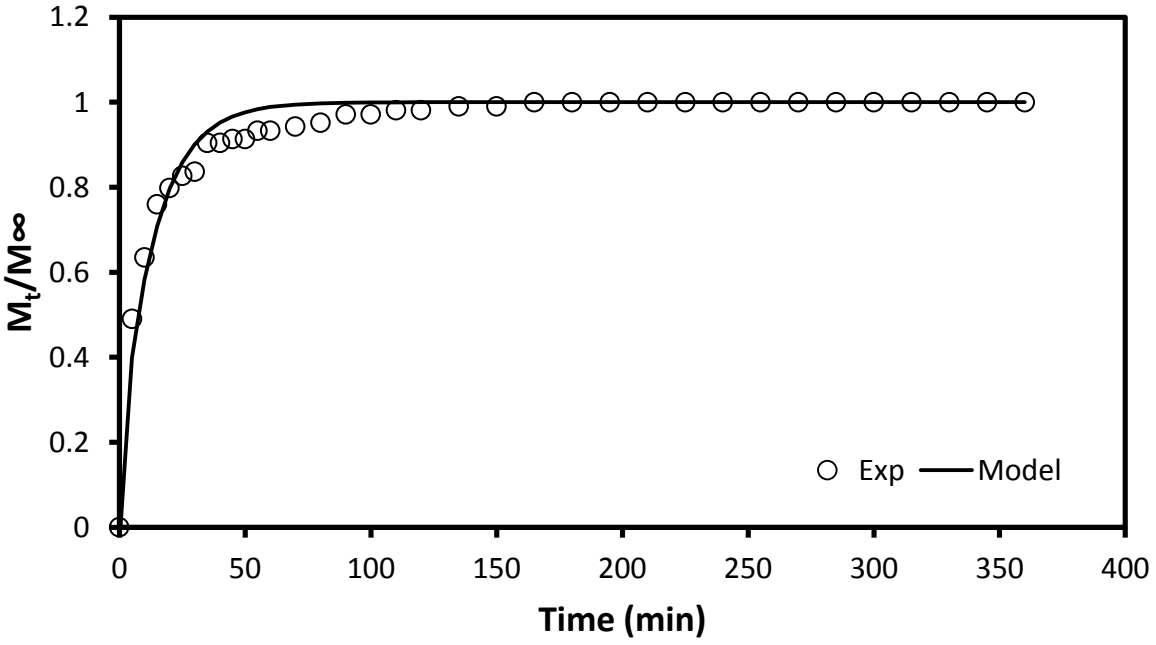

Figure B-20: Ciprofloxacin-HCl sorption kinetics, 400 ppm.

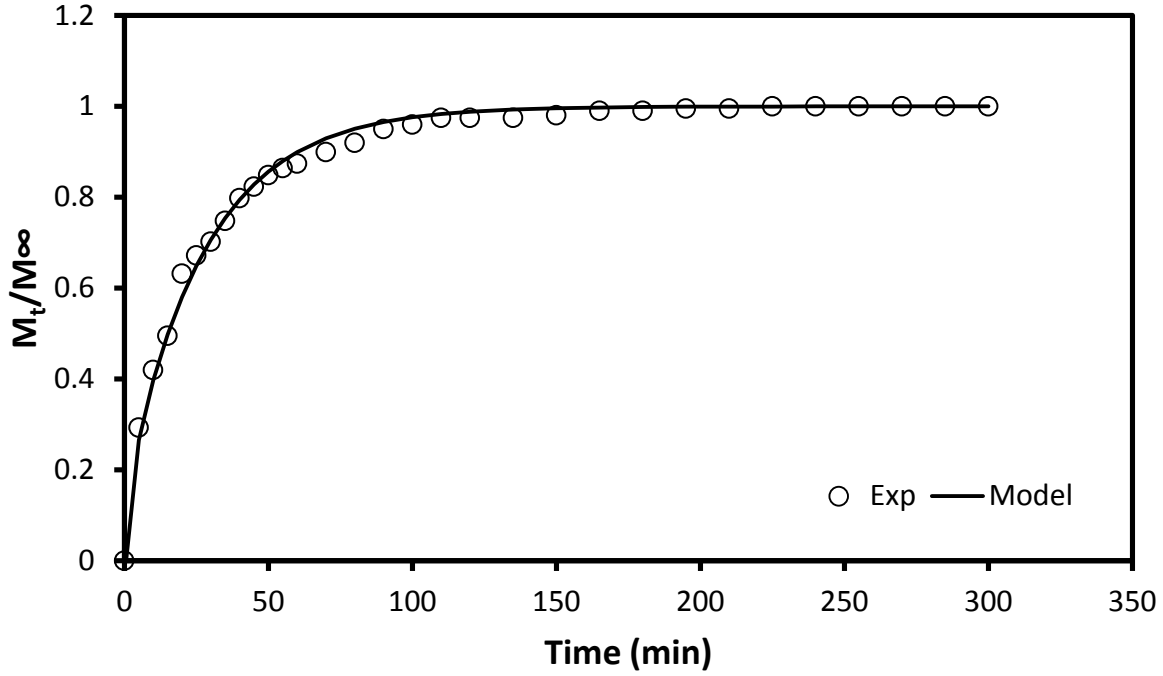

Figure B-21: Ciprofloxacin-HCl sorption kinetics, 500 ppm.

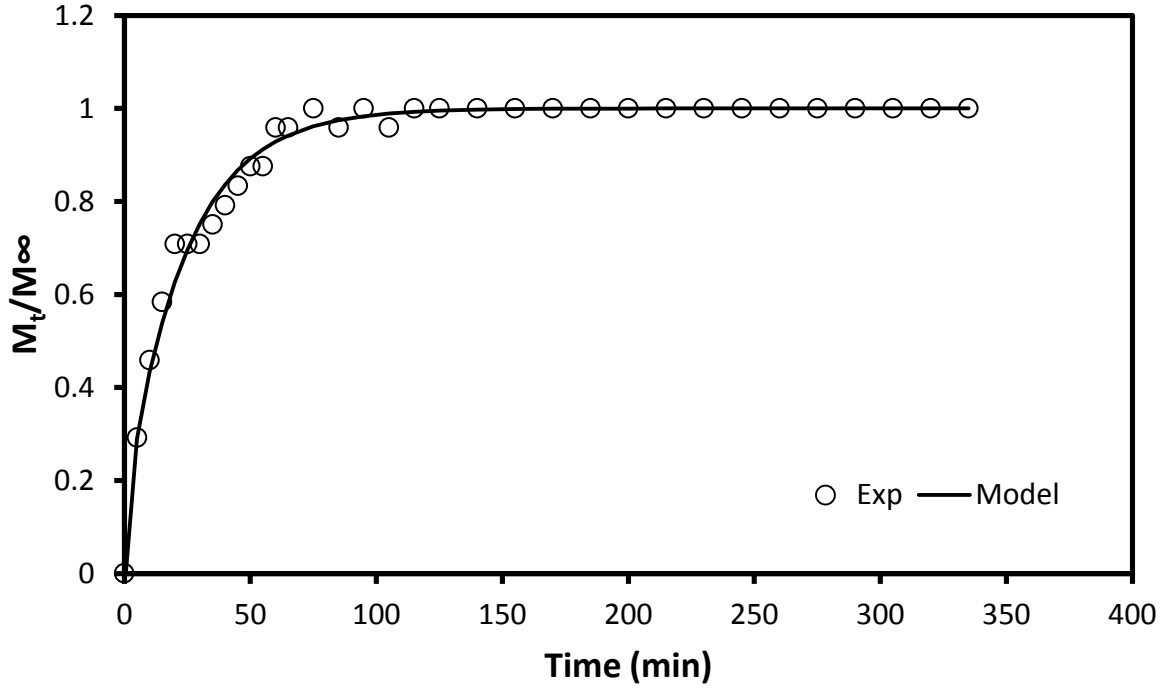

Figure B-22: Ciprofloxacin-HCl desorption kinetics, 100 ppm.

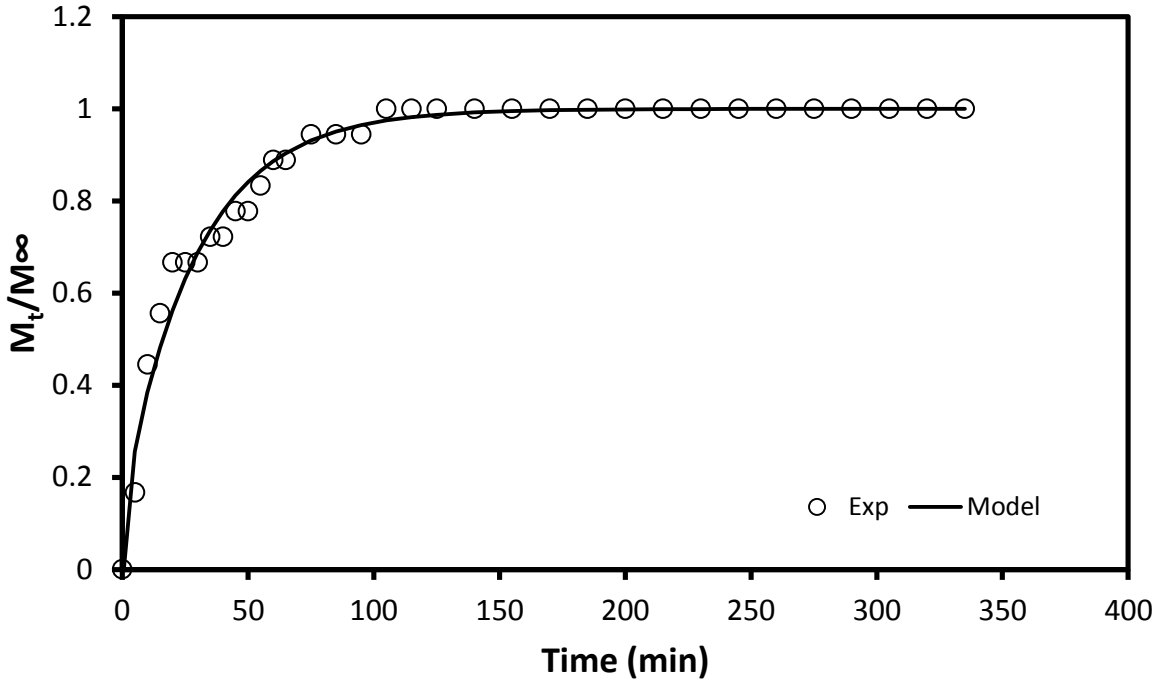

Figure B-23: Ciprofloxacin-HCl desorption kinetics, 200 ppm.

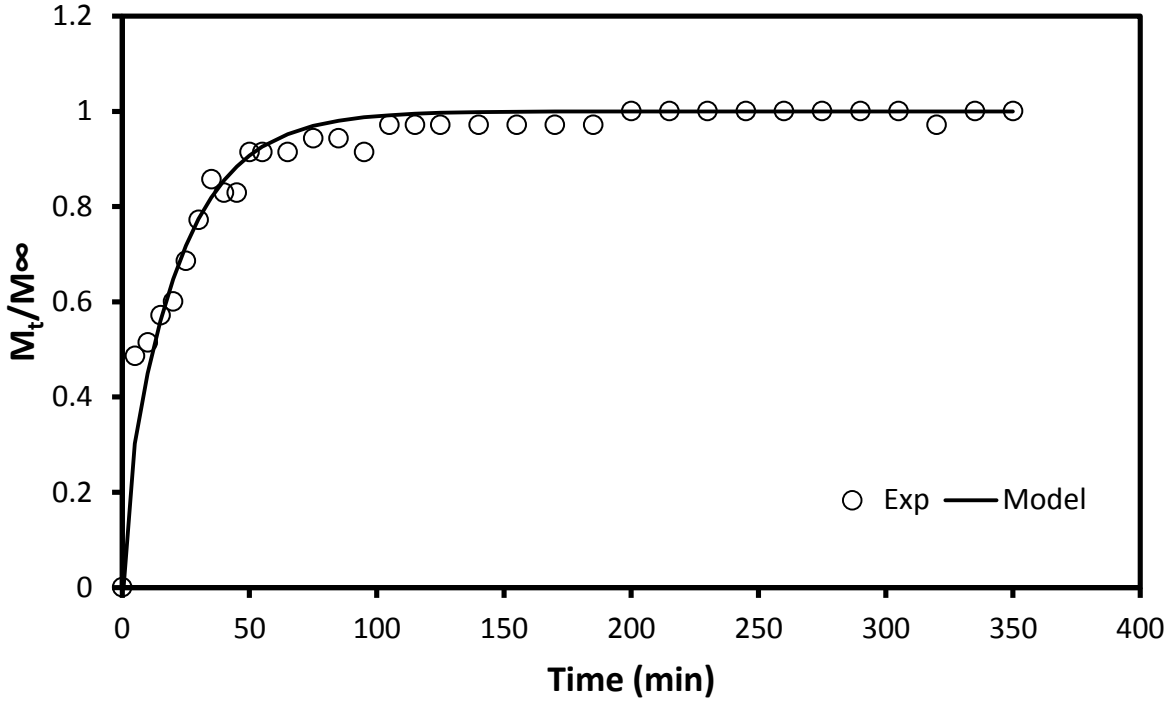

Figure B-74: Ciprofloxacin-HCl desorption kinetics, 300 ppm.

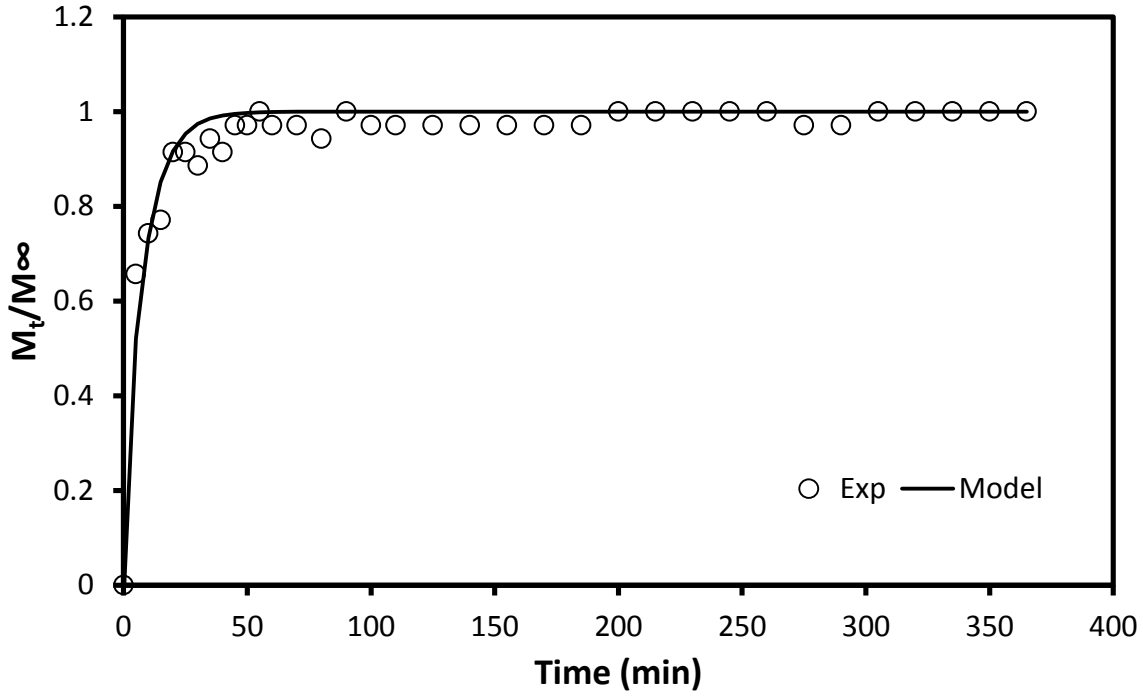

Figure B-85: Ciprofloxacin-HCl desorption kinetics, 400 ppm.

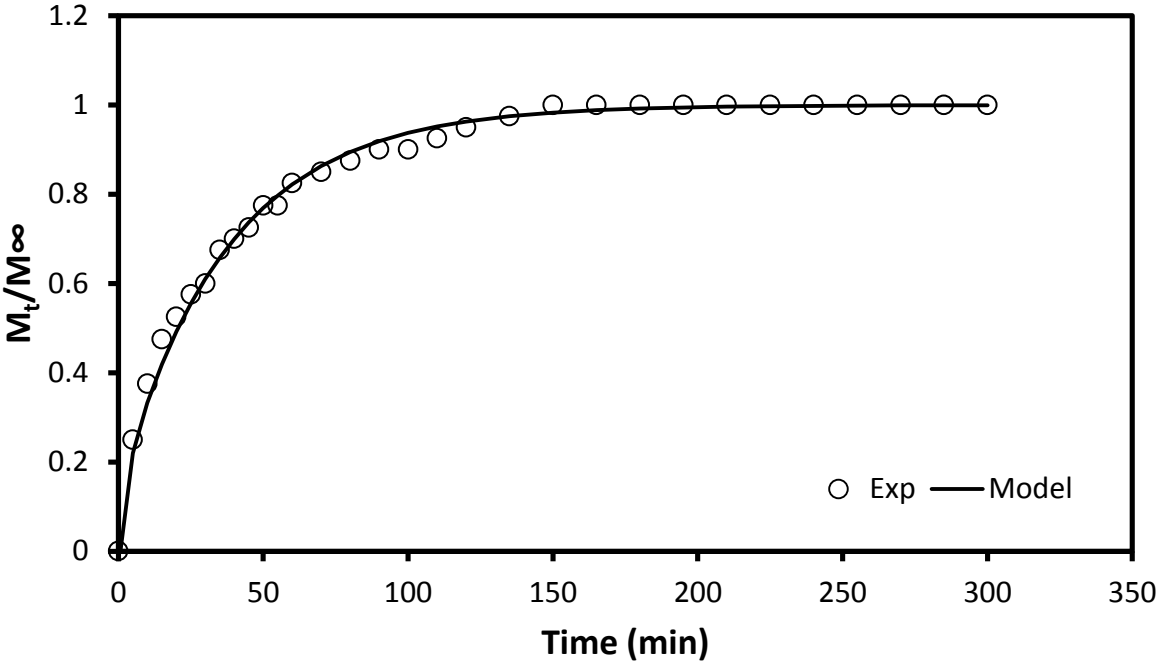

Figure B-26: Ciprofloxacin-HCl desorption kinetics, 500 ppm.

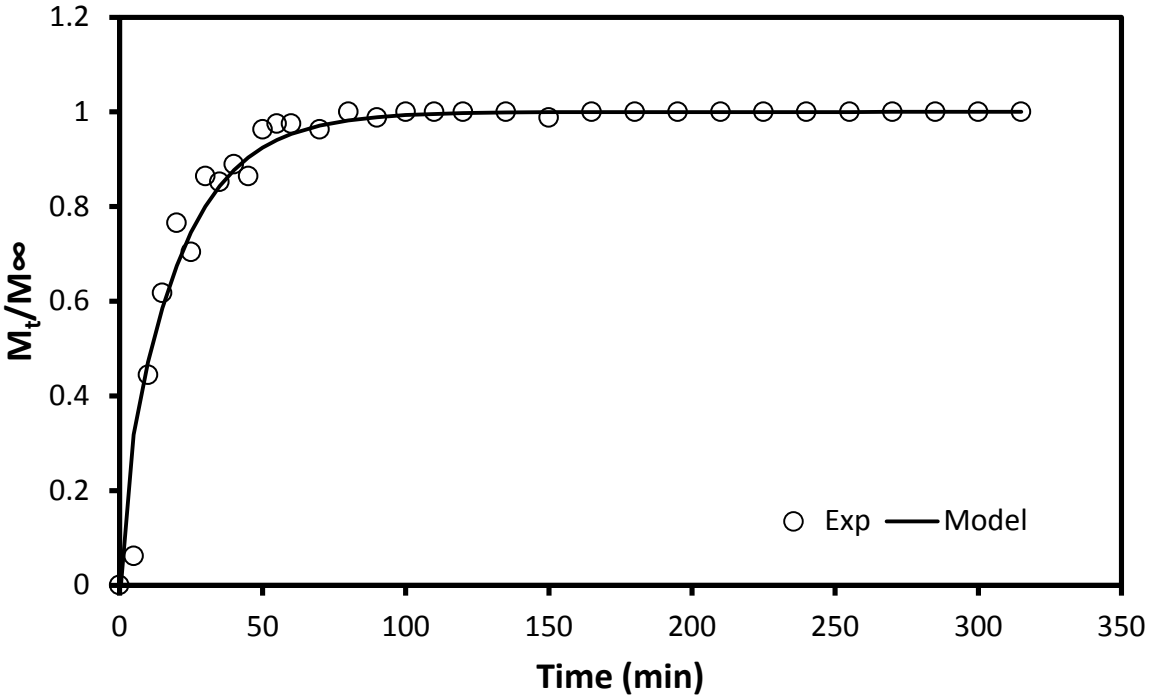

Figure B-27: Tetrahydrozoline-HCl sorption kinetics, 100 ppm.

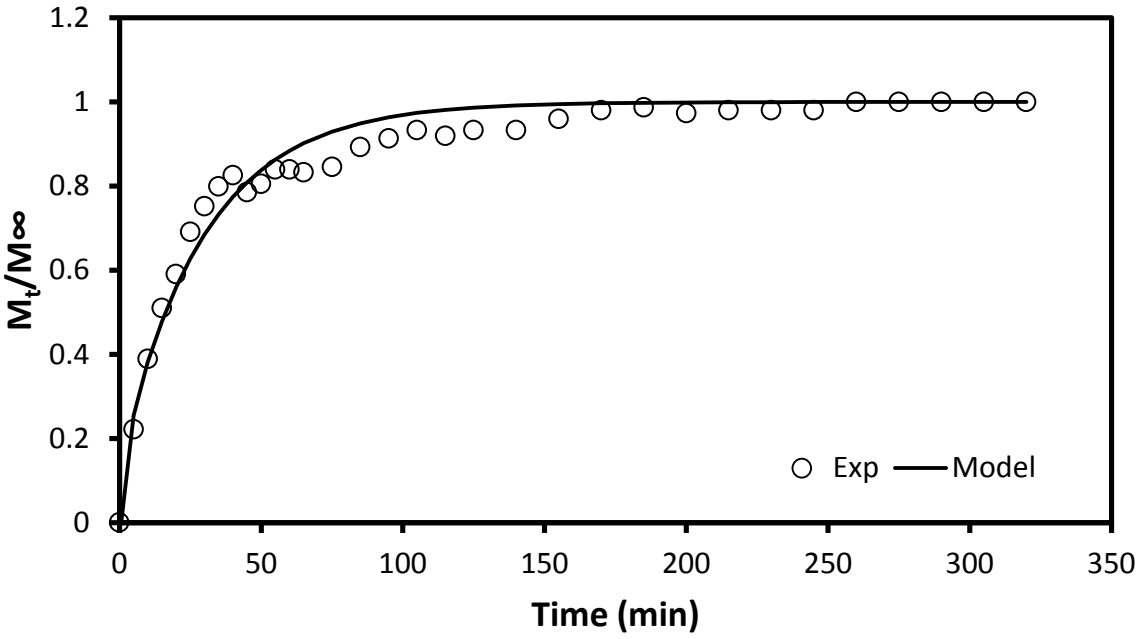

Figure B-28: Tetrahydrozoline-HCl sorption kinetics, 200 ppm.

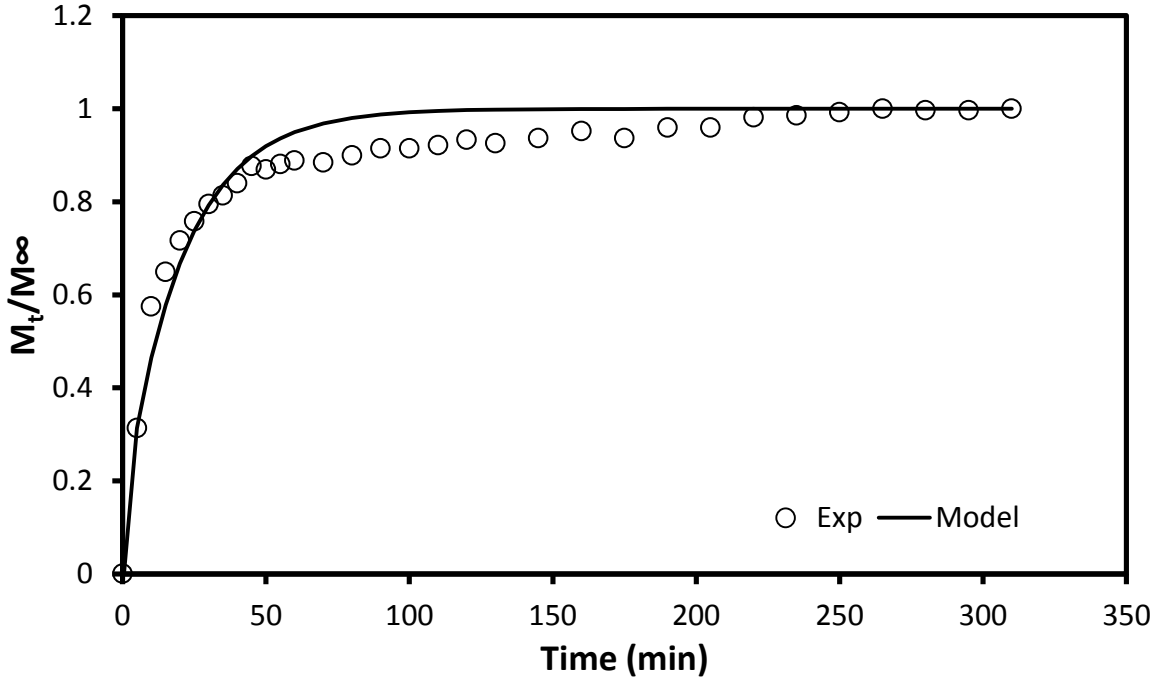

Figure B-29: Tetrahydrozoline-HCl sorption kinetics, 300 ppm.

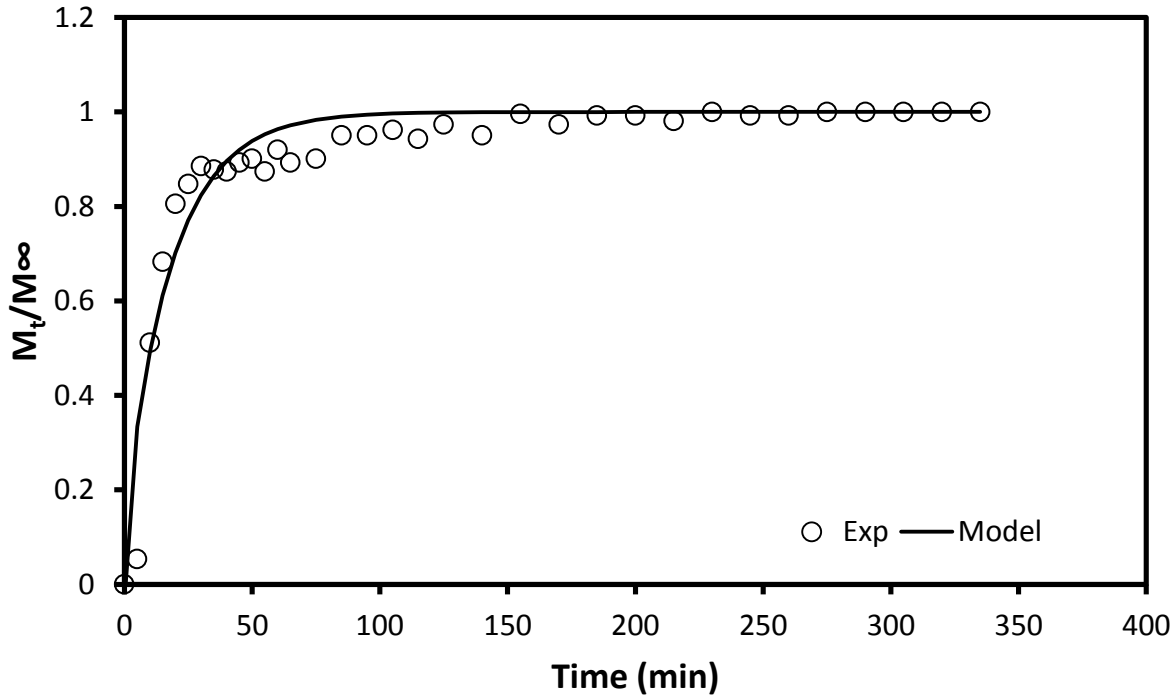

Figure B-30: Tetrahydrozoline-HCl desorption kinetics, 400 ppm.

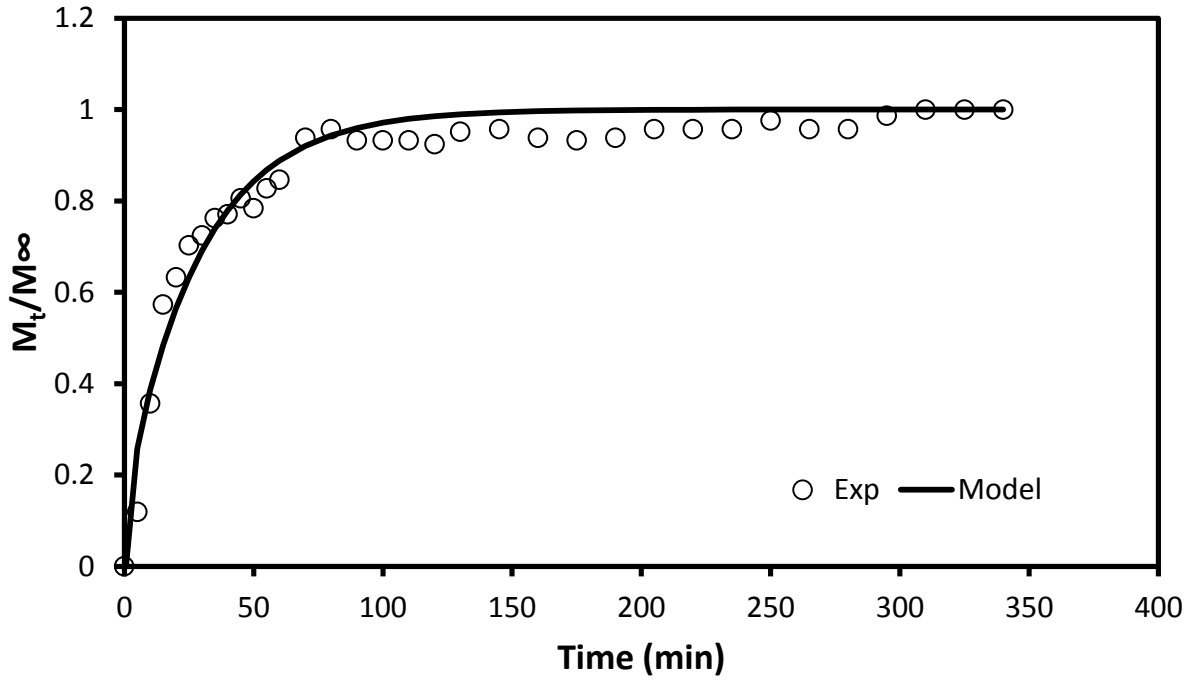

Figure B-31: Tetrahydrozoline-HCl sorption kinetics, 500 ppm.

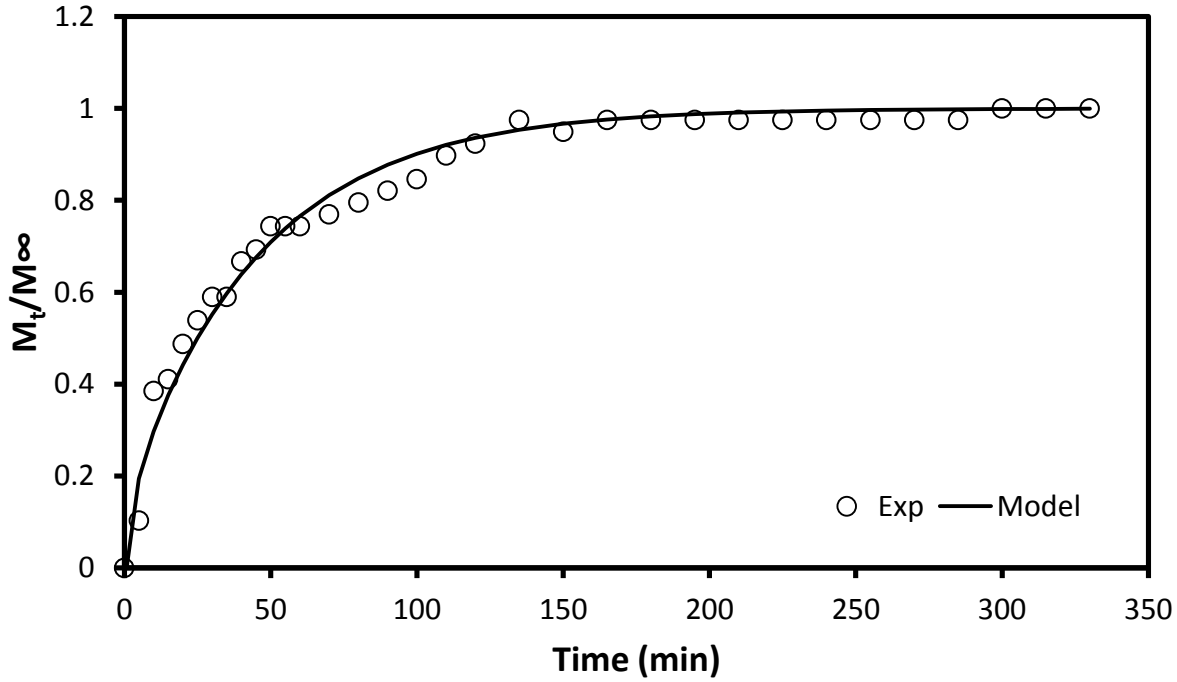

Figure B-32: Tetrahydrozoline-HCl desorption kinetics, 100 ppm.

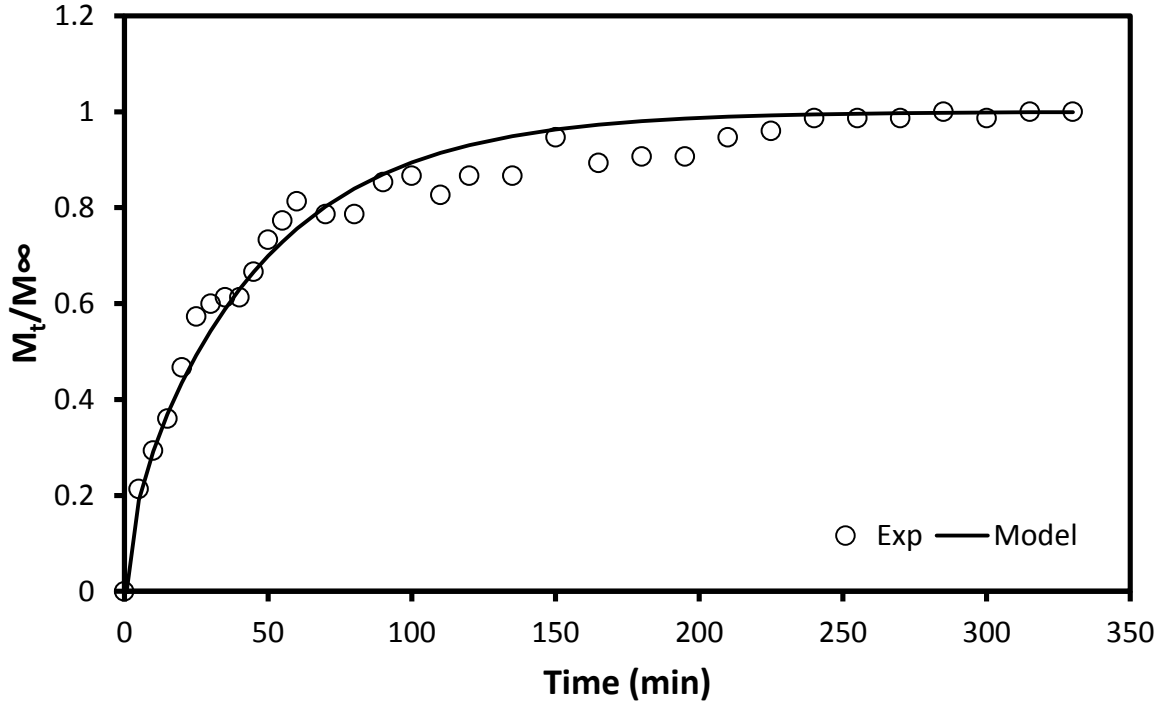

Figure B-33: Tetrahydrozoline-HCl desorption kinetics, 200 ppm.

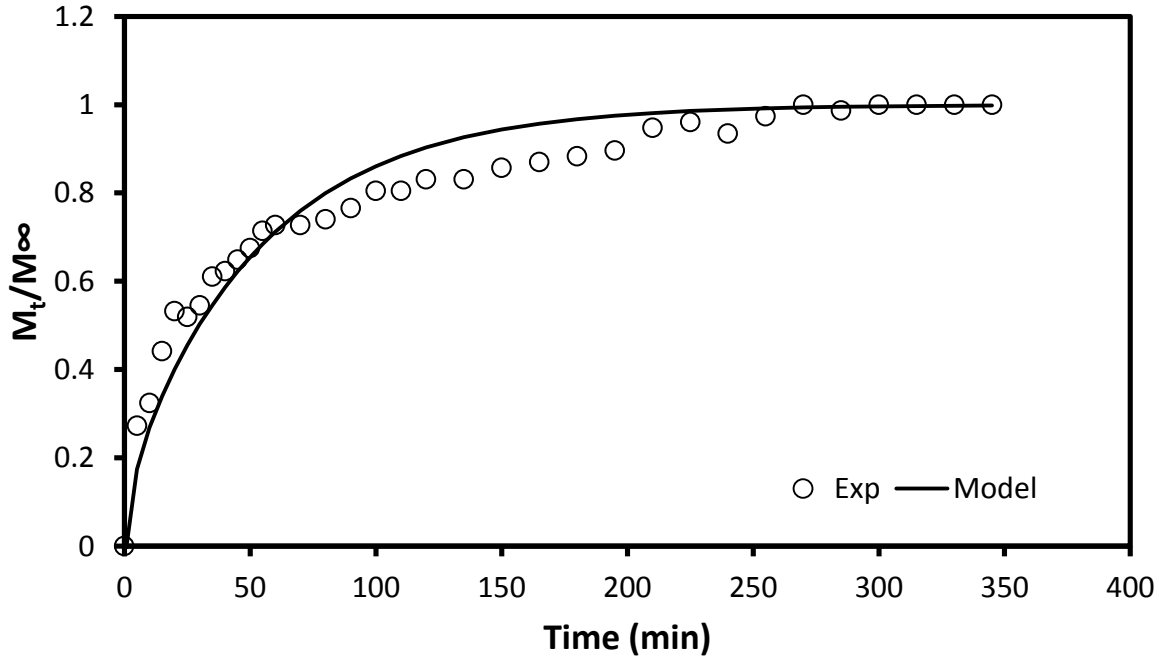

Figure B-94: Tetrahydrozoline-HCl desorption kinetics, 300 ppm.

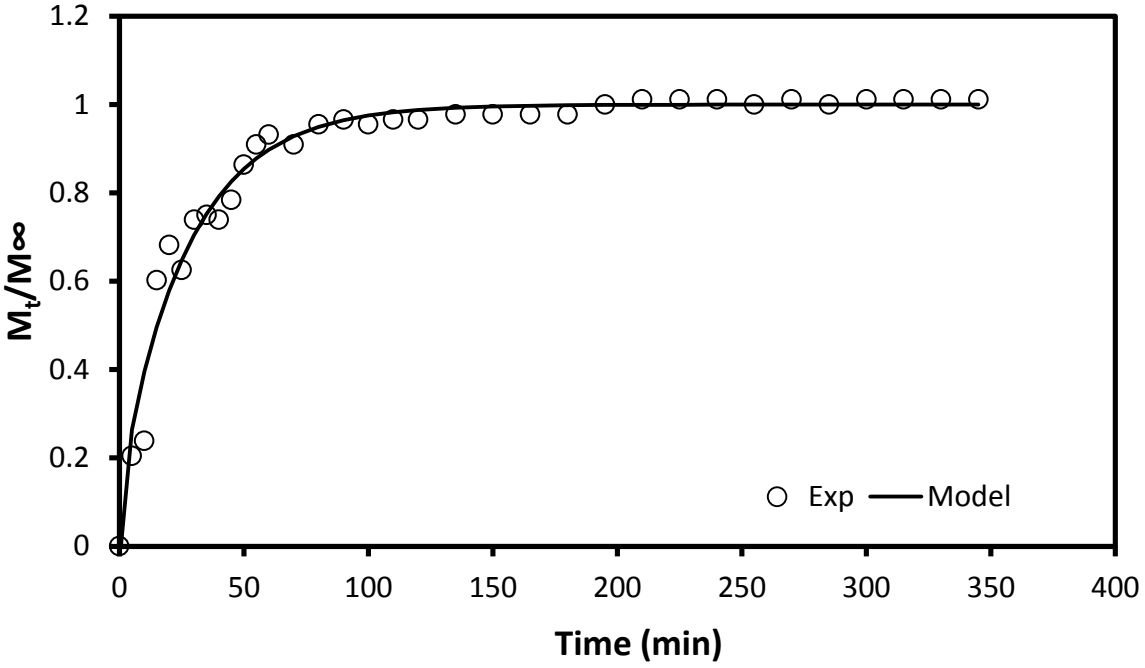

Figure B-105: Tetrahydrozoline-HCl desorption kinetics, 400 ppm.

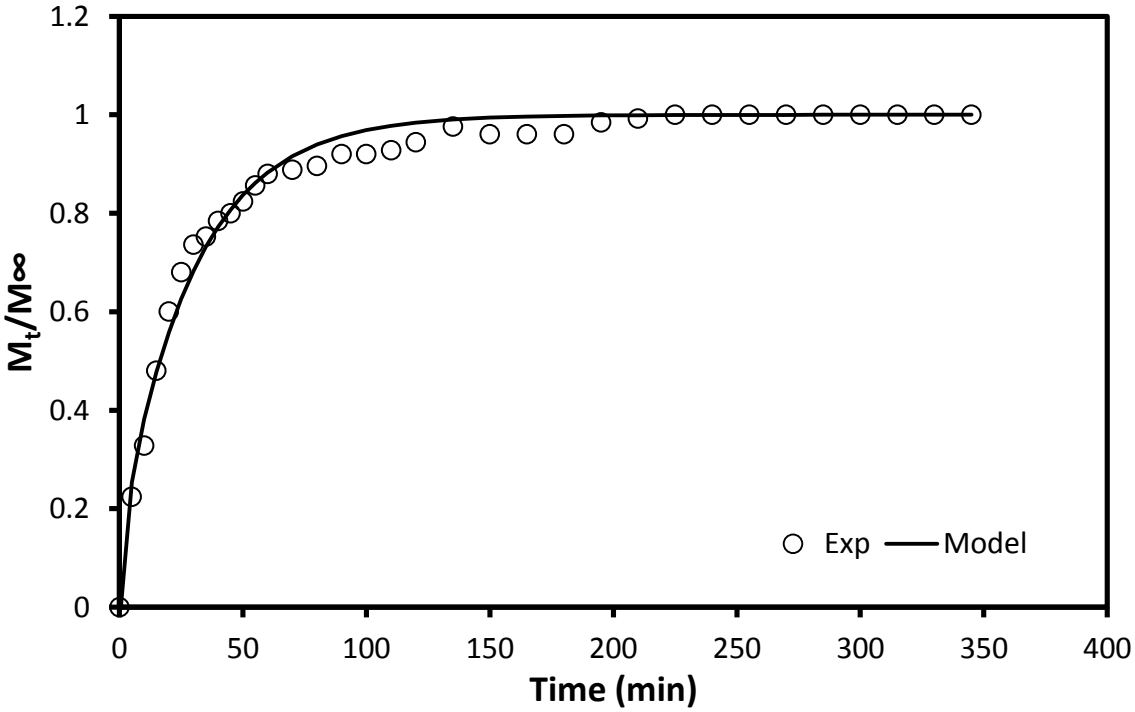

Figure B-36: Tetrahydrozoline-HCl desorption kinetics, 500 ppm.

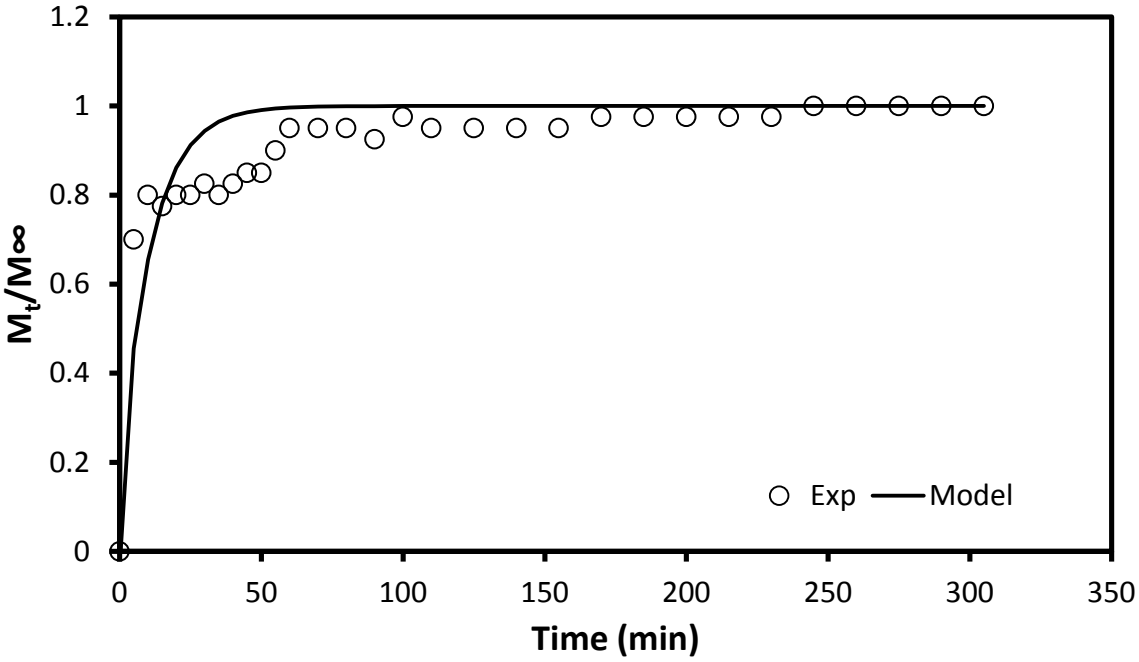

Figure B-37: Tetracycline-HCl sorption kinetics, 100 ppm.

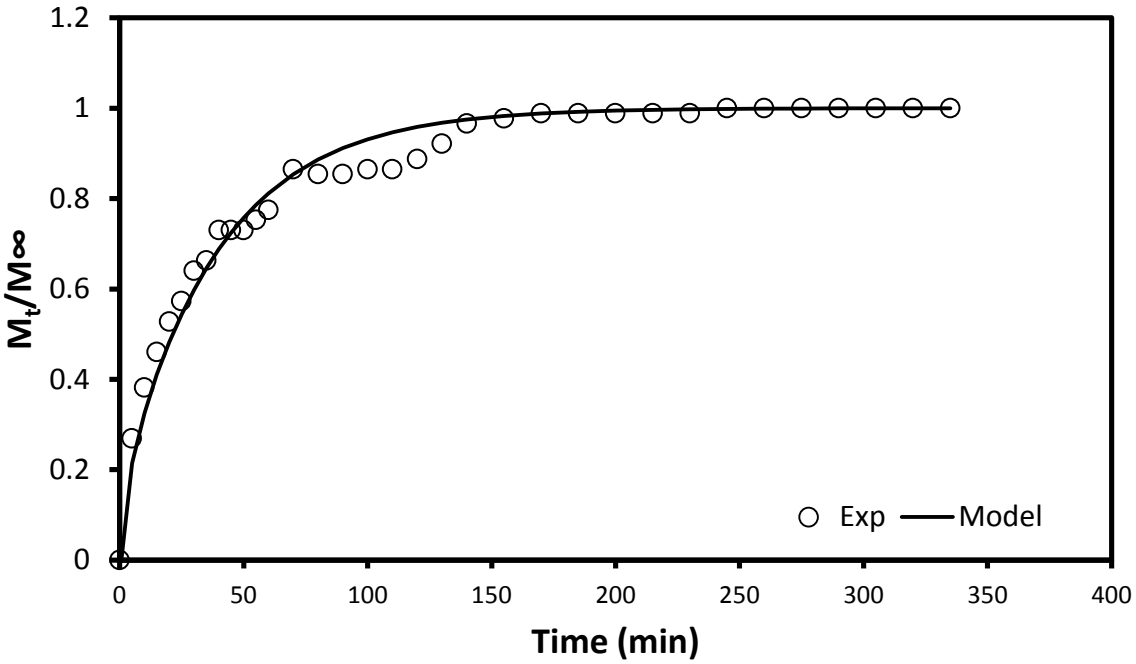

Figure B-38: Tetracycline-HCl sorption kinetics, 200 ppm.

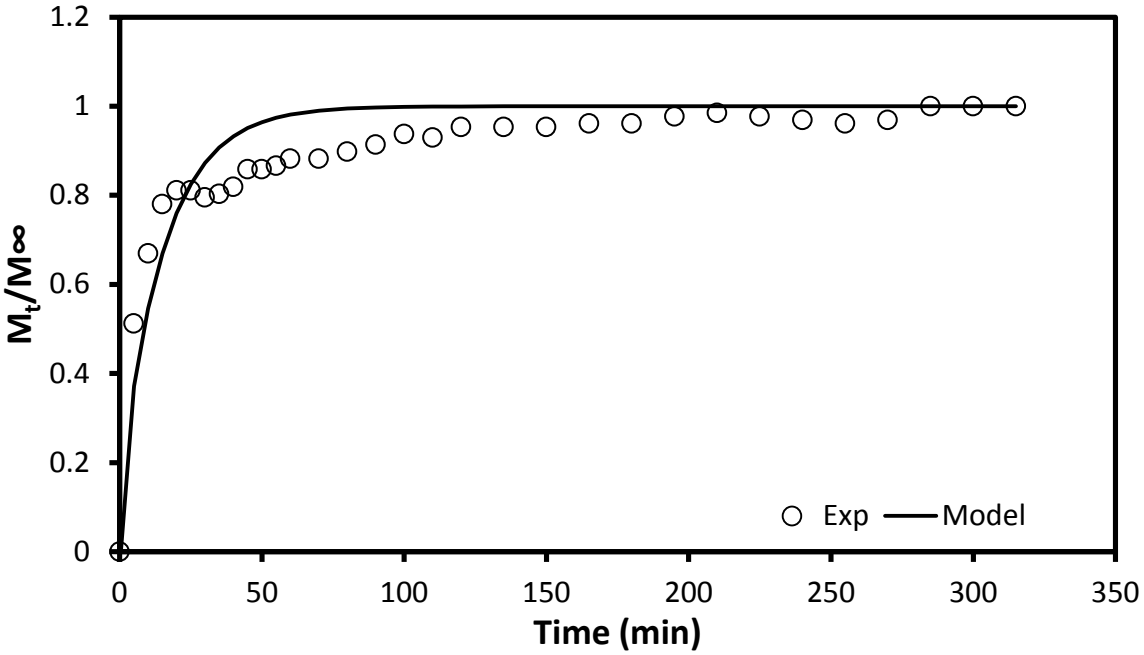

Figure B-39: Tetracycline-HCl sorption kinetics, 300 ppm.

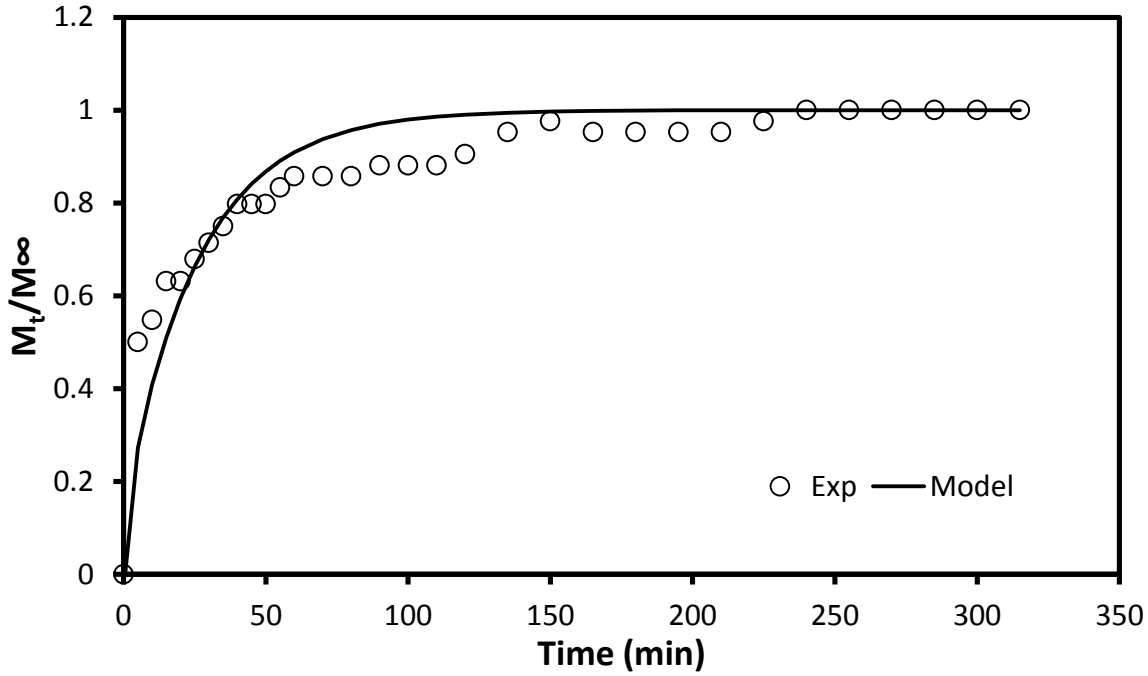

Figure B-40: Tetracycline-HCl sorption kinetics, 400 ppm.

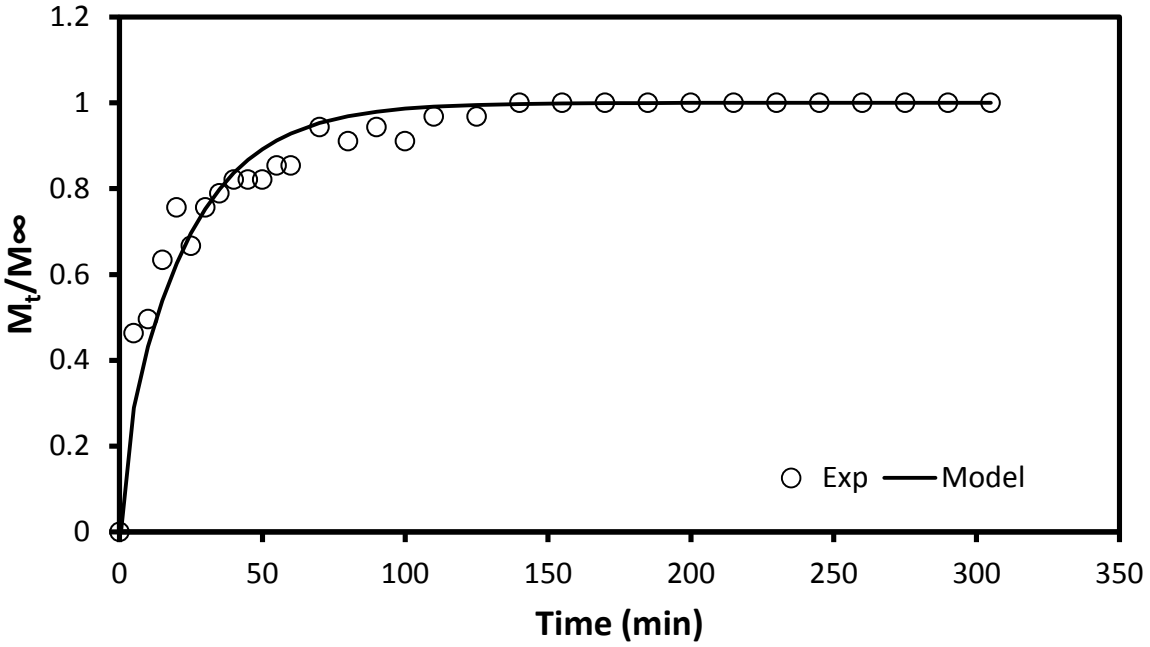

Figure B-41: Tetracycline-HCl sorption kinetics, 500 ppm.

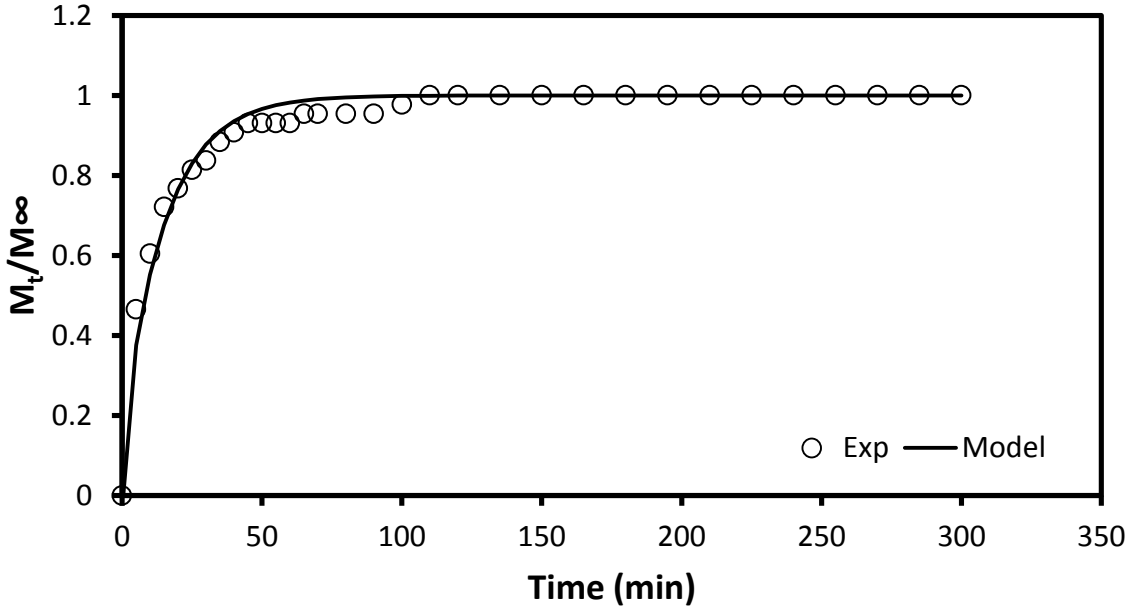

Figure B-42: Tetracycline-HCl desorption kinetics, 100 ppm.

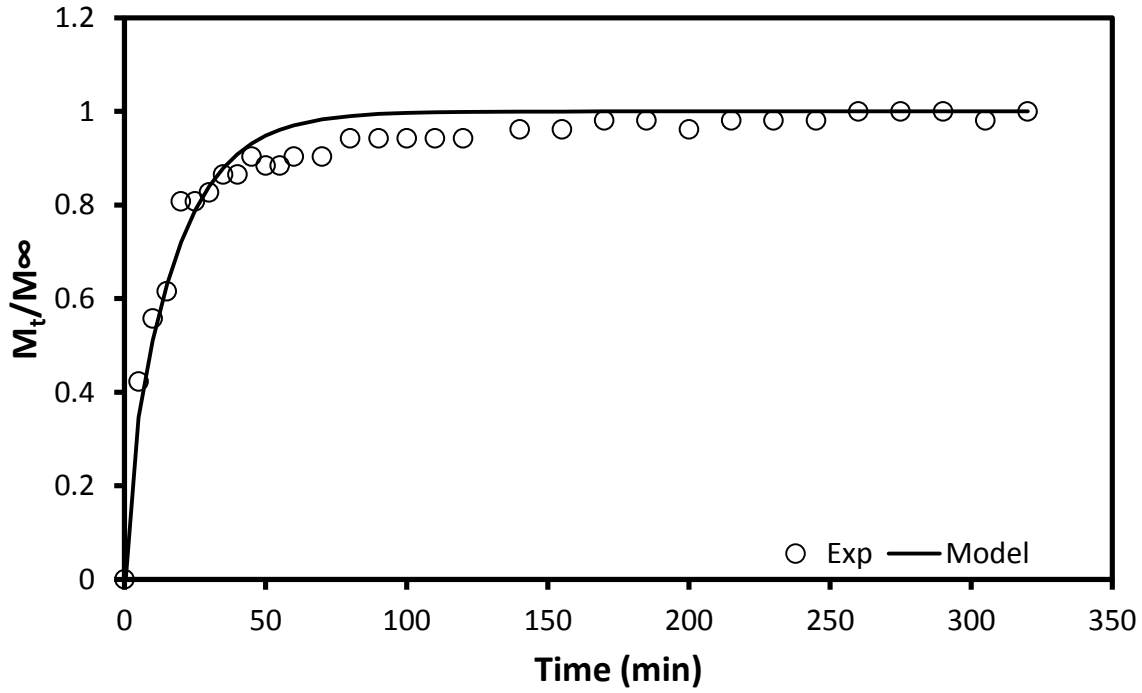

Figure B-43: Tetracycline-HCl desorption kinetics, 200 ppm.

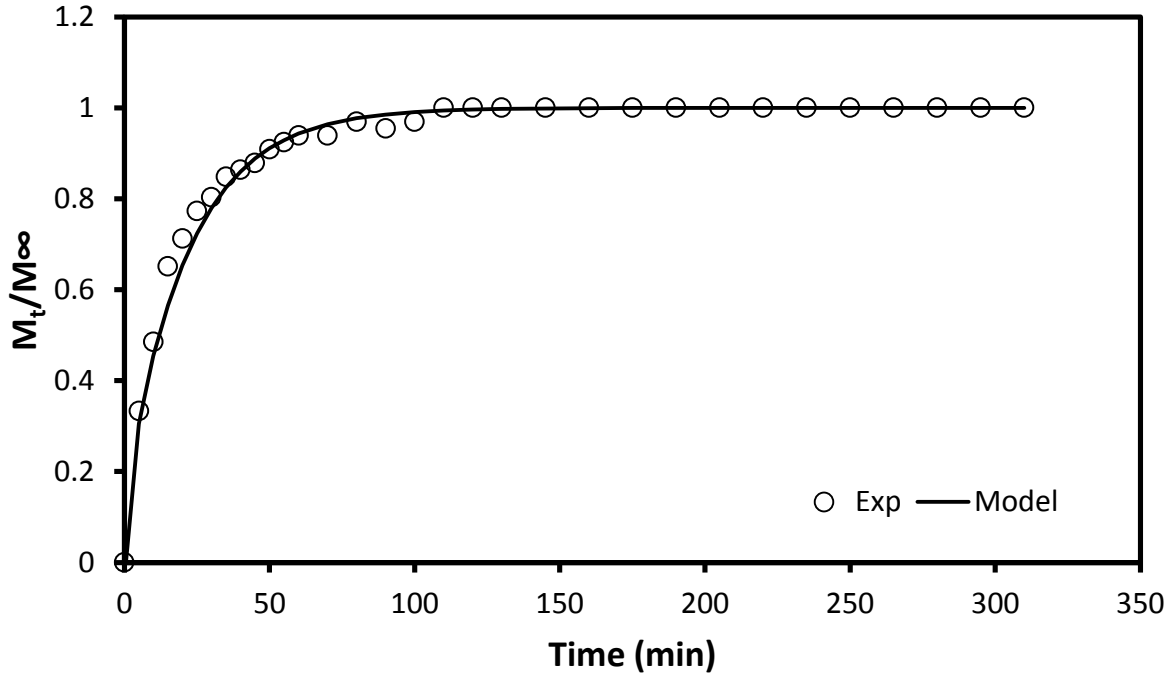

Figure B-114: Tetracycline-HCl desorption kinetics, 300 ppm.

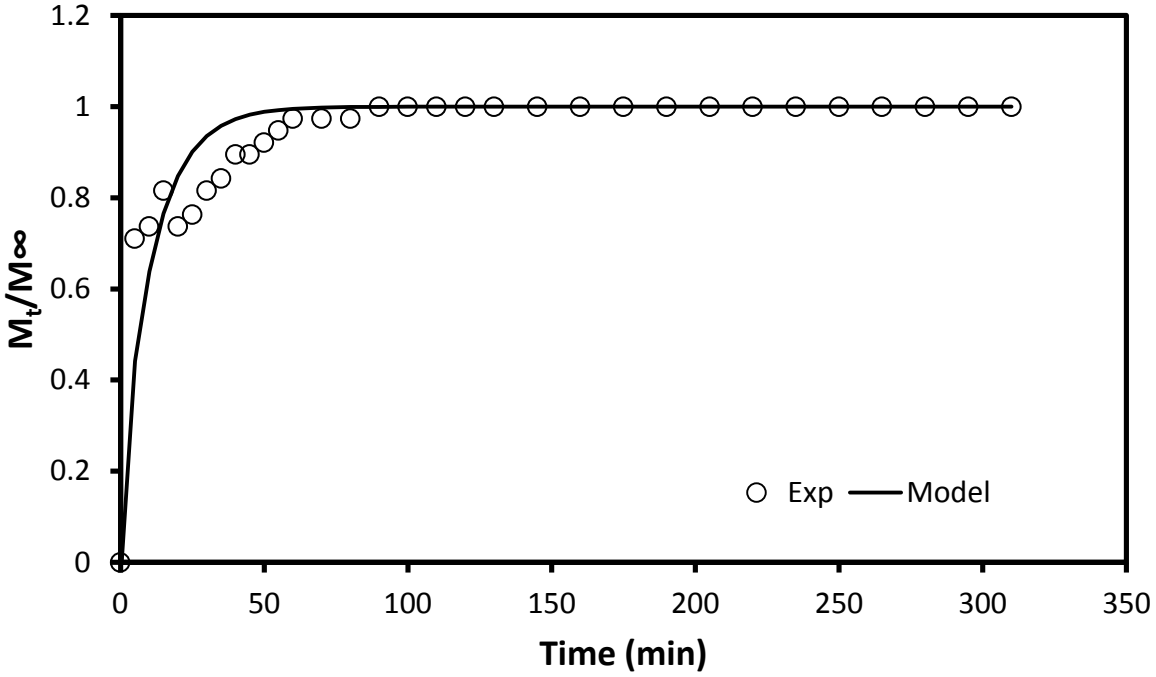

Figure B-125: Tetracycline-HCl desorption kinetics, 400 ppm.

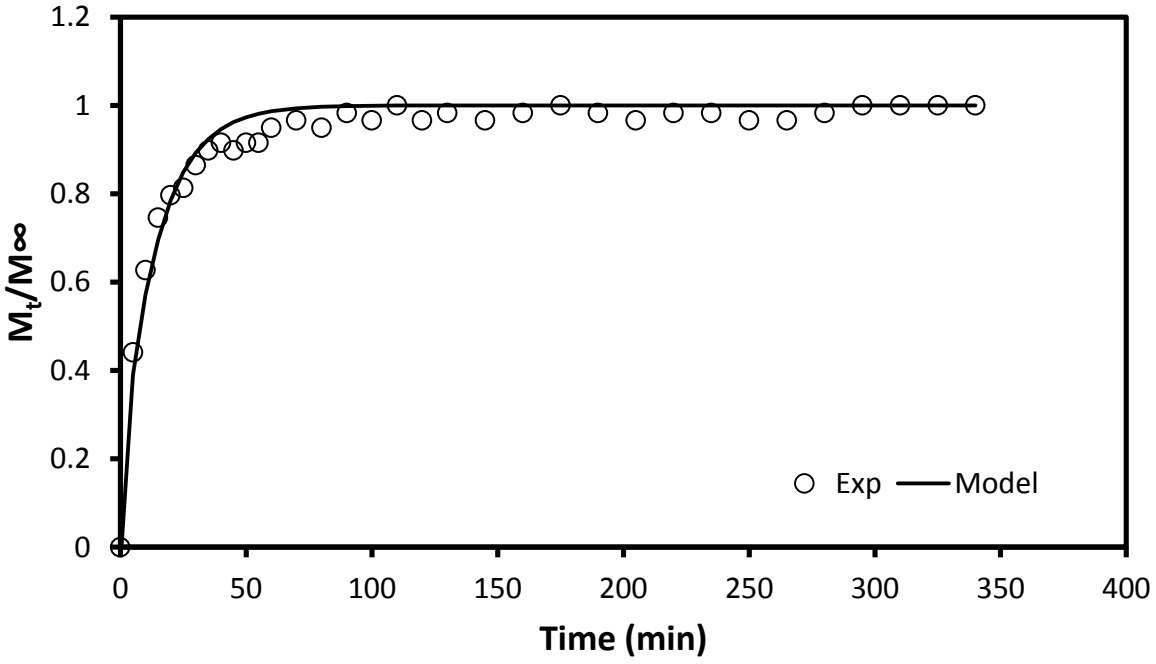

Figure B-46: Tetracycline-HCl desorption kinetics, 500 ppm.